amU
Aix Marseille Université

NNT : 2025AIXM0000

THÈSE DE DOCTORAT

Soutenue à AMU — Aix-Marseille Université
le 06 juin 2025 par

Yu-Hsi LIN

Long waves models of ideal fluids

Discipline
Sciences pour l'Ingénieur

Spécialité
Mécanique et physique des fluides

École doctorale
ED 353 Sciences pour l'ingénieur :
Mécanique, Physique, Micro et Nanoélectronique

Laboratoire/Partenaires de recherche
IUSTI UMR CNRS 7343/ECOCI

Composition du jury

Hélène MATHIS Prof., Univ. de Montpellier	Rapporteure
Mario RICCHIUTO DR, INRIA, Bordeaux	Rapporteur
Boniface NKONGA Prof., Univ. de Nice Sophia-Antipolis	Président du jury
Malek ABID MCF, Aix-Marseille Univ.	Examinateur
Ricardo BARROS Senior Lecturer, Loughborough Univ. (UK)	Examinateur
Sergey GAVRILYUK Prof., Aix-Marseille Univ.	Directeur de thèse
Michel BENOIT Senior Researcher, EDF R&D LNHE & LHSV	Co-directeur de thèse

IUSTI

Affidavit

I, Lin, Yu-Hsi, hereby declare that the work presented in this manuscript is my own work, carried out under the scientific direction of Sergey Gavrilyuk and Michel Benoit, in compliance with the principles of honesty, integrity and responsibility inherent in the research mission. The research work and the writing of this manuscript were carried out in compliance with both the french national charter for Research Integrity and the Aix-Marseille University charter on the fight against plagiarism.

This work has not been previously submitted in France or abroad in an identical or similar version to an examining body.

Marseille, 27 March 2025

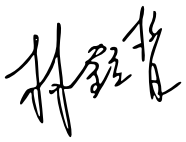

Cette oeuvre est mise à disposition selon les termes de la Licence Creative Commons Attribution - Pas d'Utilisation Commerciale - Pas de Modification 4.0 International.

List of publications and conference participation

List of publications and/or patents produced as part of the thesis project :

1. Sergey Gavrilyuk, Yu-Hsi Lin et Keh-Ming Shyue. « Hyperbolicity study of the modulation equations for the Benjamin–Bona–Mahony equation ». In : *Studies in Applied Mathematics* 151.2 (2023), p. 536-554

Participation in conferences and summer schools during the thesis period :

1. Ecoulements diphasiques, la mécanique des milieux continus et les systèmes d'équations hyperboliques (2022, CIRM, Marseille)
2. « INSTABILITES » (2023, IMI, Marseille)
3. Journées de Modélisation des Vagues à Phases Résolues (2023, Ile D'Aix)
4. Colloquium in memory of Serguei Godunov (2023 Marseille)
5. Advanced Numerical Methods for Hyperbolic PDE (30/1/2023 - 3/2/2023) (online)

Résumé

Dans le chapitre 1, les équations de modulation de l'équation Benjamin-Bona-Mahony (BBM) sont étudiées. La frontière de stabilité des équations de modulation est dérivée. Approximativement, lorsque le nombre d'onde adimensionnel est $k > \sqrt{3}$, le système d'équations de Whitham n'est pas hyperbolique.

Au chapitre 2, une étude mathématique et numérique d'un écoulement bicouche décrit par les équations de Benney est présentée. Le système est hyperbolique même si l'énergie totale n'est pas convexe. Les invariants de Riemann pour ce système peuvent être dérivés explicitement. L'étude des champs de direction propres a été réalisée. Deux champs de direction propres correspondant aux ondes de surface rapides et lentes sont vraiment non-linéaires au sens de Lax. Le troisième champ de direction propre, correspondant au transport de vorticité, n'est ni vraiment non-linéaire, ni linéairement dégénéré au sens de Lax. La région où tous les champs de direction propres sont vraiment non-linéaires est déterminée, dans laquelle l'inégalité « d'entropie » garantit la stabilité d'un choc pour tous les champs. Cependant, lorsque le troisième champ de direction propre n'est ni vraiment non-linéaire, ni linéairement dégénéré, on peut avoir un choc stable même si l'entropie mathématique augmente au cours du choc.

Au chapitre 3, les équations d'Euler sont formulées en coordonnées semi-Lagrangiennes. Une condition limite de pression sur le fond du domaine dépendant de la courbure du fond est dérivée. Un schéma numérique perspectif est proposé et testé dans le cas d'une onde longue non-linéaire périodique se propageant dans une profondeur d'eau uniforme.

Mots clés : équation BBM, hyperbolicité, équations de Benney, stabilité, coordonnées semi-lagrangiennes

Abstract

In Chapter 1, the modulation equations of the BBM equation are studied. The boundary of modulational stability is derived. Approximately, when the wave number is $k > \sqrt{3}$, the system is modulationally unstable.

In Chapter 2, a study of a two-layer flow described by the Benney equations is presented. The system is hyperbolic even though the total energy is not convex. The Riemann invariants for this system can be derived explicitly. The study of the eigenfields has been done. Two eigenfields corresponding to the fast and slow surface waves are genuinely nonlinear in the sense of Lax. The third eigenfield corresponding to the vorticity transport is neither genuinely nonlinear nor linear degenerate in the sense of Lax. The region where all eigenfields are genuinely nonlinear is found, in which the "entropy" inequality guarantees the stability of a shock for all fields. However, when the third eigenfield is neither genuinely nonlinear nor linear degenerate, one can have a stable shock even when the mathematical "entropy" increases through the shock.

In Chapter 3, the Euler equations are formulated in semi-Lagrangian coordinates. A curvature-dependent bottom boundary condition for pressure is derived. A perspective numerical scheme is proposed and tested in the case of a nonlinear long periodic wave propagating in uniform water depth.

Keywords: BBM equation, hyperbolicity, Benney equations, stability, semi-Lagrangian coordinates

Acknowledgments

I express my gratitude to the IUSTI laboratory for hosting me. I sincerely thank both of my supervisors, Prof. Sergey Gavrilyuk and Dr. Michel Benoit, for their generous and priceless support throughout these years. I would like to thank my wife, Shu-Chen, and my family for their invaluable support. Last but not least, I would like to thank all the researchers and doctoral researchers who helped me improve my work through their advice and comments, in particular, Kevin, Joris, Houssine, Jordan, Valentin, Gabriel, Alexandre, Yann, Chong-Wei, Solène, Quentin, Léa, Estelle, and Priya.

Table of Contents

Résumé 4

Abstract 5

Acknowledgments 7

List of Figures 9

Introduction 11
0.1 General setup and the construction of the thesis 11
APPENDIX 17
A Derivation of approximate models from the Euler equations 17
A.1 Dimensionless variables 18
A.2 Dispersive waves 19
A.3 Benney equations 23

1 Hyperbolicity study of the modulation equations for the Benjamin-Bona-Mahony equation 25
1.1 Introduction 26
1.2 Whitham modulation equations for the BBM system 28
1.3 Hyperbolicity study in the variables $\mathbf{q} = (D, a, m)^T$ 30
1.4 Numerical study of eigenfields in $(\overline{u}, a, m)$ variables 34
1.5 Stokes expansion for the BBM modulation system 35
1.6 Stability of the BBM periodic solutions 37
APPENDIX: The nondegeneracy of the Jacobian matrix in $(\overline{u}, a, k)$ varialbes 43

2 Shear Shallow Water Flow Approximation based on Benney equations 45
2.1 Introduction 46
2.1.1 Recall on hyperbolic conservation laws 46
2.1.2 Shallow water equations with piecewise linear velocity profiles 53
2.2 Two-layer stratified flow with continuous velocity profile 55
2.2.1 Total momentum equation 56
2.2.2 Vorticity equation 57
2.2.3 Energy equation 58
2.2.4 Riemann invariants and eigenvalues 58

2.3 System study . . . 60
2.3.1 Study of $\nabla\lambda_j \cdot \mathbf{r}_j$ . . . 60
2.3.2 Convexity of energy . . . 64
2.3.3 Rankine-Hugoniot locus and "entropy" inequality . . . 70
2.4 Numerical results . . . 71
2.4.1 The fast characteristic field . . . 72
2.4.2 The second characteristic field . . . 83
2.5 Conclusion . . . 86
APPENDIX . . . 87
B Recall on shallow water equations . . . 87
C Recall on the basic algorithms for finite volume methods . . . 90
C.1 Godunov method . . . 91
C.2 The HLL approximate Riemann solver . . . 92

3 Modelling of the Euler equations with arbitrary vorticity over variable topography in semi-Lagrangian coordinates 94
3.1 Introduction . . . 95
3.2 Two-dimensional Euler equations in semi-Lagrangian coordinates . . . 96
3.3 Equation for the pressure . . . 98
3.3.1 Boundary condition for the pressure on the bottom . . . 99
3.3.2 Bottom boundary condition of the pressure in semi-Lagrangian coordinates . . . 102
3.4 Equation for Energy . . . 103
3.5 Three-dimensional Euler equations in semi-Lagrangian coordinates . . . 104
3.5.1 Divergence operator . . . 104
3.5.2 Laplacian operator of pressure . . . 106
3.5.3 Reduction from 3D to 2D . . . 106
3.6 Numerical scheme . . . 108
3.6.1 Overview of the numerical solution strategy . . . 108
3.6.2 Discretizations . . . 109
3.6.3 Partial numerical results . . . 112
3.7 Conclusion . . . 119

Conclusion and perspective 120

Bibliography 121

List of Figures

1 Sketch of the domain $\mathfrak{D}$ where the Euler equations are valid. 11
2 The solid blue line is the boundary between the hyperbolic and elliptic regions; the dashed blue line is the wave number $k = \sqrt{3}$. . . 13
3 Sketch of a two-layer flow of a homogeneous fluid with a piecewise linear continuous horizontal velocity profile. 14
4 Illustration of the change of variables from (x, z) to (x, λ). 16
5 Long waves models derived from Euler equations. 17

2.1 Sketch of the pressure $p(\tau)$ in p-system 48
2.2 Illustration of the Lax condition Eqn. (2.15) on (q, t)-plane 50
2.3 Illustration of the function $p(\tau)$, for the right facing shock. 52
2.4 p-system 52
2.5 p-system when the eigenfields are not genuinely nonlinear 53
2.6 Illustration of a piecewise linear velocity profile in $i^{\text{th}} -$ layer. 53
2.7 Illustration of two-layer stratified flow with continuous velocity profile 56
2.8 The blue continuous curves are level sets of $g(h_1, h_2) = \nabla\lambda_2 \cdot \mathbf{r}_2 = 0$; The dashed black lines are the tangent lines to $g = 0$ at $h_1 = h_2 = 0$, The expression of the tangent lines is: $h_1 = \dfrac{\omega_1 - 2\omega_2}{2\omega_1 - \omega_2} h_2$ 63
2.9 The 3 characteristic fields are genuinely nonlinear in the red region $\dfrac{1}{2} \leq \dfrac{|\omega_1|}{|\omega_2|} \leq 2$ 65
2.10 The second principal minor of E'' is negative in the red region, which implies the total energy is not a convex function. The black line is where the term $A = 0$; and the blue line is where the term $B = 0$. . 69
2.11 The evolutions of $\mathcal{E}(h_1^-, h_2^-) = 0$ and Rankine-Hugoniot locus $\mathcal{H}(h_1^-, h_2^-)$ varying the vorticity in the upper layer ω_2 from negative to positive. 76
2.12 Numerical results of the points marked in Fig. 2.11. 78
2.13 Numerical results of observing the angle of the cusp when the averaged vorticity is zero $\Omega \equiv 0$. 82
2.14 Two examples of the second characteristic field of $g(h_1, h_2) = 0$, $\mathcal{E}(h_1^-, h_2^-) = 0$, and the Rankine-Hugoniot locus $\mathcal{H}(h_1^-, h_2^-)$ on (h_1^-, h_2^-)-plane. 84
2.15 Numerical results showing two stable shocks in unstable region . . . 85
2.16 Illustration of HLL method 92

3.1 Two-dimensional domain $\mathfrak{D}_{\mathbf{x}}$ in Eulerian coordinates 95

3.2 Illustration of geometrical parameters 101
3.3 Illustration of bottom boundary condition for pressure 102
3.4 Locations of the unknown variables in a staggered grid. 110
3.5 The tested case marked on Le Méhauté diagram (the diagram was taken from Wikipedia) 113
3.6 Partial numerical results 118

Introduction

Table of Content

0.1 General setup and the construction of the thesis 11
APPENDIX 17
A Derivation of approximate models from the Euler equations 17
A.1 Dimensionless variables 18
A.2 Dispersive waves 19
A.2.1 The Serre-Green-Naghdi equations 19
A.2.2 Boussinesq equation, long waves of small amplitude 21
A.2.3 Unidirectional models: Korteweg-de Vries equation and Benjamin-Bona-Mahony equations 21
A.3 Benney equations 23

0.1. General setup and the construction of the thesis

Ideal fluid is assumed to have a constant density and is described by the Euler equations. Fig. 1 shows a sketch of the flow domain $\mathfrak{D}$. The piecewise smooth

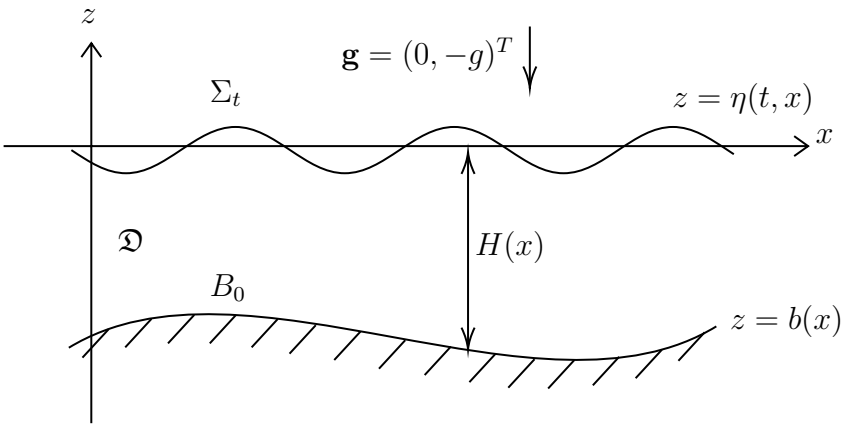

Figure 1. – Sketch of the domain $\mathfrak{D}$ where the Euler equations are valid.

boundaries B_0 and Σ_t are defined as:

$$B_0 \coloneqq \{x, z | z = b(x)\},$$
$$\Sigma_t \coloneqq \{x, z | z = \eta(t, x)\},$$

where the sea bed elevation is denoted by $b(x)$, which is time independent t, and $\eta(t,x)$ represent the free surface evolution. Moreover, the total water depth can be defined as:

$$h(t,x) \coloneqq \eta(t,x) - b(x).$$

With constant density ρ, the Euler equations in domain $\mathfrak{D}$ take the form:

$$\operatorname{div} \mathbf{u} = 0, \tag{0.1}$$

$$\rho \frac{\mathrm{d}\mathbf{u}}{\mathrm{d}t} + \nabla p = \rho \mathbf{g}, \tag{0.2}$$

with $\mathbf{g} = (0, -g)^T$ being the gravity field, and $\dfrac{\mathrm{d}}{\mathrm{d}t} \coloneqq \dfrac{\partial}{\partial t} + \mathbf{u} \cdot \nabla$ being the total derivative. The unknown variables are the velocity vector $\mathbf{u} = (u, w)^T$, the pressure p depending on $\mathbf{x} = (x, z)^T$, and the time t. There are two boundary conditions on the free surface, Σ_t:

$$\eta_t + u_s \eta_x = w_s, \tag{0.3}$$

$$p_s = 0, \tag{0.4}$$

where the subscript "s" denotes the unknown variables at the free surface. At the sea bed, B_0, the boundary condition takes the form:

$$u_b b_x = w_b. \tag{0.5}$$

where the subscript "b" denotes the unknown variables at the bottom.

Various wave models exist, based on different kinds of simplification, regarding two important wave properties, nonlinearity and dispersion. These two properties can be characterized by the wave amplitude and the wavelength compared to the water depth. Denote the wave amplitude by a, and the characteristic wavelength by L, and the characteristic water depth is denoted by H. These two important parameters can be defined as:

$$\mu \coloneqq \frac{H}{L}, \tag{0.6}$$

$$\varepsilon \coloneqq \frac{a}{H}. \tag{0.7}$$

To be more precise, the term long waves or shallow waves refers to $\mu \ll 1$ while the term short waves or deep waves refers to $\mu \gg 1$. On the other hand, the small-amplitude waves correspond to $\varepsilon \ll 1$.

In this thesis, three topics would be covered, including two long-wave models derived from the Euler equations, and the semi-Lagrangian formulation of the Euler equations. The first case is a long wave with small amplitude assumption, which is referred to the Benjamin-Bona-Mahony (BBM) equation (Thomas Brooke Benjamin,

Bona, and Mahony 1972); the second case is only a long-wave approximation, which is referred to the Benney equations (Benney 1973).

In Chapter 1, the hyperbolicity of Whitham's modulational equations (G. Whitham 1967, Gerald Beresford Whitham 2011) for the BBM equation is studied. The hyperbolicity of the modulational equations (modulational stability), from the mathematical point of view, is a necessary condition for the spectral stability of periodic traveling waves (see Benzoni-Gavage, Noble, and Rodrigues 2014). Moreover, from the physical point of view, the Benjamin-Feir instability (T Brooke Benjamin and Feir 1967) is related to the ellipticity of the modulational equations. In Tso 1992, has mentioned that Whitham's modulational equations of the BBM equation can be not hyperbolic; however, the study of the equations is not done. The Benjamin-Feir instability for the BBM equation is studied in Hur and Pandey 2016. They have shown that the traveling wave is spectrally unstable when the wave number $k > \sqrt{3}$, but the precise boundary of stability is not defined. Numerical and analytical studies of the limit case, the wave number $k \to 0$ (solitary waves) are present in Gavrilyuk and Shyue 2021. In Chapter 1, the boundary between the hyperbolic and elliptic regions is found. Furthermore, when the wave amplitude is small, this boundary is approximated to the wave number $k = \sqrt{3}$. Here, we share the same results as in Hur and Pandey 2016. This boundary is shown in Fig. 2 as the solid blue line. In which, the parameter m on the horizontal axis is related to the wave amplitude. A more precise definition can be found on page 28.

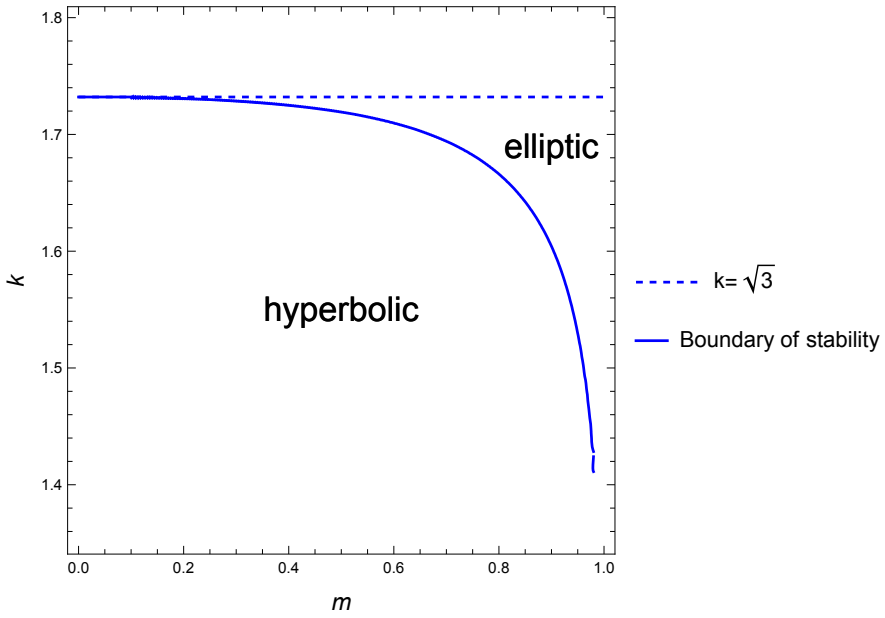

Figure 2. – The solid blue line is the boundary between the hyperbolic and elliptic regions; the dashed blue line is the wave number $k = \sqrt{3}$.

In Chapter 2, a two-layer flow of ideal homogeneous fluid described by the Benney equations is studied, in which the horizontal velocity in each layer is linear with

respect to the vertical coordinate:

$$\frac{\partial u_1}{\partial z} = \omega_1, \tag{0.8}$$

$$\frac{\partial u_2}{\partial z} = \omega_2. \tag{0.9}$$

Here u_1, u_2 and ω_1, ω_2 are horizontal velocities and constant vorticities in each layer, respectively. A sketch of the system is shown in Fig. 3

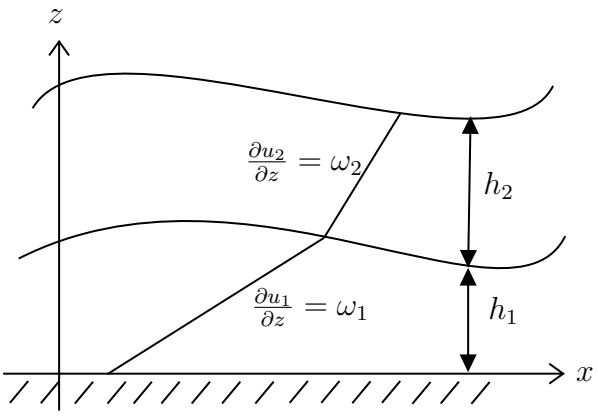

Figure 3. – Sketch of a two-layer flow of a homogeneous fluid with a piecewise linear continuous horizontal velocity profile.

A long wave problem is usually described by the classical shallow water equations (Stoker 2019), which only considers the averaged horizontal velocity, and the horizontal velocity u is independent of z: $u(t, x, z) \approx u(t, x)$. Therefore, with the mass conservation equation: $u_x + w_z = 0$, the vertical velocity for the classical shallow water equations takes the form:

$$w = -\int_0^z u_x(t, x, s)\mathrm{d}s \approx -u_x(t, x)z.$$

Equations of a long non-linear wave in shear flow (the horizontal velocity u can depend on z) are provided in (Benney 1973). The Benney equations imply an infinite number of conservation laws (Benney 1973). A finite multi-layered fluid based on the Benney system with piecewise constant horizontal velocity in z with infinite conservation laws is provided in Zakharov 1980. Such a finite multi-layered fluid with a piecewise linear velocity profile in z in each layer is discussed in Chesnokov, El, Gavrilyuk, and Pavlov 2017. Notice that the velocity between each layer is not required to be continuous. The criteria of hyperbolicity of the governing equations and the existence of corresponding Riemann invariants are given. In Chapter 2, we consider a two-layer flow with a continuous piecewise linear velocity profile. In this case, the system is hyperbolic, and it becomes possible to study the

nature of the eigenfields (genuinely nonlinear or linear degenerate). Furthermore, the conditions for shock stability in the sense of Lax are studied.

In Chapter 3, the Euler equations are discussed. The difficulty of the full Euler equation is to deal with the moving boundary, the free surface. Therefore, it is necessary to transform the moving domain into a fixed domain with flat boundaries. A classical method is the so-called σ-transformation (Phillips 1957), the mapping function σ is defined as:

$$\sigma := \frac{z - b(x)}{h(t,x)}; \quad \sigma \in [0,1],$$

here using the notation of Fig. 1. Although this method is the simplest transformation, but it lacks of physical meaning, and extra terms are generated while taking derivative with respect to $\mathbf{x} = (x,z)^T$, and the time t. An alternative mapping method is applying the semi-Lagrangian coordinates (x,λ), which is introduced by Zakharov 1980. The Lagrangian coordinate λ is defined in the region $\lambda \in (0,1)$. The definition of the Lagrangian variable λ is the total derivative of λ is zero,

$$\frac{\mathrm{d}}{\mathrm{d}t}\lambda = \lambda_t + u\lambda_x + w\lambda_z = 0.$$

The free surface $z = \eta(t,x)$ corresponds to the value $\lambda = 1$; and the bottom $z = b(x)$ corresponds to the value $\lambda = 0$. The mapping function of the changing variables $(x,z) \to (x,\lambda)$ is:

$$z = \Phi(t,x,\lambda),$$

where $\Phi(t,x,\lambda)$ is the solution of the equation

$$\Phi_t + \tilde{u}\Phi_x = \tilde{w}, \tag{0.10}$$

with the initial condition:

$$\Phi|_{t=0} = (1-\lambda)b(x) + \lambda\eta_0(x) = b(x) + \lambda h_0(x).$$

Here the subscript "0" is the initial value of the corresponding variables, and the "tilde" sign denotes the variables in (x,λ) coordinates. Remark that as defined above, $h_0(x) := \eta_0(x) - b(x)$ denotes the initial total water depth. The curves $\Phi(t,x,\lambda = \text{const.})$ represent a foliation of the domain in (x,z) variables indexed by λ. In which, the bottom B_0 and the free surface Σ_t are included. Notice that Eqn. (0.10) indicates there is no mass passing through the curves $\Phi(t,x,\lambda = \text{const.})$. Moreover, since Φ is a smooth function, there is no intersection between any two curves $\Phi(t,x,\lambda = \text{const.})$. In other words, $\Phi_\lambda \neq 0$. Therefore, the limit of this model is obvious, this model is not suitable to simulate the wave-breaking process. Fig. 4 shows the mapping of the domain in (x,z) to the domain in (x,λ). For any physical variable in (x,z) domain, $F(t,x,z)$, with the definition of changing

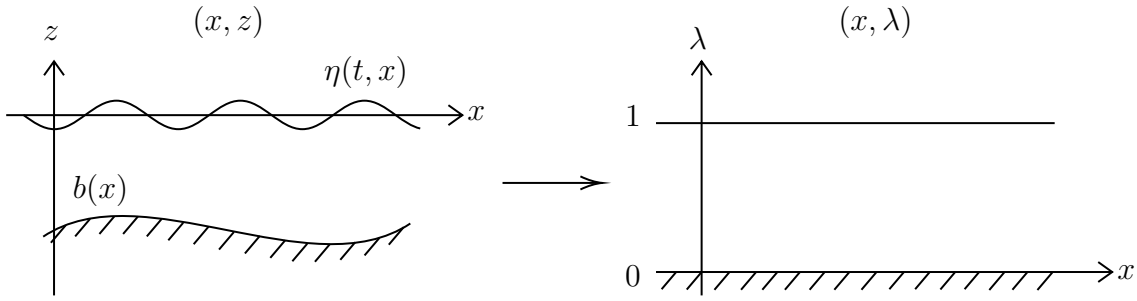

Figure 4. – Illustration of the change of variables from (x, z) to (x, λ).

variables, the corresponding physical variable in (x, λ) domain, $\tilde{F}(t, x, \lambda)$, can be expressed as:

$$F(t, x, z) = F(t, x, \Phi(t, x, \lambda)) = \tilde{F}(t, x, \lambda).$$

Taking partial derivative of any physical variable with respect to t, x, and λ the following relation can be obtained:

$$F_t + F_z\Phi_t = \tilde{F}_t; \quad F_x + F_z\Phi_x = \tilde{F}_x; \quad F_z\Phi_\lambda = \tilde{F}_\lambda.$$

Therefore, the material derivative takes the form:

$$\begin{aligned}\frac{\mathrm{d}F(t, x, z)}{\mathrm{d}t} &= F_t + uF_x + wF_z \\ &= F_t + uF_x + (\Phi_t + u\Phi_x)F_z \\ &= \tilde{F}_t + \tilde{u}\tilde{F}_x = \frac{\tilde{\mathrm{d}}\tilde{F}(t, x, \lambda)}{\tilde{\mathrm{d}}t}.\end{aligned}$$

An advantage of these changes of variables is that in semi-Lagrangian coordinates, the term involving the vertical velocity in the material derivative vanishes.

Several works have been studied on this semi-Lagrangian coordinates recently. A clear definition of the semi-Lagrangian is present in V. M. Teshukov 1985 and V. M. Teshukov 1992, In Di Martino, El Hassanieh, Godlewski, et al. 2024, the Benney equations are written in semi-Lagrangian coordinates, the equivalence between the system in domain (x, z) and domain (x, λ) is rigorously proved. Such a change of variables is also proposed by Alexandris-Galanopoulos, Papadakis, and Belibassakis 2024, but the energy conservation equation is not present.

In Chapter 3, the conservation laws of mass, moment, and energy are derived. Moreover, the bottom boundary condition for Poisson's equation of pressure for arbitrary bottom topography $B_0(x)$ is derived. However, there are several difficulties while we are doing numerical studies of the system. An important issue is to satisfy the condition of a divergence-free velocity field. When this condition is not satisfied, the system becomes numerically unstable. We have tried a couple of methods to deal with this problem. However, the problem is not fully understood yet. However,

a possible numerical scheme is presented.

APPENDIX

A. Derivation of approximate models from the Euler equations

A brief classification of approximate models is shown in Fig. 5. The approximate models can be classified into two families: with and without dispersion.

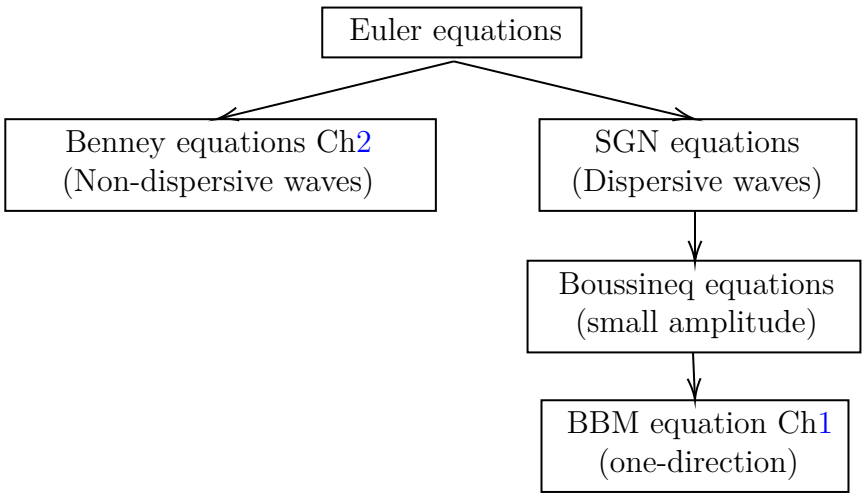

Figure 5. – Long waves models derived from Euler equations.

As mentioned above, two properties are commonly used to classify wave models, namely nonlinearity and dispersion. Here, a brief derivation of approximate dimensionless Euler equations is presented. First, a zero-order long-wave approximation (shallow water), called the Benney equations, is derived. Then, a second-order long-wave approximation, called the Serre-Green-Naghdi equations, is presented. After that, combined with the small-amplitude assumption, a weakly nonlinear long-wave model, the Boussinesq equations, is derived. Finally, considering a traveling wave propagating in a unique direction, the KdV equation and the BBM equation are derived. These derivations can be found in many books (see, for example, the book of Lannes 2013. Here we follow the structure of Chiang, Stiassnie, and Yue 2005, Mitsotakis 2013, SL Gavrilyuk, Makarenko, and Sukhinin 2017, and Thomas Brooke Benjamin, Bona, and Mahony 1972.

A.1. Dimensionless variables

Using the notation in Fig. 1, the two-dimensional Euler equations with flat bottom $b(x) \equiv -H$ take the form:

$$\begin{aligned} u_x + w_z &= 0, \\ \rho(u_t + uu_x + wu_z) + p_x &= 0, \\ \rho(w_t + uw_x + ww_z) + p_z &= -\rho g. \end{aligned}$$

The corresponding boundary conditions at the free surface η are:

$$\begin{aligned} \eta_t + u_s\eta_x &= w_s, \\ p_s &= 0, \\ w_b &= 0. \end{aligned}$$

Let us introduce:

$$\mu \coloneqq \frac{H}{L}, \quad \varepsilon \coloneqq \frac{a}{H},$$

where L is the characteristic wavelength and a is the wave amplitude. The dimensionless scale variables are:

$$x = Lx', \quad z = Hz', \quad \eta = a\eta', \quad p = \rho gHp', \quad t = \frac{L}{\sqrt{gH}}t'.$$

The dimensionless velocity components are:

$$u = \sqrt{gH}u', \quad w = \frac{H}{L}\sqrt{gH}w'.$$

The Euler equations are written in dimensionless variables are:

$$u'_{x'} + w'_{z'} = 0, \tag{0.11}$$

$$u'_{t'} + u'u'_{x'} + w'u'_{z'} + p'_{x'} = 0, \tag{0.12}$$

$$\mu^2(w'_{t'} + w'w'_{x'} + w'w'_{z'}) + p'_{z'} = -1. \tag{0.13}$$

The corresponding boundary conditions are:

$$\varepsilon(\eta'_{t'} + u'_s\eta'_{x'}) = w'_s, \quad p'_s = 0, \quad w'_b = 0.$$

A.2. Dispersive waves

A.2.1. The Serre-Green-Naghdi equations

From now on, the "prime" for the dimensionless variables is omitted to simplify the notation. We assume the horizontal velocity is weakly dependent on z:

$$u(t,x,z) \approx u(t,x). \tag{0.14}$$

A rigorous justification of this assumption can be found in Barros, SL Gavrilyuk, and V. Teshukov 2007. The averaged horizontal velocity can be approximated as:

$$\overline{u}(t,x) \coloneqq \frac{1}{h}\int_{-1}^{\varepsilon\eta} u(t,x,s)\mathrm{d}s \approx u(t,x), \tag{0.15}$$

where $h \coloneqq \varepsilon\eta + 1$. Then from mass conservation Eqn. (0.11), the vertical velocity can be defined as:

$$w = -\int_{-1}^{z} u_x(t,x,s)\mathrm{d}s \approx -u_x(t,x)(z+1). \tag{0.16}$$

Then the vertical momentum equation Eqn. (0.13) can be written as:

$$-\mu^2(z+1)\left(u_{xt} + uu_{xx} - u_x^2\right) + p_z \approx -1 \tag{0.17}$$

Integrate the above equation from z to $\varepsilon\eta$, with the free surface boundary condition of pressure $p_s = 0$, we have:

$$p(t,x,z) \approx (\varepsilon\eta - z) - \frac{\mu^2}{2}\left[h^2 - (z+1)^2\right]\left(u_{xt} + uu_{xx} - u_x^2\right) \tag{0.18}$$

With the kinematic boundary condition on the free surface, the integral form of the mass equation Eqn. (0.11) takes the form:

$$\begin{aligned}\int_{-1}^{\varepsilon\eta}(u_x + w_z)\,\mathrm{d}z &= w_s - w_b + \frac{\partial}{\partial x}\left(\int_{-1}^{\varepsilon\eta} u\mathrm{d}z\right) - \varepsilon u_s\eta_x \\ &\approx \varepsilon\eta_t + (hu)_x \\ &= h_t + (hu)_x = 0.\end{aligned} \tag{0.19}$$

The integral form of the horizontal momentum equation Eqn. (0.12) become:

$$\begin{aligned}\int_{-1}^{\varepsilon\eta}\left(u_t + (u^2)_x + (wu)_z + p_x\right)\mathrm{d}z &= \frac{\partial}{\partial t}\int_{-1}^{\varepsilon\eta} u\mathrm{d}z + \frac{\partial}{\partial x}\int_{-1}^{\varepsilon\eta} u^2\mathrm{d}z + \frac{\partial}{\partial x}\int_{-1}^{\varepsilon\eta} p\mathrm{d}z \\ &\quad - u_s(\varepsilon\eta_t + \varepsilon u_s\eta_x - w_s) \\ &\approx (hu)_t + \left(hu^2 + \int_{-1}^{\varepsilon\eta} p\mathrm{d}z\right)_x = 0.\end{aligned} \tag{0.20}$$

Here, the integration of the pressure takes the form:

$$\begin{aligned}\int_{-1}^{\varepsilon\eta} p\mathrm{d}z &\approx \int_{-1}^{\varepsilon\eta}(\varepsilon\eta - z)\mathrm{d}z - \frac{\mu^2}{2}\left(u_{xt} + uu_{xx} - u_x^2\right)\int_{-1}^{\varepsilon\eta}\left[h^2 - (z+1)^2\right]\mathrm{d}z \\ &= \frac{h^2}{2} - \mu^2\frac{h^3}{3}\left(u_{xt} + uu_{xx} - u_x^2\right).\end{aligned}$$

Then the dimensionless Serre-Green-Naghdi equations take the form:

$$h_t + (hu)_x = 0, \tag{0.21}$$

$$u_t + uu_x + h_x = \frac{\mu^2}{3h}\left(h^3\left(u_{xt} + uu_{xx} - u_x^2\right)\right)_x. \tag{0.22}$$

The dispersive terms of Eqn. (0.22) can be written in other form by using the notation of the total derivative of h from Eqn. (0.21):

$$u_x = -\frac{1}{h}\left(h_t + uh_x\right) = -\frac{1}{h}\frac{\mathrm{d}h}{\mathrm{d}t}. \tag{0.23}$$

The dispersive terms then become:

$$\begin{aligned}h^3\left(u_{xt} + uu_{xx} - u_x^2\right) &= h^3\left(\frac{\mathrm{d}}{\mathrm{d}t}u_x - u_x^2\right) = -h^3\left[\frac{\mathrm{d}}{\mathrm{d}t}\left(\frac{1}{h}\frac{\mathrm{d}h}{\mathrm{d}t}\right) + \frac{1}{h^2}\left(\frac{\mathrm{d}h}{\mathrm{d}t}\right)^2\right] \\ &= -h^2\ddot{h},\end{aligned} \tag{0.24}$$

where $\ddot{h} \coloneqq \dfrac{\mathrm{d}^2h}{\mathrm{d}t^2}$. Hence, the other form of the Serre-Green-Naghdi equations are:

$$h_t + (hu)_x = 0, \tag{0.25}$$

$$u_t + uu_x + h_x + \frac{\mu^2}{3h}\left(h^2\ddot{h}\right)_x = 0. \tag{0.26}$$

Going back to dimensional variables, with $h = H + \eta$, Eqn. (0.21) and Eqn. (0.22) become:

$$h_t + (hu)_x = 0, \tag{0.27}$$

$$u_t + uu_x + gh_x = \frac{1}{3h}\left(h^3\left(u_{xt} + uu_{xx} - u_x^2\right)\right)_x \tag{0.28}$$

The other form of the Serre-Green-Naghdi equations Eqn. (0.25) and Eqn. (0.26) become,

$$h_t + (hu)_x = 0, \tag{0.29}$$

$$u_t + uu_x + gh_x + \frac{1}{3h}\left(h^2\ddot{h}\right)_x = 0. \tag{0.30}$$

A.2.2. Boussinesq equation, long waves of small amplitude

Considering long waves of small amplitude, and the dimensionless variables are described in the form:

$$h(t,x) = 1 + \varepsilon^2 \eta(t,x), \quad u(t,x) = \varepsilon^2 v(t,x). \tag{0.31}$$

Then the dimensionless system Eqn. (0.21) and Eqn. (0.22), can be approximated up to order $\mathcal{O}(\varepsilon^4, \varepsilon^2\mu^2)$ are:

$$\eta_t + v_x + \varepsilon^2(\eta v)_x = 0, \tag{0.32}$$

$$v_t + \eta_x + \varepsilon^2 v v_x = \frac{\mu^2}{3} v_{xxt}. \tag{0.33}$$

The leading order of Eqn. (0.32) is: $\eta_t + v_x = 0$, thus $v_{xxt} \approx -\eta_{xtt}$, we get:

$$\eta_t + v_x + \varepsilon^2(\eta v)_x = 0, \tag{0.34}$$

$$v_t + \eta_x + \varepsilon^2 v v_x + \frac{\mu^2}{3}\eta_{xtt} = 0. \tag{0.35}$$

This is exactly the approximation of Eqn. (0.25) and Eqn. (0.26). Going back to the dimensional variables, the dimensional Boussinesq equations (good Boussinesq equations) are:

$$h_t + (hu)_x = 0, \tag{0.36}$$

$$u_t + u u_x + g h_x = \frac{1}{3} H^2 u_{xxt}. \tag{0.37}$$

The other form (bad Boussinesq equations) is:

$$h_t + (hu)_x = 0, \tag{0.38}$$

$$u_t + u u_x + g h_x + \frac{1}{3} H^2 h_{xtt} = 0. \tag{0.39}$$

A.2.3. Unidirectional models: Korteweg-de Vries equation and Benjamin-Bona-Mahony equations

We are seeking a dimensionless solution propagating in positive x direction, of the form: $h(\tau, \xi)$ and $u(\tau, \xi)$ with

$$\tau = \varepsilon^2 t; \quad \xi = x - C_0 t, \tag{0.40}$$

in which, C_0 is a positive constant which will be determined later. In terms of these variables, the derivatives become:

$$\frac{\partial}{\partial t} \to \varepsilon^2 \frac{\partial}{\partial \tau} - C_0 \frac{\partial}{\partial \xi}; \quad \frac{\partial}{\partial x} \to \frac{\partial}{\partial \xi}.$$

Substitute the above derivatives into the dimensionless Boussinesq equations, Eqn. (0.32) and Eqn. (0.33), we have up to order $\mathcal{O}(\varepsilon^2, \mu^2)$:

$$\varepsilon^2 \eta_\tau - C_0 \eta_\xi + v_\xi + \varepsilon^2 (\eta v)_\xi = 0, \tag{0.41}$$

$$\varepsilon^2 v_\tau - C_0 v_\xi + \eta_\xi + \varepsilon^2 v v_\xi + C_0 \frac{\mu^2}{3} v_{\xi\xi\xi} = 0. \tag{0.42}$$

The leading order of the above two equations are:

$$v_\xi = C_0 \eta_\xi, \tag{0.43}$$

$$\eta_\xi = C_0 v_\xi. \tag{0.44}$$

This implies that: $C_0 = 1$. The next order of Eqn. (0.42) shows:

$$\varepsilon^2 v_\tau + \varepsilon^2 v v_\xi + \frac{\mu^2}{3} v_{\xi\xi\xi} = 0. \tag{0.45}$$

The v in the above equation may be replaced by η, and returning back to the variables t and x, the classic dimensionless KdV equation can be obtained:

$$\eta_t + \eta_x + \varepsilon^2 \eta \eta_x + \frac{\mu^2}{3} \eta_{xxx} = 0. \tag{0.46}$$

The leading order of the KdV equation is: $\eta_t + \eta_x = 0$, and thus $\eta_{xxx} = -\eta_{xxt}$. Finally, the dimensionless BBM equation takes the form:

$$\eta_t + \eta_x + \varepsilon^2 \eta \eta_x - \frac{\mu^2}{3} \eta_{xxt} = 0. \tag{0.47}$$

In dimensional variables, the KdV equation takes the form:

$$\eta_t + \sqrt{gH}\eta_x + \frac{3}{2}\sqrt{\frac{g}{H}}\eta\eta_x + \frac{H^3}{6}\sqrt{\frac{g}{H}}\eta_{xxx} = 0. \tag{0.48}$$

The dimensional BBM equation can be expressed in the form:

$$\eta_t + \sqrt{gH}\eta_x + \frac{3}{2}\sqrt{\frac{g}{H}}\eta\eta_x - \frac{H^2}{6}\eta_{xxt} = 0. \tag{0.49}$$

A.3. Benney equations

Considering the zero-order long waves approximation, namely $\mu \to 0$, the vertical momentum equation Eqn. (0.13) shows,

$$p'_{z'} = -1. \tag{0.50}$$

This indicates that the pressure is hydrostatic. In dimensional variables, the pressure takes the form:

$$p = \rho g(\eta - z). \tag{0.51}$$

The dimensional mass conservation equation and the horizontal momentum equation:

$$u_x + w_z = 0, \tag{0.52}$$
$$\rho(u_t + uu_x + wu_z) + p_x = 0, \tag{0.53}$$

with the boundary conditions:

$$\eta_t + u_s\eta_x = w_s, \tag{0.54}$$
$$p_s = 0, \tag{0.55}$$
$$w_b = 0. \tag{0.56}$$

The vertical velocity can be obtained by integrating the mass equation Eqn (0.52) with respect to z, from the bottom $z = -H$ to a chosen z, combining with the kinematic boundary condition at the bottom:

$$w = -\int_{-H}^{z} u_x(t, x, s)\mathrm{d}s. \tag{0.57}$$

On the other hand, the integration form of the mass conservation can be obtained by integrating the mass conservation equation Eqn (0.52) with respect to z, from the bottom to the free surface:

$$\int_{-H}^{\eta} (u_x + w_z)\,\mathrm{d}z = w_s - w_b + \frac{\partial}{\partial x}\left(\int_{-H}^{\eta} u\mathrm{d}z\right) - u_s\eta_x = 0.$$

Applying the boundary conditions Eqn. (0.54) and Eqn. (0.56), the above equation can be simplified as:

$$\eta_t + \frac{\partial}{\partial x}\left(\int_{-H}^{\eta} u\mathrm{d}z\right) = 0. \tag{0.58}$$

To sum up, Eqn. (0.58), Eqn. (0.53) and Eqn. (0.57) are called the Benney equations, or shallow-water equations for shear flows.

$$\begin{aligned}
&\eta_t + \frac{\partial}{\partial x}\left(\int_{-H}^{\eta} u \mathrm{d}z\right) = 0, \\
&u_t + uu_x + wu_z + g\eta_x = 0, \\
&w = -\int_{-H}^{z} u_x(t, x, s)\mathrm{d}s.
\end{aligned}$$

Often, the reference frame has $z = 0$ as the bottom instead of $z = -H$. The governing equations are then obtained by changing $z \to z + H$.

1. Hyperbolicity study of the modulation equations for the Benjamin-Bona-Mahony equation

Article

The work on this topic is fully included in the following paper:

Sergey Gavrilyuk, Yu-Hsi Lin, and Keh-Ming Shyue. "Hyperbolicity study of the modulation equations for the Benjamin–Bona–Mahony equation". In: *Studies in Applied Mathematics* 151.2 (2023), pp. 536–554

Check for updates

Received: 10 February 2023 | Revised: 2 May 2023 | Accepted: 16 May 2023

DOI: 10.1111/sapm.12602

ORIGINAL ARTICLE

STUDIES IN APPLIED MATHEMATICS WILEY

Hyperbolicity study of the modulation equations for the Benjamin–Bona–Mahony equation

Sergey Gavrilyuk[1] | **Yu-Hsi Lin**[1] | **Keh-Ming Shyue**[2]

[1]Aix Marseille Univ, CNRS, IUSTI, UMR, Marseille, France

[2]Institute of Applied Mathematical Sciences, National Taiwan University, Taipei, Taiwan

Correspondence
Sergey Gavrilyuk, Aix Marseille Univ, CNRS, IUSTI, UMR 7343, Marseille, France.
Email: sergey.gavrilyuk@univ-amu.fr

Funding information
Isaac Newton Institute for Mathematical Sciences; Ministry of Science and Technology, Taiwan, Grant/Award Number: 110-2115-M-002-004-MY2; EPSRC, Grant/Award Number: EP/R014604/1

Abstract

A complete study of the modulation equations for the Benjamin–Bona–Mahony equation is performed. In particular, the boundary between the hyperbolic and elliptic regions of the modulation equations is found. When the wave amplitude is small, this boundary is approximately defined by $k = \sqrt{3}$, where k is the wave number. This particular value corresponds to the inflection point of the linear dispersion relation for the BBM equation. Numerical results are presented showing the appearance of the Benjamin–Feir instability when the periodic solutions are inside the ellipticity region.

KEYWORDS
dispersive equations, modulational instability

JEL CLASSIFICATION
35L65, 35Q35

1 | INTRODUCTION

The Benjamin–Bona–Mahony (BBM) equation is an unidirectional model of weakly nonlinear waves in shallow water[1]:

$$v_t + v_x + vv_x - v_{txx} = 0.$$

It involves one dependent variable $v(t, x)$ and two independent variables t (time) and x (space coordinate). The last term v_{txx} is responsible for the nonlocal nature of the BBM equation. It also

© 2023 Wiley Periodicals LLC.

14679590, 2023, 2, Downloaded from https://onlinelibrary.wiley.com/doi/10.1111/sapm.12602 by Inrae - Dipso-Paris, Wiley Online Library on [24/02/2025]. See the Terms and Conditions (https://onlinelibrary.wiley.com/terms-and-conditions) on Wiley Online Library for rules of use; OA articles are governed by the applicable Creative Commons License

appears as an asymptotic model of finite amplitude waves propagating in one-dimensional rods made of a compressible neo-Hookean material.[2] After the change of variables $v = u - 1$, one gets the equation

$$u_t + uu_x - u_{txx} = 0. \tag{1}$$

The dispersion relation to (1) linearized on a constant solution $u = u_0$ is

$$c_p = \frac{u_0}{1 + k^2}, \tag{2}$$

where c_p is the phase velocity, and k is the wave number. The phase and group velocities are uniformly bounded for any waves numbers.

P. Olver[3] justified that (1) admits only three independent conservation laws

$$(u - u_{xx})_t + \left(\frac{u^2}{2}\right)_x = 0, \tag{3a}$$

$$\left(\frac{u^2}{2} + \frac{u_x^2}{2}\right)_t + \left(\frac{u^3}{3} - uu_{tx}\right)_x = 0, \tag{3b}$$

$$\left(\frac{u^3}{3}\right)_t - \left(u_t^2 - u_{xt}^2 + u^2u_{xt} - \frac{u^4}{4}\right)_x = 0, \tag{3c}$$

and proposed a Hamiltonian formulation of the BBM equation.[4] In particular, the Lagrangian for the BBM equation is

$$\mathcal{L} = -\frac{\varphi_t\varphi_x}{2} + \frac{\varphi_t\varphi_{xxx}}{2} - \frac{\varphi_x^3}{6}, \quad u = \varphi_x. \tag{4}$$

The conservation law (3a) is the Euler–Lagrange equation for (4). The conservation laws (3b) and (3c) are the consequence of the Noether's theorem that correspond to the invariance of the Lagrangian under space and time translations.

Much work has been done for the BBM equation, both mathematical (e.g., Ref. 5 and references therein) and numerical (e.g., Ref. 6 and references therein). Here, we study the hyperbolicity of the corresponding Whitham's modulation equations. The study of the hyperbolic character or not of the Whitham system is important at least for two reasons. From the physical point of view, the ellipticity of the modulation equations is "responsable" for the Benjamin–Feir instability, well known in the theory of water waves.[7] From the mathematical point of view, the modulational stability (hyperbolicity of the modulational equations) is necessary for the spectral stability of periodic traveling waves.[8] The study of the Benjamin–Feir instability for the BBM equation in the case of small amplitudes can be found in Ref. 9. The singular soliton limit ($k \to 0$) was studied analytically and numerically in Ref. 10. In this limit, the governing equations for the wave amplitude and its wave mean are hyperbolic. Such a singular limit is obtained by using the action integral for the modulation equations for (3) following the papers Refs. 11, 12. It was mentioned in Ref. 13 that the modulation equations for the BBM equation could be elliptic, but the whole study of the modulation equations was not performed. Here, we provide the analysis of the hyperbolicity in the whole three-dimensional domain of wave parameters. The analytical results are illustrated by the numerical ones.

2 | WHITHAM MODULATION EQUATIONS FOR THE BBM SYSTEM

The periodic traveling wave solutions of the BBM equation (1) in the form

$$u = u(\xi), \quad \xi = x - Dt$$

satisfy the equation

$$-Du' + uu' + Du''' = 0. \tag{5a}$$

Here, "prime" means the derivative with respect to ξ. In what follows, we will study only the solutions with positive D. The case with negative D is recovered by the change of variables $u \to -u$, and $D \to -D$. Performing two integrations, we have

$$(u')^2 = \frac{2}{D}\left(-\frac{u^3}{6} + D\frac{u^2}{2} + c_1 u + c_2\right), \tag{5b}$$

where c_1 and c_2 are constants. Equation (5b) has real periodic solutions if and only if the right-hand side of (5b), which is a cubic polynomial, has three different real roots u_i, $i = 1, 2, 3$, $u_1 < u_2 < u_3$. For this, the discriminant of this polynomial should be positive. We introduce $P(u) = (u - u_1)(u - u_2)(u_3 - u)$, and write (5b) as:

$$(u')^2 = \frac{1}{3D}P(u) = \frac{1}{3D}(u - u_1)(u - u_2)(u_3 - u). \tag{5c}$$

The relations between these new constants and D, c_1, and c_2 are

$$D = \frac{1}{3}(u_1 + u_2 + u_3),\ c_1 = -\frac{1}{6}(u_1u_2 + u_1u_3 + u_2u_3),\ c_2 = \frac{1}{6}u_1u_2u_3.$$

From (5c), the three-parameter family of periodic solutions defined up to a shift in space, takes the form:

$$u(\xi) = u_2 + a\ \mathrm{cn}^2(\eta, m), \tag{6}$$

where

$$m = \frac{u_3 - u_2}{u_3 - u_1}, \quad a = u_3 - u_2, \quad \eta = \frac{\xi + \xi_0}{2\sqrt{3D}}\sqrt{\frac{a}{m}}, \quad \xi_0 = \text{const}.$$

Here, $\mathrm{cn}(\eta, m) = \cos(\varphi(\eta, m))$, where φ is defined implicitly from

$$\eta = \int_0^{\varphi(\eta,m)} \frac{d\theta}{\sqrt{1 - m\sin^2\theta}}.$$

The wavelength L is given as

$$L = \int_{\xi_2}^{\xi_3} d\xi = 2\int_{u_2}^{u_3} \frac{\sqrt{3D}}{\sqrt{P(u)}}\, du = 4\sqrt{\frac{3Dm}{a}}\, K(m), \tag{7}$$

14679590, 2023, 2, Downloaded from https://onlinelibrary.wiley.com/doi/10.1111/sapm.12602 by Inrae - Dipso-Paris, Wiley Online Library on [24/02/2025]. See the Terms and Conditions (https://onlinelibrary.wiley.com/terms-and-conditions) on Wiley Online Library for rules of use; OA articles are governed by the applicable Creative Commons License

where the interval $[\xi_2, \xi_3]$ has the length L, and

$$K(m) = \int_0^{\pi/2} \frac{d\theta}{\sqrt{1 - m\sin^2\theta}}$$

is the complete elliptic integral of the first kind.[14] In particular, the solitary wave solution obtained in the limit $L \to \infty$ and for the values $u_1 = u_2 > 0$, $a = u_3 - u_2$ is in the form

$$u(\xi) = u_2 + \frac{a}{\cosh^2(\eta)}, \quad \eta = \frac{\xi + \xi_0}{2\sqrt{1 + (3u_2/a)}}, \quad D = u_2 + \frac{a}{3}, \quad \xi_0 = \text{const}.$$

We will define the wave averaged of any function $f(u)$ as

$$\overline{f(u)} = \frac{1}{L}\int_{\xi_2}^{\xi_3} f(u)\, d\xi = \frac{2}{L}\int_{u_2}^{u_3} f(u)\frac{\sqrt{3D}}{\sqrt{P(u)}}\, du.$$

In particular, the wave averaged of u (denoted below by $\overline{u}$) is given by:

$$\begin{aligned} \overline{u} &= \int_{u_2}^{u_3} \frac{u du}{\sqrt{P(u)}} \Big/ \int_{u_2}^{u_3} \frac{du}{\sqrt{P(u)}} \\ &= u_1 + (u_3 - u_1)Q(m) = u_2 + \frac{a}{m}(Q(m) + m - 1), \quad Q(m) = \frac{E(m)}{K(m)}. \end{aligned} \tag{8}$$

Here, $E(m)$ is the complete elliptic integral of the second kind[14]:

$$E(m) = \int_0^{\pi/2} \sqrt{1 - m\sin^2\theta}\, d\theta.$$

In Whitham's modulation theory, we are interested in the three-parameter solution (6), which is periodic with respect to ξ and whose parameters u_1, u_2, and u_3 vary slowly with respect to T and X. The solution period L is thus also a slowly varying function. Commutating the averaging with respect to ξ, and time and space derivatives, we obtain the BBM modulation system in conservation form[10,13]:

$$\boldsymbol{F}(\boldsymbol{q})_T + \boldsymbol{G}(\boldsymbol{q})_X = 0, \tag{9}$$

with the state vector $\boldsymbol{F}$ and the flux $\boldsymbol{G}$ given as

$$\boldsymbol{F}(\boldsymbol{q}) = \begin{bmatrix} \bar{u} \\ \overline{u^2}/2 + \overline{u'^2}/2 \\ k \end{bmatrix} \quad \text{and} \quad \boldsymbol{G}(\boldsymbol{q}) = \begin{bmatrix} \overline{u^2}/2 \\ \overline{u^3}/3 - D\overline{u'^2} \\ Dk \end{bmatrix}. \tag{10}$$

Here, $\boldsymbol{q}$ is a state vector, for example, $\boldsymbol{q} = (u_1, u_2, u_3)^T$ and $k = 2\pi/L$ is the wave number. The last equation for k is the phase conservation law. It is equivalent to the averaged equation (3c). To simplify the notations, we will use in the following for the independent variables again the notations (x, t) instead of (X, T).

The choice of variables $\boldsymbol{q}$ in which the hyperbolicity of Whitham's system of modulation equations is studied is not essential if the Jacobian matrices corresponding to the change of variables

14679590, 2023, 2, Downloaded from https://onlinelibrary.wiley.com/doi/10.1111/sapm.12602 by Inrae - Dipso-Paris, Wiley Online Library on [24/02/2025]. See the Terms and Conditions (https://onlinelibrary.wiley.com/terms-and-conditions) on Wiley Online Library for rules of use; OA articles are governed by the applicable Creative Commons License

14679590, 2023, 2, Downloaded from https://onlinelibrary.wiley.com/doi/10.1111/sapm.12602 by Inrae - Dipso-Paris, Wiley Online Library on [24/02/2025]. See the Terms and Conditions (https://onlinelibrary.wiley.com/terms-and-conditions) on Wiley Online Library for rules of use; OA articles are governed by the applicable Creative Commons License

are nondegenerate. In other words, if the modulation equations are hyperbolic in one set variables, they are hyperbolic in another set of variables provided the coordinate change between them is invertible. However, a specific choice of $\boldsymbol{q}$ can simplify the study of the modulation equations. We will use several such change of variables. For example, by their better physical interpretation, the choice $\boldsymbol{q} = (\bar{u}, a, m)^T$ or $\boldsymbol{q} = (D, a, m)^T$ is sometimes more suitable than that of (u_1, u_2, u_3). The corresponding Jacobian matrices are nondegenerate[10]:

$$\det\left(\frac{\partial(u_1, u_2, u_3)}{\partial(\overline{u}, a, m)}\right) = \frac{a}{m^2} \neq 0$$

and

$$\det\left(\frac{\partial(D, a, m)}{\partial(\overline{u}, a, m)}\right) = \frac{\partial D}{\partial \overline{u}} = 1.$$

In the limit of small amplitudes, the choice $\boldsymbol{q} = (\overline{u}, a, k)^T$ is also appropriate. The nondegeneracy of the corresponding Jacobian matrix is proven in the Appendix.

3 | HYPERBOLICITY STUDY IN THE VARIABLES $\boldsymbol{q} = (\boldsymbol{D}, \boldsymbol{a}, \boldsymbol{m})^T$

For further analysis, we will write the governing equations in quasilinear form by using the variables $\boldsymbol{q} = (D, a, m)^T$. One can find the following expressions for the averaged quantities[10]:

$$\begin{aligned}
\overline{u} &= D + a f_1(m),\\
\overline{u^2} &= D^2 + 2a f_1(m) D + a^2 f_2(m),\\
\overline{u^3} &= D^3 + 3a f_1(m) D^2 + 3a^2 f_2(m) D + a^3 f_3(m),\\
\overline{P} &= a^3 \tilde{P}(m),\\
L &= 4\sqrt{3}\sqrt{\frac{Dm}{a}} K(m),
\end{aligned}$$

with

$$\begin{aligned}
f_1(m) &= \frac{1}{m}\left(Q - \frac{2-m}{3}\right),\\
f_2(m) &= \frac{1 - m + m^2}{9m^2},\\
f_3(m) &= \frac{27(1 - m + m^2)Q + 5m^3 - 21m^2 + 33m - 22}{135m^3},\\
\tilde{P}(m) &= \frac{2(1 - m + m^2)Q - m^2 + 3m - 2}{15m^3},\\
Q(m) &= \frac{E(m)}{K(m)}.
\end{aligned}$$

14679590, 2023, 2, Downloaded from https://onlinelibrary.wiley.com/doi/10.1111/sapm.12602 by Inrae - Dipso-Paris, Wiley Online Library on [24/02/2025]. See the Terms and Conditions (https://onlinelibrary.wiley.com/terms-and-conditions) on Wiley Online Library for rules of use; OA articles are governed by the applicable Creative Commons License

The corresponding quasilinear system is:

$$\boldsymbol{F}(\boldsymbol{q})_t + \boldsymbol{G}(\boldsymbol{q})_x = \frac{\partial \boldsymbol{F}}{\partial \boldsymbol{q}}\boldsymbol{q}_t + \frac{\partial \boldsymbol{G}}{\partial \boldsymbol{q}}\boldsymbol{q}_x = \boldsymbol{A}\boldsymbol{q}_t + \boldsymbol{B}\boldsymbol{q}_x = 0.$$

Here,

$$\mathbf{F} = \begin{bmatrix} D + af_1 \\ 3D^2 + 6af_1D + 3a^2f_2 + \frac{a^3\tilde{P}}{D} \\ \sqrt{\frac{a}{Dm}}\frac{1}{K} \end{bmatrix},$$

$$\mathbf{G} = \begin{bmatrix} \frac{D^2}{2} + af_1D + \frac{a^2f_2}{2} \\ 2D^3 + 6af_1D^2 + 6a^2f_2D + 2a^3f_3 - 2a^3\tilde{P} \\ \sqrt{\frac{aD}{m}}\frac{1}{K} \end{bmatrix},$$

$$\mathbf{A} = \begin{bmatrix} 1 & f_1 & af_1' \\ 6D + 6af_1 - \frac{a^3\tilde{P}}{D^2} & 6f_1D + 6af_2 + 3\frac{a^2\tilde{P}}{D} & 6af_1'D + 3a^2f_2' + \frac{a^3\tilde{P}'}{D} \\ -\frac{1}{2}\sqrt{\frac{a}{D^3m}}\frac{1}{K} & \frac{1}{2}\sqrt{\frac{1}{aDm}}\frac{1}{K} & -\frac{1}{2}\sqrt{\frac{a}{Dm^3}}\frac{1}{K}\frac{Q(m)}{1-m} \end{bmatrix},$$

$$\mathbf{B} = \begin{bmatrix} D + af_1 & f_1D + af_2 & af_1'D + \frac{a^2f_2'}{2} \\ 6D^2 + 12af_1D + 6a^2f_2 & B_{22} & B_{23} \\ \frac{1}{2}\sqrt{\frac{a}{Dm}}\frac{1}{K} & \frac{1}{2}\sqrt{\frac{D}{am}}\frac{1}{K} & -\frac{1}{2}\sqrt{\frac{aD}{m^3}}\frac{1}{K}\frac{Q(m)}{1-m} \end{bmatrix},$$

$$B_{22} = 6f_1D^2 + 12af_2D + 6a^2f_3 - 6a^2\tilde{P},$$

$$B_{23} = 6af_1'D^2 + 6a^2f_2'D + 2a^3f_3' - 2a^3\tilde{P}',$$

with $(\cdot)' \equiv \frac{\partial(\cdot)}{\partial m}$. The system would be hyperbolic if the three roots $\lambda_1, \lambda_2, \lambda_3$ of the third-degree polynomial

$$\det(\mathbf{B} - \lambda\mathbf{A}) = 0$$

are real. After some simplification, and letting $\alpha = a/D$, we can transform the above equation to

$$g(\beta, m, \alpha) = \det(\tilde{\mathbf{B}} - \beta\tilde{\mathbf{A}}) = 0, \quad \beta = \frac{\lambda/D - 1}{\alpha},$$

with

$$\tilde{\mathbf{A}} = \begin{bmatrix} m^2 & m\left(Q - \frac{2-m}{3}\right) & \frac{m}{2}\left(\frac{1-m}{3} - Q^2\right) \\ 2m^2(3Q - (2-m)) & \tilde{A}_{22} & \tilde{A}_{23} \\ -\alpha & 1 & -Q \end{bmatrix},$$

$$\tilde{\mathbf{B}} = \begin{bmatrix} m\left(Q - \frac{2-m}{3}\right) & \frac{1-m+m^2}{9} & \frac{-(2-m)(1-m)}{18} \\ \tilde{B}_{21} & \frac{(1-2m)(2+m-m^2)}{9} & \frac{(m^2+2m-2)(1-m)}{9} \\ 2 & 0 & 0 \end{bmatrix},$$

$$\tilde{A}_{22} = \frac{2m(1-m+m^2)}{3} + \frac{2\alpha}{15}[2(1-m+m^2)Q - (1-m)(2-m)],$$

$$\tilde{A}_{23} = \frac{-m(2-m)(1-m)}{3} + \frac{\alpha}{15}\left[5(1-m)^2 - 3(2-m)(1-m)Q + (1-m+m^2)Q^2\right],$$

$$\tilde{B}_{21} = \frac{2m(1-m+m^2)}{3} - \frac{\alpha}{15}[2(1-m+m^2)Q - (1-m)(2-m)].$$

Notice that, since D and α are real numbers, β_i would be real if and only if λ is real. The coefficient of β^3 is $-\det\tilde{\mathbf{A}}$, which is not 0. Therefore, the above equation $g(\beta, m, \alpha)$ is a third-degree polynomial.

Notice that its coefficients are determined only by two parameters: α and m. We have already supposed that $D > 0$, which implies that the domain to study the corresponding third-degree polynomial is: $\alpha = a/D > 0$ and $0 < m < 1$.

Using Wolfram Mathematica, we can plot in the (m, α)-plane the resultant of the polynomials g and its derivative g_β with respect to β, $R(m, \alpha) = \mathrm{res}(g, g_\beta) = 0$, which is shown by red line in Figure 1A.

Below the red line, three roots are real and the system of modulation equations is hyperbolic. It has been numerically verified that on the red line two coinciding eigenvalues $\beta_1 = \beta_2$ are negative, the third one, β_3, is positive. In terms of the eigenvalues λ, it means that on this curve, one has $\lambda_1 = \lambda_2 < D$ and $\lambda_3 > D$. In the domain above the curve the system is elliptic: two eigenvalues become complex. A special case, $u_1 = 0$ is shown in Figure 1A in blue line. Below this curve, the roots u_i, $u_1 < u_2 < u_3$ of the polynomial $P(u)$ (5c) are positive. In the (m, α)-plane the curve $u_1 = 0$ is given by the relation $\alpha = \frac{3m}{2-m}$. In particular, for $0 \le u_1 < u_2 < u_3$, the modulation equations are hyperbolic.

We study now the behavior of the curve $R(m, \alpha) = 0$ separating the hyperbolic and elliptic region. For small m, we parameterize this curve as $\alpha = \alpha(m)$, with $\alpha = \gamma_1 m + \gamma_2 m^2 + \cdots$, with unknown coefficients γ_i, $i = 1, 2, \ldots$. Replacing this asymptotic expression into $R(m, \alpha(m)) = 0$, one can find $\gamma_1 = 9$ and $\gamma_2 = \frac{9}{2}$. Thus, for small m, one has $\alpha \approx 9m + \frac{9}{2}m^2$. Analogously, in the soliton limit, when $m \to 1$, one can show, by using symbolic computations, that $\alpha \to 3(5 + 2\sqrt{10})$. Now, we map the (m, α)-plane to the (m, k)-plane where k is the wave number. By definition,

$$k = \frac{2\pi}{L} = \frac{\pi}{2\sqrt{3}}\sqrt{\frac{\alpha}{m}}\frac{1}{K(m)}.$$

When $m \to 0$, one has $\alpha \approx 9m + \frac{9}{2}m^2$, and $K(m) \to \frac{\pi}{2}$. Therefore, $k \to \sqrt{3}$. Furthermore, one can check the corresponding slope is vanishing: $\lim_{m\to 0}\frac{dk}{dm} = 0$. When $m \to 1$, $\alpha \to 3(5 + 2\sqrt{10})$, and $K(m) \to \infty$, so $k \to 0$.

The qualitative behavior of the resultant in the (m, k)-plane is shown in continuous red line in Figure 1B. It is interesting to note that in the ellipticity region, one always has $k > \sqrt{3}$. This specific value of $k = \sqrt{3}$ corresponds to the inflection point in the linear dispersion relation (2) (see Figure 2). Indeed, Equation (2) can be written as

$$\omega = \frac{u_0 k}{1 + k^2}. \tag{11}$$

14679590, 2023, 2, Downloaded from https://onlinelibrary.wiley.com/doi/10.1111/sapm.12602 by Inrae - Dipso-Paris, Wiley Online Library on [24/02/2025]. See the Terms and Conditions (https://onlinelibrary.wiley.com/terms-and-conditions) on Wiley Online Library for rules of use; OA articles are governed by the applicable Creative Commons License

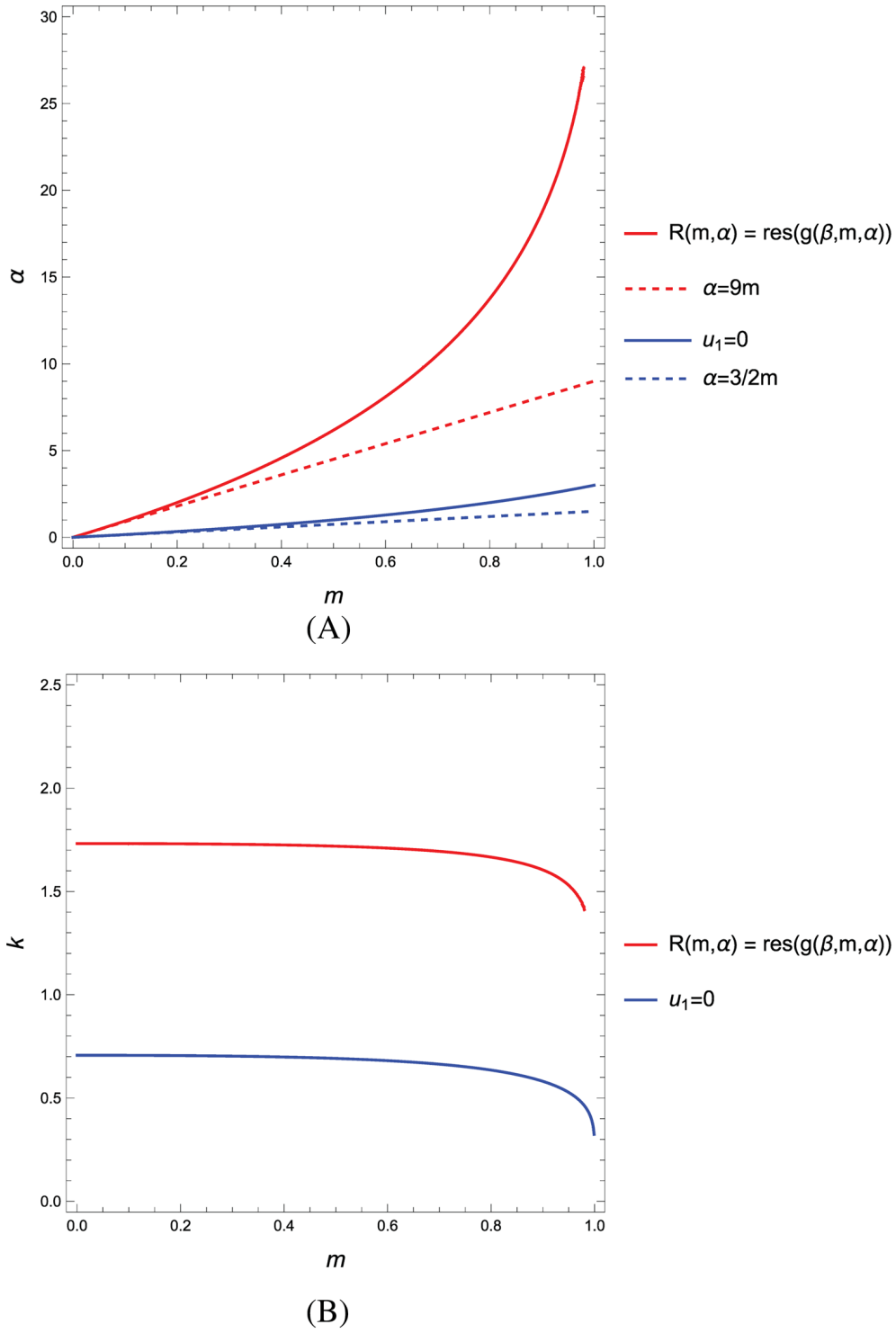

FIGURE 1 The hyperbolicity region in the (m, α)-plane (A) and (m, k)-plane (B). The red continuous curve is the boundary between elliptic (above the red curve) and hyperbolic (below the red curve) regions. The blue curve corresponds to $u_1 = 0$ (below the blue curve we have the inequality $0 < u_1 < u_2 < u_3$). The dashed blue and red straight lines in (A) are tangent lines to the corresponding continuous curves at $m = 0$.

14679590, 2023, 2, Downloaded from https://onlinelibrary.wiley.com/doi/10.1111/sapm.12602 by Inrae - Dipso-Paris, Wiley Online Library on [24/02/2025]. See the Terms and Conditions (https://onlinelibrary.wiley.com/terms-and-conditions) on Wiley Online Library for rules of use; OA articles are governed by the applicable Creative Commons License

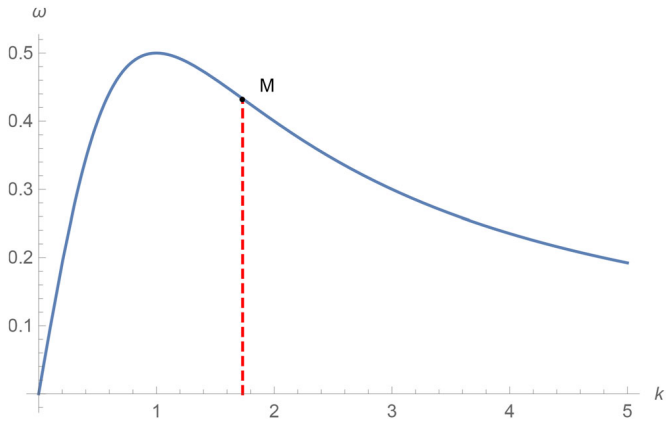

FIGURE 2 The point M of the dispersion curve having the abscissa $\sqrt{3}$ is the inflection point of the dispersion relation (11).

The second derivative $\omega''(k)$ is

$$\omega''(k) = 2\frac{u_0 k(k^2-3)}{(1+k^2)^3}.$$

Thus, $k = \sqrt{3}$ corresponds to the inflection point of the dispersion relation $\omega = \omega(k)$. The curve in the $(m-k)$-plane corresponding to $u_1 = 0$ is also shown in blue.

4 | NUMERICAL STUDY OF EIGENFIELDS IN $(\overline{\boldsymbol{u}}, \boldsymbol{a}, \boldsymbol{m})$ VARIABLES

Let λ_j be the eigenvalue, $\boldsymbol{\ell}_j$ and $\boldsymbol{r}_j$ be the left and right eigenvectors of the quasi-linear system of the BBM modulation system satisfying $\boldsymbol{\ell}_j(\boldsymbol{B}-\lambda_j\boldsymbol{A}) = 0$ and $(\boldsymbol{B}-\lambda_j\boldsymbol{A})\boldsymbol{r}_j = 0$, respectively. Assume that the solution is self-similar in the variable $\zeta = x/t$, that is, $\boldsymbol{q}(x,t) = \boldsymbol{q}(\zeta)$ is the simple wave solution, the modulation system is reduced to a system of ordinary differential equations (ODEs):

$$(\boldsymbol{B}-\boldsymbol{A}\zeta)\frac{d\boldsymbol{q}}{d\zeta} = 0. \tag{12}$$

If $\nabla_{\boldsymbol{q}}\lambda_j \cdot \boldsymbol{r}_j \neq 0$, the simple wave solution of (12) corresponding to the eigenfield j is determined by a set of ODEs in the form[15]:

$$\frac{d\boldsymbol{q}}{d\zeta} = \boldsymbol{r}_j/\left(\nabla_{\boldsymbol{q}}\lambda_j \cdot \boldsymbol{r}_j\right), \quad \zeta = \lambda_j, \quad j = 1,2,3. \tag{13}$$

Unlike the case of the Korteweg-de Vries (KdV) equation where the modulation system can be written in Riemann invariant form, and where we can therefore find the closed-form solutions of the corresponding ODEs, for the BBM equation, we can only find the eigenvectors and eigenvalues and solve the ODEs (13) numerically.

In Figure 3, we present numerical results for the eigenvalues λ_j and the quantities $\nabla_{\boldsymbol{q}}\lambda_j \cdot \boldsymbol{r}_j$, $j = 1,2,3$, as a function of $m = (u_3-u_2)/(u_3-u_1)$ for $u_1 = 0$ and $u_3 = 1$. As it has been proved in Section 3 (see Figure 1A,B), in this case (since $u_1 = 0$) the equations are hyperbolic. We observe the occurrence of double characteristic roots only in the limits $m \to 0$ and $m \to 1$ as it is usually the case of integrable (cf. Ref. 11) and nonintegrable (cf. Ref. 16) systems.

14679590, 2023, 2, Downloaded from https://onlinelibrary.wiley.com/doi/10.1111/sapm.12602 by Inrae - Dipso-Paris, Wiley Online Library on [24/02/2025]. See the Terms and Conditions (https://onlinelibrary.wiley.com/terms-and-conditions) on Wiley Online Library for rules of use; OA articles are governed by the applicable Creative Commons License

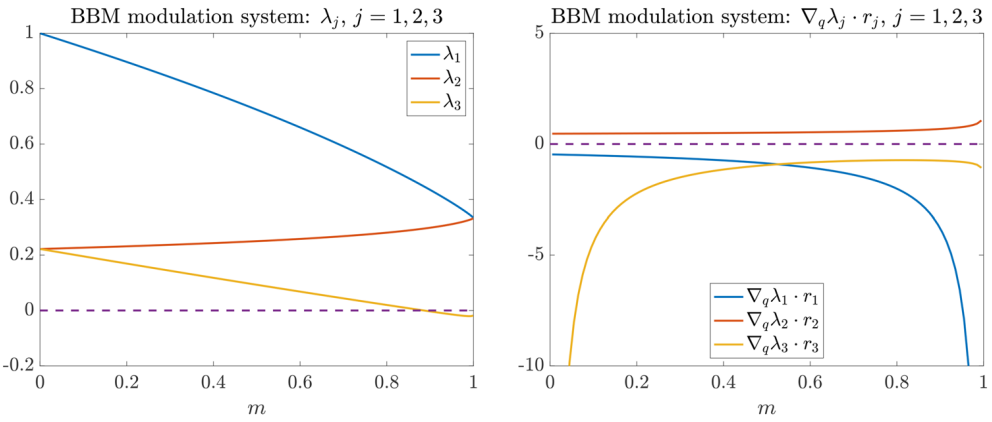

FIGURE 3 Numerical results for the eigenvalue problem of the Benjamin–Bona–Mahony (BBM) modulation system in $(\overline{u}, a, m)$ variables. On the left column, the eigenvalues λ_1, λ_2, and λ_3 are shown as a function of $m = (u_3 - u_2)/(u_3 - u_1)$ with $u_1 = 0$ and $u_3 = 1$. As has been mentioned in Section 3 (see Figure 3), in this case (since $u_1 = 0$), the equations are hyperbolic. On the right column, the quantities $\nabla_{\boldsymbol{q}} \lambda_1 \cdot \boldsymbol{r}_1$, $\nabla_{\boldsymbol{q}} \lambda_2 \cdot \boldsymbol{r}_2$, and $\nabla_q \lambda_3 \cdot \boldsymbol{r}_3$ are shown.

In addition, we observe the genuine nonlinearity of all the characteristic fields with this set of parameter values ($\nabla_{\boldsymbol{q}} \lambda_i \cdot \boldsymbol{r}_i \neq 0$). Obviously, the property of the genuine nonlinearity is not satisfied if the wave parameters are in the vicinity of the hyperbolic–elliptic boundary.

To give an example for the undular bore solution of the BBM equation (1) and the simple wave solution of the BBM modulation system (9), we consider an initial-boundary value problem studied in Ref. 17 for the magma equation. For the undular bore part of the problem, the boundary conditions we take on the left at $x = 0$ is $u_L = 1$ at all time, and on the right at $x = 100$ is the non-reflecting boundary. Initially, in the interior of the domain where $x \in (0, 100]$, we take $u = 1/2$. For the simple wave solution problem, the solution is an expansion fan along the λ_2 characteristic field. On the left of this expansion fan, we have the acoustic wave limit $m_L \to 0$, $\bar{u}_L \to 1$, and on the right of the fan, we have the soliton limit $m_R \to 1$ and $\bar{u}_R \to 1/2$; the parameter on the amplitude a_L and a_R in the state vector $q = (\bar{u}, a, m)$ of the modulation system can be determined numerically once the phase velocities are set on the left and on the right, respectively. Figure 4 shows the numerical results, at time $t = 100$, observing qualitative agreement of the results on the wave envelopes and the average state between the BBM bore solution and the modulation simple wave solution. Numerical results obtained using the hyperbolized BBM model (BBMH)[18] are included also where $\hat{c} = c = 10^3$ is used in the computation (see Ref. 18 for details). Here, $\hat{c}$ and c are two parameters of the hyperbolized model. The BBMH model is a very accurate hyperbolic approximation of the exact BBM equation and is obtained as the Euler–Lagrange equations for a two-parameter "extended" Lagrangian. The advantage of such an hyperbolic approximation is a possibility to use a full arsenal of numerical methods developed for hyperbolic systems of conservations laws. Such a method of "extended" Lagrangian was efficiently used for dispersive models appearing both in classical and quantum fluids (e.g., Refs. 18–24). map

5 | STOKES EXPANSION FOR THE BBM MODULATION SYSTEM

If the flow state of interests is in the weakly nonlinear regime, we can obtain an approximate periodic solution via the Stokes expansion[25]:

14679590, 2023, 2, Downloaded from https://onlinelibrary.wiley.com/doi/10.1111/sapm.12602 by Inrae - Dipso-Paris, Wiley Online Library on [24/02/2025]. See the Terms and Conditions (https://onlinelibrary.wiley.com/terms-and-conditions) on Wiley Online Library for rules of use; OA articles are governed by the applicable Creative Commons License

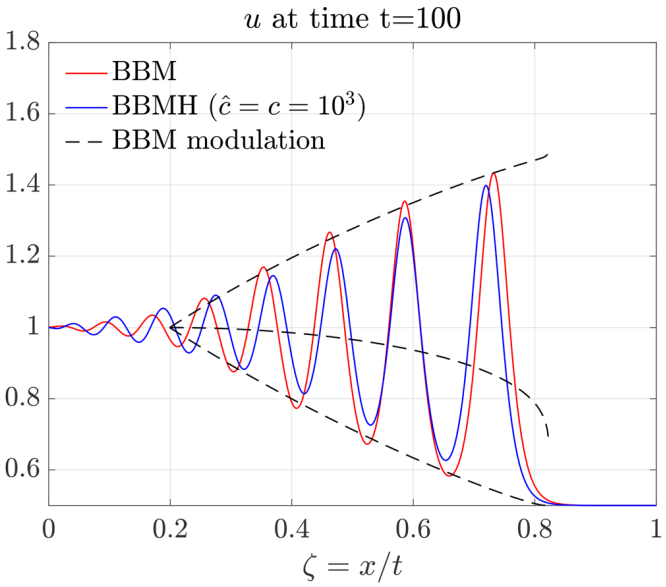

FIGURE 4 Numerical results for the initial-boundary value problem of the Benjamin–Bona–Mahony (BBM) equation and the BBM modulation system. In the graph, the solid red line is the solution obtained using the BBM equation (1), the blue solid line is the solution obtained using the hyperbolized BBM equation,[18] and the black dashed line is the solution using the BBM modulation system (13).

$$u(\xi) = \bar{u} + \varepsilon\tilde{u}_1(\xi) + \varepsilon^2\tilde{u}_2(\xi) + \varepsilon^3\tilde{u}_3(\xi) + \cdots,$$

$$D(k) = \frac{\bar{u}}{1+k^2} + \varepsilon D_1(k) + \varepsilon^2 D_2(k) + \cdots$$

for $0 < \varepsilon \ll 1$. It follows from (8) that the condition to be imposed on each $\tilde{u}_j$ is

$$\int_{\xi_2}^{\xi_3} \tilde{u}_j(\xi)\, d\xi = 0, \quad j = 1, 2, \ldots.$$

Inserting this ansatz into (5a), and collecting terms of the equal powers of ε, we find the solution up to $O(\varepsilon^2)$:

$$u(\xi) = \bar{u} + \varepsilon\cos(k\xi) + \varepsilon^2\left(\frac{1+k^2}{12\bar{u}k^2}\right)\cos(2k\xi) + O(\varepsilon^3),$$

$$D(k) = \frac{\bar{u}}{1+k^2} + \frac{\varepsilon^2}{24\bar{u}k^2} + O(\varepsilon^3).$$

Now if we assume the wave amplitude $a = 2\varepsilon$, from the above equations, we arrive at the approximate periodic solution to the BBM equation:

$$u(\xi) = \bar{u} + \frac{a}{2}\cos(k\xi) + a^2\left(\frac{1+k^2}{48\bar{u}k^2}\right)\cos(2k\xi) + O(a^3), \tag{14a}$$

$$D(k) = \frac{\bar{u}}{1+k^2} + \frac{a^2}{96\bar{u}k^2} + O(a^3). \tag{14b}$$

By definition, this series is an asymptotic one, if with a given ξ_0 we have $|u_2| \ll |u_1|$ for $\xi \to \xi_0$, which means

$$a \ll \frac{24\bar{u}k^2}{1+k^2}.$$

14679590, 2023, 2, Downloaded from https://onlinelibrary.wiley.com/doi/10.1111/sapm.12602 by Inrae - Dipso-Paris, Wiley Online Library on [24/02/2025]. See the Terms and Conditions (https://onlinelibrary.wiley.com/terms-and-conditions) on Wiley Online Library for rules of use; OA articles are governed by the applicable Creative Commons License

14679590, 2023, 2, Downloaded from https://onlinelibrary.wiley.com/doi/10.1111/sapm.12602 by Inrae - Dipso-Paris, Wiley Online Library on [24/02/2025]. See the Terms and Conditions (https://onlinelibrary.wiley.com/terms-and-conditions) on Wiley Online Library for rules of use; OA articles are governed by the applicable Creative Commons License

We continue by inserting (14) into (9) that gives the approximate modulation system up to $O(a^2)$:

$$\bar{u}_t + \left(\frac{1}{2}\bar{u}^2 + \frac{a^2}{16}\right)_x = 0, \tag{15a}$$

$$\left(\frac{1}{2}\bar{u}^2 + \frac{a^2}{16}(1+k^2)\right)_t + \left(\frac{1}{3}\bar{u}^3 + \frac{a^2}{8}\frac{\bar{u}}{1+k^2}\right)_x = 0, \tag{15b}$$

$$k_t + \left(\frac{k\bar{u}}{1+k^2} + \frac{a^2}{96k\bar{u}}\right)_x = 0. \tag{15c}$$

Assume that the state vector $\boldsymbol{q}$ is given by $\boldsymbol{q} = (\overline{u}, a, k)^T$. In a matrix form, the approximate model (15) can be written as

$$\boldsymbol{A}\boldsymbol{q}_t + \boldsymbol{B}\boldsymbol{q}_x = 0,$$

where the matrices $\boldsymbol{A}$ and $\boldsymbol{B}$ (by abuse of notations, we use the same symbols for the approximate matrices) are defined by

$$\boldsymbol{A} = \begin{bmatrix} 1 & 0 & 0 \\ \bar{u} & \frac{a(1+k^2)}{8} & \frac{a^2 k}{8} \\ 0 & 0 & 1 \end{bmatrix}, \quad \boldsymbol{B} = \begin{bmatrix} \bar{u} & \frac{a}{8} & 0 \\ \bar{u}^2 + \frac{a^2}{8(1+k^2)} & \frac{a\bar{u}}{4(1+k^2)} & \frac{-a^2 k\bar{u}}{4(1+k^2)^2} \\ \frac{k}{1+k^2} - \frac{a^2}{96k\bar{u}^2} & \frac{a}{48k\bar{u}} & \frac{(1-k^2)\bar{u}}{(1+k^2)^2} - \frac{a^2}{96k^2\bar{u}} \end{bmatrix},$$

respectively.

Employing the standard perturbation procedures (cf. Ref. 26), one obtains the eigenvalues of $\tilde{\mathcal{A}} = \boldsymbol{A}^{-1}\boldsymbol{B}$ computed from the equation $\det(\boldsymbol{B} - \lambda\boldsymbol{A}) = 0$ in the form

$$\lambda_{\tilde{\mathcal{A}},1} = \bar{u} + O(a^2),$$

$$\lambda_{\tilde{\mathcal{A}},2} = \frac{(1-k^2)\bar{u}}{(1+k^2)^2} + \frac{a}{12}\sqrt{\frac{3(3+5k^2)(3-k^2)}{(3+k^2)(1+k^2)^3}} + O(a^2),$$

$$\lambda_{\tilde{\mathcal{A}},3} = \frac{(1-k^2)\bar{u}}{(1+k^2)^2} - \frac{a}{12}\sqrt{\frac{3(3+5k^2)(3-k^2)}{(3+k^2)(1+k^2)^3}} + O(a^2).$$

Again, we recover the critical value $k = \sqrt{3}$ below, which the modulation equations for waves of small amplitude are hyperbolic.

Figure 5 shows a comparison plot of the approximate periodic solution to the analytic solution, where the parameters we used are $\bar{u} = 1, a = 1/5$, and $k = 1$, observing good agreement of results.

6 | STABILITY OF THE BBM PERIODIC SOLUTIONS

Here, we present numerical results on the stability or instability of periodic solutions depending whether the parameters of the periodic solution belong to the hyperbolic or elliptic region of the modulation equations. The numerical results are consistent with the analytical estimations of the boundary between hyperbolic and elliptic regions of the modulation equations.

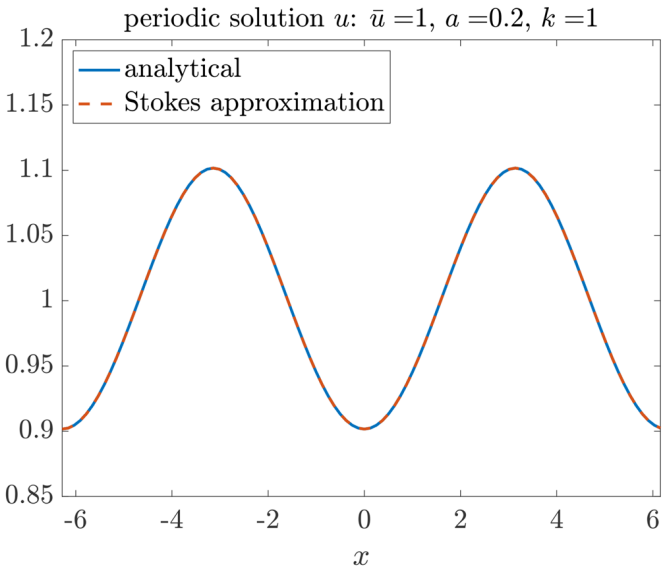

FIGURE 5 Numerical comparison of the periodic Stokes wave approximation to the analytic Benjamin–Bona–Mahony (BBM) solution; parameters $\bar{u} = 1$, $a = 1/5$, and $k = 1$ were used in the computation.

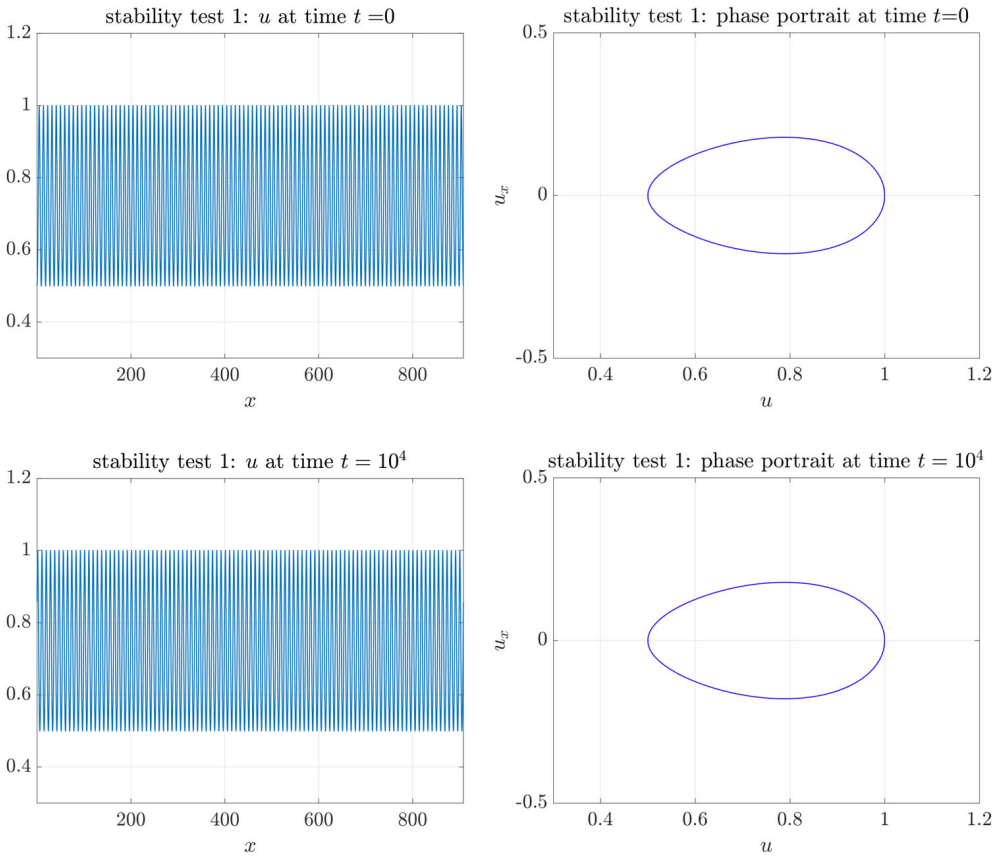

FIGURE 6 Numerical results for the modulational stability of Benjamin–Bona–Mahony (BBM) periodic solutions with the parameters $\bar{u} \approx 0.728473$, $a = 0.5$, and $k \approx 0.691747$ belonging to the hyperbolic region of the exact modulation equations (9)–(10). The BBM solution is shown on the left column, and the phase portrait of the solution is shown on the right column.

14679590, 2023, 2, Downloaded from https://onlinelibrary.wiley.com/doi/10.1111/sapm.12602 by Inrae - Dipso-Paris, Wiley Online Library on [24/02/2025]. See the Terms and Conditions (https://onlinelibrary.wiley.com/terms-and-conditions) on Wiley Online Library for rules of use; OA articles are governed by the applicable Creative Commons License

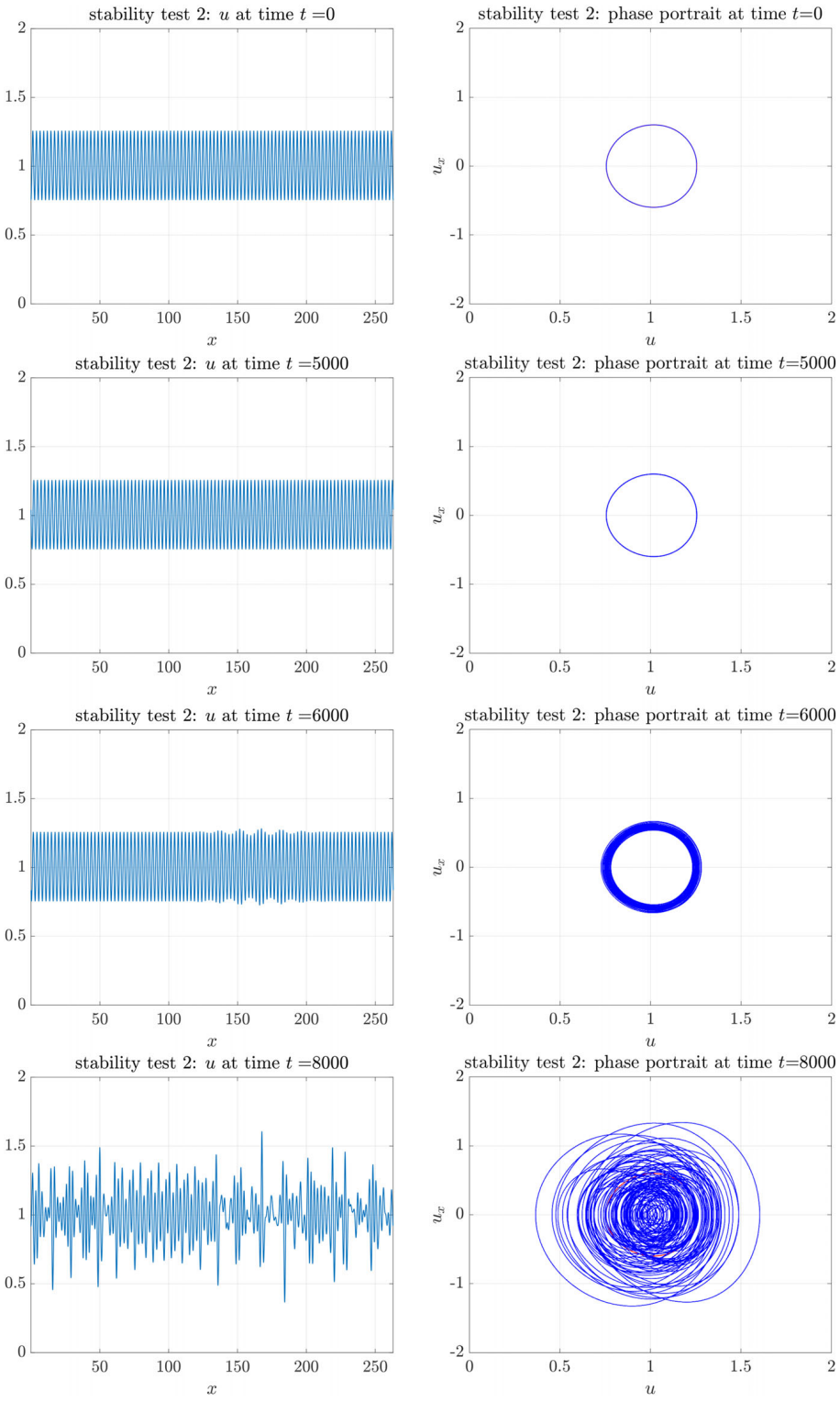

FIGURE 7 Numerical results for the modulational stability of Benjamin–Bona–Mahony (BBM) periodic solutions with the parameters $\bar{u} = 1$, $a = 0.5$, and $k = 2.3895$ belonging to the elliptic region of the exact modulation equations (9)–(10). The graphs are displayed in the same manner as in Figure 6.

14679590, 2023, 2, Downloaded from https://onlinelibrary.wiley.com/doi/10.1111/sapm.12602 by Inrae - Dipso-Paris, Wiley Online Library on [24/02/2025]. See the Terms and Conditions (https://onlinelibrary.wiley.com/terms-and-conditions) on Wiley Online Library for rules of use; OA articles are governed by the applicable Creative Commons License

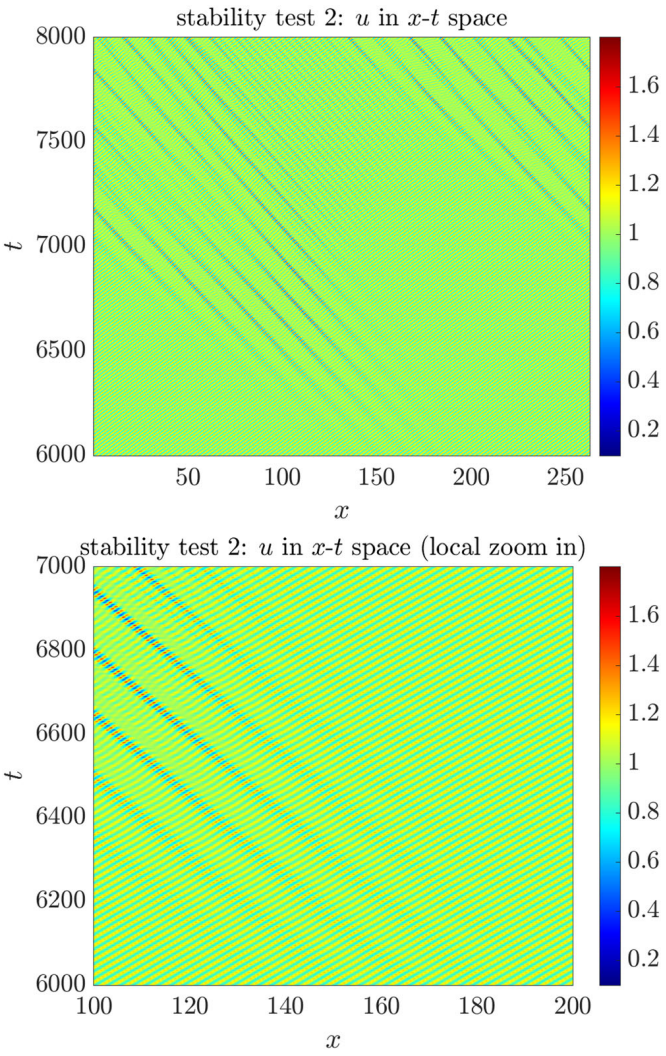

FIGURE 8 The pseudo-color plot of the numerical solution in the (x,t)-plane for the test shown in Figure 7. On the top the solutions in the time interval $t \in [6000, 8000]$ are shown, and on the bottom the zoom-in solutions for $(x,t) \in [100, 200] \times [6000, 7000]$ are shown.

The perturbations are introduced only by the numerical method solving directly the BBM equation (1). The numerical method we used is described in Refs. 10, 18.

We first choose the parameters $\bar{u}$, a, and m for the solution of a single periodic wave over a wave length L. We then setup the problem initially by forming a wave train that consists of N aforementioned single periodic waves (6). In the tests shown below, we take $N = 100$.

In the first example, we take the parameters of periodic wave belonging to the hyperbolicity region: $\bar{u} \approx 0.728473$, $a = 0.5$, and $k \approx 0.691747$. The corresponding value of m can be estimated as $m \approx 0.5$. It gives the real eigenvalues $\lambda_1 \approx 0.0929218$, $\lambda_2 \approx 0.250354$, and $\lambda_3 \approx 0.724104$. The numerical solution shown in Figure 6 is stable up to time $t = 10^4$.

In the second example, we take the parameters of periodic wave belonging to the ellipticity region: $\bar{u} = 1$, $a = 0.5$, and $k \approx 2.3895$. The corresponding value of m can be estimated as $m \approx 0.177317$. It gives two complex conjugate and one real eigenvalue: $\lambda_1 \approx -0.104009 - i\,0.0129987$, $\lambda_2 \approx -0.104009 + i\,0.0129987$, and $\lambda_3 \approx 0.997296$. The numerical solution shown in Figure 7 is stable up to time $t \approx 5 \times 10^3$, becomes unstable at time $t \approx 6 \times 10^3$, and proceeds afterwards. It is clearly seen from the pseudo-color plot of the solution in the x-t plane shown in Figure 8 for $t \in [6000, 8000]$ and the zoom-in for $(x,t) \in [100, 200] \times [6000, 7000]$.

14679590, 2023, 2, Downloaded from https://onlinelibrary.wiley.com/doi/10.1111/sapm.12602 by Inrae - Dipso-Paris, Wiley Online Library on [24/02/2025]. See the Terms and Conditions (https://onlinelibrary.wiley.com/terms-and-conditions) on Wiley Online Library for rules of use; OA articles are governed by the applicable Creative Commons License

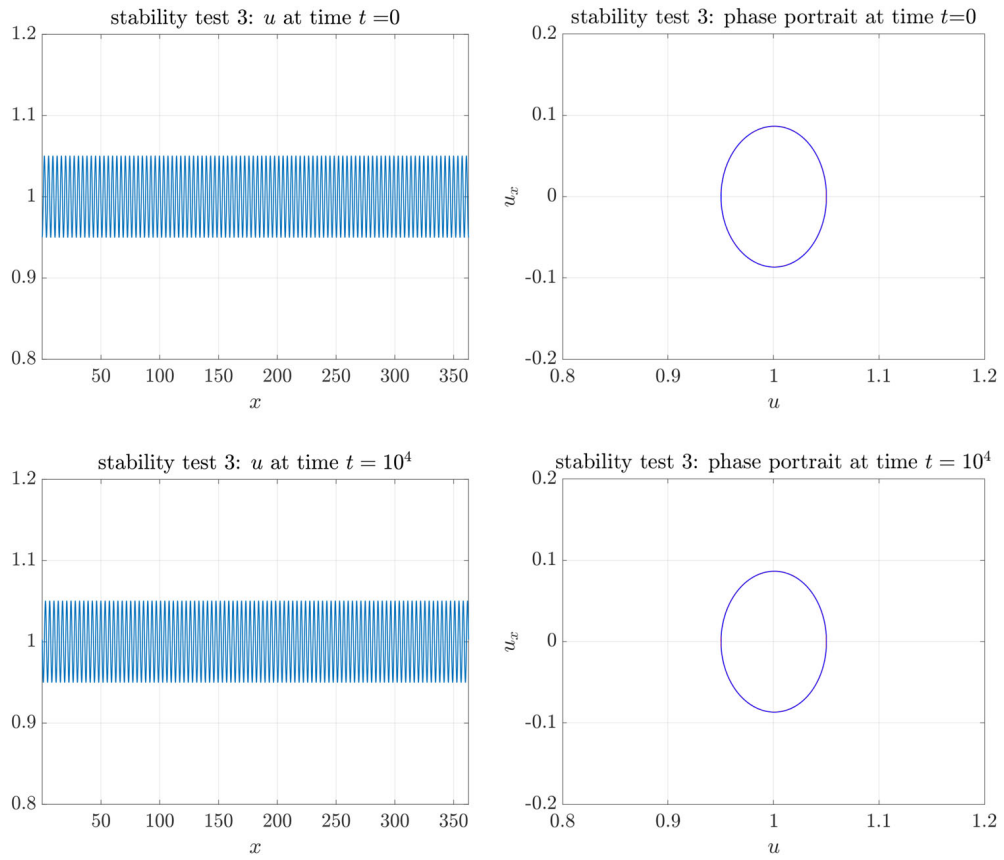

FIGURE 9 Numerical results for the modulational stability of Benjamin–Bona–Mahony (BBM) periodic solutions with the parameters $\bar{u} = 1$, $a = 0.1$, and $k = 1.73242$ belonging to the boundary between elliptic and hyperbolic region of the exact modulation equations (9)–(10). The graphs are displayed in the same manner as in Figure 6.

Finally, in the third example, we take the parameters of periodic wave at the boundary between hyperbolic and elliptic regions: $\bar{u} = 1$, $a = 0.1$, and $k \approx 1.73242$. The corresponding value of m can be estimated as $m \approx 0.04346$. It gives the multiple eigenvalues $\lambda_1 = \lambda_2 \approx -0.124983$ and $\lambda_3 \approx 0.999861$. The numerical solution shown in Figure 9 is stable up to time $t = 10^4$.

ACKNOWLEDGMENTS

We thank the reviewers for their constructive remarks. SG would like to thank the Isaac Newton Institute for Mathematical Sciences, Cambridge, for support and hospitality during the programme "Dispersive hydrodynamics: mathematics, simulation and experiments, with applications in nonlinear waves" where work on this paper was undertaken. This work was supported by EPSRC grant no EP/R014604/1. KMS was partially supported by the Grant of the Ministry of Science and Technology, Taiwan 110-2115-M-002-004-MY2.

DATA AVAILABILITY STATEMENT

The data that support the findings of this study are available from the corresponding author upon reasonable request.

14679590, 2023, 2, Downloaded from https://onlinelibrary.wiley.com/doi/10.1111/sapm.12602 by Inrae - Dipso-Paris, Wiley Online Library on [24/02/2025]. See the Terms and Conditions (https://onlinelibrary.wiley.com/terms-and-conditions) on Wiley Online Library for rules of use; OA articles are governed by the applicable Creative Commons License

ORCID

Sergey Gavrilyuk https://orcid.org/0000-0003-4605-8104

REFERENCES

1. Benjamin TB, Bona JL, Mahony JJ. Model equations for long waves in nonlinear dispersive systems. *Philos Trans R Soc London, Ser A*. 1972;272(1220):47-78.
2. Dai HH. Model equations for nonlinear dispersive waves in a compressible Mooney–Rivlin rod. *Acta Mech*. 1998;127(1-4):193-207.
3. Olver PJ. Euler operators and conservation laws of the BBM equation. *Math Proc Cambridge Philos Soc*. 1979;85(1):143-160.
4. Olver PJ. On the Hamiltonian structure of evolution equations. *Math Proc Cambridge Philos Soc*. 1980;88(1):71-88.
5. Bona JL, Tzvetkov N. Sharp well-posedness results for the BBM equation. *Discrete Contin Dyn Syst*. 2009;23(4):1241-1252.
6. Congy T, El G, Hoefer M, Shearer M. Dispersive Riemann problems for the Benjamin-Bona-Mahony equation. *Stud Appl Math*. 2021;147(3):1089-1145.
7. Benjamin TB, Feir JE. The disintegration of wave trains on deep water Part 1. Theory. *J Fluid Mech*. 1967;27(3):417-430.
8. Benzoni-Gavage S, Noble P, Rodrigues LM. Slow modulations of periodic waves in Hamiltonian PDEs, with application to capillary fluids. *J Nonlinear Sci*. 2014;24:711-768.
9. Hur VM, Pandey AK. Modulational instability in nonlinear nonlocal equations of regularized long wave type. *Physica D*. 2016;325:98-112.
10. Gavrilyuk S, Shyue KM. Singular solutions of the BBM equation: analytical and numerical study. *Nonlinearity*. 2021;35(1):388.
11. Gurevich A, Krylov A, El G. Nonlinear modulated waves in dispersive hydrodynamics. *Zhurnal Eksperimentalnoi i Teoreticheskoi Fiziki*. 1990;98:1605-1626.
12. Benzoni-Gavage S, Mietka C, Rodrigues LM. Modulated equations of hamiltonian PDEs and dispersive shocks. *Nonlinearity*. 2021;34(1):578.
13. Tso T. *The Zero Dispersion Limits of Nonlinear Wave Equations*. The University of Arizona; 1992.
14. Abramowitz M, Stegun IA. *Handbook of Mathematical Functions with Formulas, Graphs, and Mathematical Tables*, vol. 55. US Government Printing Office; 1948.
15. Lax PD. *Hyperbolic Systems of Conservation Laws and the Mathematical Theory of Shock Waves*. SIAM; 1973.
16. Tkachenko S, Gavrilyuk S, Shyue KM. Hyperbolicity of the modulation equations for the Serre-Green-Naghdi model. *Water Waves*. 2020;2:299-326.
17. Marchant TR, Smyth N. Approximate solutions for magmon propagation from a reservoir. *IMA J Appl Math*. 2005;70(6):796-813.
18. Gavrilyuk S, Shyue KM. Hyperbolic approximation of the BBM equation. *Nonlinearity*. 2022;35(3):1447.
19. Favrie N, Gavrilyuk S. A rapid numerical method for solving Serre-Green-Naghdi equations describing long free surface gravity waves. *Nonlinearity*. 2017;30(7):2718.
20. Dhaouadi F, Favrie N, Gavrilyuk S. Extended Lagrangian approach for the defocusing nonlinear Schrödinger equation. *Stud Appl Math*. 2019;142(3):336-358.
21. Busto S, Dumbser M, Escalante C, Favrie N, Gavrilyuk S. On high order ADER discontinuous Galerkin schemes for first order hyperbolic reformulations of nonlinear dispersive systems. *J Sci Comput*. 2021;87(2):48.
22. Besse C, Gavrilyuk S, Kazakova M, Noble P. Perfectly matched layers methods for mixed hyperbolic-dispersive equations. *Water Waves*. 2022;4(3):313-343.
23. Tkachenko S, Gavrilyuk S, Massoni J. Extended Lagrangian approach for the numerical study of multidimensional dispersive waves: applications to the Serre-Green-Naghdi equations. *J Comput Phys*. 2023:111 901.
24. Dhaouadi F, Gavrilyuk S, Vila JP. Hyperbolic relaxation models for thin films down an inclined plane. *Appl Math Comput*. 2022;433:127 378.
25. Whitham GB. *Linear and Nonlinear Waves*. John Wiley & Sons; 2011.
26. Hinch E. *Perturbation Methods*. Cambridge University Press and references therein; 1991.

14679590, 2023, 2, Downloaded from https://onlinelibrary.wiley.com/doi/10.1111/sapm.12602 by Inrae - Dipso-Paris, Wiley Online Library on [24/02/2025]. See the Terms and Conditions (https://onlinelibrary.wiley.com/terms-and-conditions) on Wiley Online Library for rules of use; OA articles are governed by the applicable Creative Commons License

How to cite this article: Gavrilyuk S, Lin Y-H, Shyue K-M. Hyperbolicity study of the modulation equations for the Benjamin–Bona–Mahony equation. *Stud Appl Math*. 2023;151:536–554. https://doi.org/10.1111/sapm.12602

APPENDIX: THE NONDEGENERACY OF THE JACOBIAN MATRIX IN $(\overline{u}, a, k)$ VARIABLES

In the limit of small amplitudes, the choice $\boldsymbol{q} = (\overline{u}, a, k)^T$ is also appropriate. In this case the Jacobian matrix is:

$$\det\left(\frac{\partial(u_1,u_2,u_3)}{\partial(\overline{u},a,k)}\right) = \det\left(\frac{\partial(u_1,u_2,u_3)}{\partial(\overline{u},a,m)}\right)\det\left(\frac{\partial(\overline{u},a,m)}{\partial(\overline{u},a,k)}\right)$$
$$= \det\left(\frac{\partial(u_1,u_2,u_3)}{\partial(\overline{u},a,m)}\right)\frac{\partial m}{\partial k} = \det\left(\frac{\partial(u_1,u_2,u_3)}{\partial(\overline{u},a,m)}\right)\Big/\frac{\partial k}{\partial m},$$

where first m is considered as a function of $\overline{u}, a, k$, and then k is considered as a function of $\overline{u}, a, m$. One has

$$2\pi\Big/\frac{\partial k}{\partial m} = -L^2\Big/\frac{\partial L}{\partial m}.$$

Using the formula

$$\frac{Dm}{a} = \frac{\overline{u}m}{a} + \frac{2-m}{3} - \frac{E(m)}{K(m)}$$

and formula (7), we can compute $\partial L/\partial m$. One has (for fixed $\overline{u}$ and a):

$$\frac{1}{4\sqrt{3}}\frac{\partial L}{\partial m} = \frac{\partial}{\partial m}\left(K(m)\sqrt{\frac{\bar{u}\,m}{a} + \frac{2-m}{3} - \frac{E(m)}{K(m)}}\right)$$
$$= K'(m)\sqrt{\frac{\bar{u}\,m}{a} + \frac{2-m}{3} - \frac{E(m)}{K(m)}} + K(m)\frac{\frac{\bar{u}}{a} - \frac{1}{3} - \left(\frac{E(m)}{K(m)}\right)'}{2\sqrt{\frac{\bar{u}\,m}{a} + \frac{2-m}{3} - \frac{E(m)}{K(m)}}}$$
$$= K'(m)\sqrt{\frac{D\,m}{a}} + K(m)\frac{\frac{\bar{u}}{a} - \frac{1}{3} - \left(\frac{E(m)}{K(m)}\right)'}{2\sqrt{\frac{D\,m}{a}}}$$
$$= \frac{1}{2\sqrt{\frac{D\,m}{a}}}\left(2K'(m)\frac{D\,m}{a} + \frac{K(m)}{m}\left(\frac{\bar{u}m}{a} - \frac{m}{3} - m\left(\frac{E(m)}{K(m)}\right)'\right)\right)$$
$$= \frac{1}{2\sqrt{\frac{D\,m}{a}}}\left(2K'(m)\frac{D\,m}{a} + \frac{K(m)}{m}\left(\frac{D\,m}{a} - \frac{2}{3} + \frac{E(m)}{K(m)} - m\left(\frac{E(m)}{K(m)}\right)'\right)\right)$$

14679590, 2023, 2, Downloaded from https://onlinelibrary.wiley.com/doi/10.1111/sapm.12602 by Inrae - Dipso-Paris, Wiley Online Library on [24/02/2025]. See the Terms and Conditions (https://onlinelibrary.wiley.com/terms-and-conditions) on Wiley Online Library for rules of use; OA articles are governed by the applicable Creative Commons License

$$= \frac{1}{2\sqrt{\frac{D\,m}{a}}}\left(\frac{D\,m}{a}\left(2K'(m)+\frac{K(m)}{m}\right)+\frac{K(m)}{m}\left(\frac{E(m)}{K(m)}-\frac{2}{3}-m\left(\frac{E(m)}{K(m)}\right)'\right)\right)$$

$$= \frac{1}{2\sqrt{\frac{D\,m}{a}}}\left(\frac{D}{a}\frac{E(m)}{(1-m)}+\frac{K(m)}{m}\left(\frac{E^2(m)}{K^2(m)}\frac{1}{2(1-m)}-\frac{1}{6}\right)\right).$$

Here, "prime" means the derivative with respect to m. Since

$$\frac{E^2(m)}{K^2(m)} > 1-m, \quad m \in (0,1),$$

one has

$$\frac{E^2(m)}{K^2(m)}\frac{1}{2(1-m)}-\frac{1}{6} > \frac{1}{3}, \quad m \in (0,1).$$

Hence, the corresponding Jacobian also does not change sign.

14679590, 2023, 2, Downloaded from https://onlinelibrary.wiley.com/doi/10.1111/sapm.12602 by Inrae - Dipso-Paris, Wiley Online Library on [24/02/2025]. See the Terms and Conditions (https://onlinelibrary.wiley.com/terms-and-conditions) on Wiley Online Library for rules of use; OA articles are governed by the applicable Creative Commons License

2. Shear Shallow Water Flow Approximation based on Benney equations

Table of Content

2.1 Introduction . . . 46
2.1.1 Recall on hyperbolic conservation laws . . . 46
2.1.1.1 p-system . . . 47
2.1.1.2 Oleinik-Liu condition for p-system . . . 51
2.1.2 Shallow water equations with piecewise linear velocity profiles 53
2.2 Two-layer stratified flow with continuous velocity profile . . . 55
2.2.1 Total momentum equation . . . 56
2.2.2 Vorticity equation . . . 57
2.2.3 Energy equation . . . 58
2.2.4 Riemann invariants and eigenvalues . . . 58
2.3 System study . . . 60
2.3.1 Study of $\nabla\lambda_j \cdot \mathbf{r}_j$ . . . 60
2.3.1.1 Region where 3 characteristic fields are all genuinely nonlinear . . . 62
2.3.2 Convexity of energy . . . 64
2.3.2.1 Study of convexity of energy when all characteristic fields are genuinely nonlinear . . . 66
2.3.3 Rankine-Hugoniot locus and "entropy" inequality . . . 70
2.3.3.1 Rankine-Hugoniot locus . . . 70
2.3.3.2 "Entropy" inequality . . . 71
2.4 Numerical results . . . 71
2.4.1 The fast characteristic field . . . 72
2.4.1.1 Potential-like flow $\Omega = 0$ . . . 79
2.4.2 The second characteristic field . . . 83
2.5 Conclusion . . . 86
APPENDIX . . . 87
B Recall on shallow water equations . . . 87
C Recall on the basic algorithms for finite volume methods . . . 90
C.1 Godunov method . . . 91

C.2 The HLL approximate Riemann solver 92

2.1. Introduction

In this chapter, a two-layer flow of an ideal homogeneous fluid described by the Benney equations derived in the Introduction is studied. We suppose that the horizontal velocity in each layer is linear with respect to the vertical coordinate:

$$\frac{\partial u_1}{\partial z} = \omega_1; \tag{2.1}$$

$$\frac{\partial u_2}{\partial z} = \omega_2. \tag{2.2}$$

Here u_1, u_2 and ω_1, ω_2 are horizontal velocities and constant vorticities in each layer, respectively. A sketch of the system is presented in Fig. 3. The governing equations have been proven to be hyperbolic, and it becomes possible for us to study the nature of the eigenfields (genuinely nonlinear or linear degenerate) related to the shock stability.

2.1.1. Recall on hyperbolic conservation laws

Consider a quasi-linear system of conservation laws:

$$u_t + f(u)_x = 0, \quad u = u(x,t) \in \mathbb{R}^n, \quad f(u) \in \mathbb{R}^n, \tag{2.3}$$

where f is a smooth vector field. The quasi-linear form of the above strictly hyperbolic system is:

$$u_t + A(u)u_x = 0.$$

The Jacobian matrix $A(u) \coloneqq \dfrac{\partial f(u)}{\partial u}$ has n real and distinct eigenvalues, and can be arranged in increasing order:

$$\lambda_1(u) < \lambda_2(u) < \cdots < \lambda_n(u).$$

The corresponding right eigenvectors of $A(u)$ are denoted by $r_1(u)$, $r_2(u)$, $\cdots$, $r_n(u)$. For any $j = 1, \cdots, n$, we call the pair (λ_j, r_j) $j-$characteristic field, and it is genuinely nonlinear in the sense of Lax when

$$\nabla_u \lambda_j(u) \cdot r_j(u) \neq 0,$$

and linearly degenerate in the sense of Lax when

$$\nabla_u \lambda_j(u) \cdot r_j(u) = 0.$$

Suppose the energy-flux pair (E, F), of Eqn. (2.3) satisfies an additional conser-

vation law:

$$E(u)_t + F(u)_x = 0,$$

with the relation:

$$\frac{\partial E}{\partial u}\frac{\partial f}{\partial u} = \frac{\partial F}{\partial u}.$$

Notice that when the energy E is strictly convex, i.e. the corresponding Hessian matrix $(E'')_{ij} \coloneqq \partial_{u_i}\partial_{u_j}E(u)$ is positive definite, then the system can be symmetrized by the Godunov, Friedrichs and Lax method (Godunov 1961, Friedrichs and Lax 1971). This implies the well-posedness of the Cauchy problem for the governing equations (Serre 1999). A piecewise continuous function u is a weak solution to Eqn. (2.3), if the states u^+, u^- and D satisfy the following Rankine-Hugoniot jump relation across the line of discontinuity

$$-D[u] + [f] = 0, \tag{2.4}$$

here u^+, u^- are limit values of u at the discontinuity, $[u] = u^+ - u^-$ denotes the jump across the line of discontinuity, and $D \coloneqq \dfrac{\mathrm{d}x}{\mathrm{d}t}$ is the velocity of the discontinuity. On the other hand, in the region where u is smooth, the Eqn. (2.3) are satisfied in a usual sense.

In general, there are at least two criteria for choosing an admissible discontinuity between all possible discontinuities:

1. If the eigenfields are genuinely nonlinear the Lax stability condition is satisfied:

$$\begin{aligned} &\lambda_{j-1}(u^-) < D < \lambda_j(u^-), \\ &\lambda_j(u^+) < D < \lambda_{j+1}(u^+). \end{aligned} \tag{2.5}$$

2. One also use the "entropy" inequality condition in the case of convex energy E: $\mathcal{E}(u^+, u^-) \coloneqq -D[E] + [F] \leq 0$.

When the characteristic field is neither genuinely nonlinear nor linear degenerate, the Oleinik-Liu condition should be verified (T. P. Liu 1974, T.-P. Liu 1975). A classical hyperbolic system is presented in the following section: the Euler equations of compressible fluids in the mass Lagrangian coordinates (p-system) for which the above conditions are satisfied. A particular case of p-system written in Eulerian coordinates (shallow water equations) is pressent in appendix B.

2.1.1.1. p-system

The Euler equations of compressible fluids in the mass Lagrangian coordinates (t, q), are also called the "p-system". The mass Lagrangian coordinate q is defined as,

$$q \coloneqq \int_0^X \rho_0(\xi)\mathrm{d}\xi,$$

ρ_0 being the initial density, and X being the Lagrangian coordinate. The p-system takes the form:

$$\begin{cases} \tau_t - u_q = 0, \\ u_t + (p(\tau))_q = 0, \end{cases} \tag{2.6}$$

in which $\tau \coloneqq \dfrac{1}{\rho}$ denotes the specific volume, ρ is the density, u is the velocity, and $p(\tau)$ is the pressure. Eqn. (2.6) can also be written in the Eulerian coordinates by using the density ρ:

$$\begin{cases} \rho_t + (\rho u)_x = 0, \\ (\rho u)_t + (\rho u^2 + p)_x = 0, \end{cases} \tag{2.7}$$

where x is the Eulerian coordinate. The relation between the Eulerian and Lagrangian coordinates is:

$$\frac{\mathrm{d}x}{\mathrm{d}t} = u(t, x); \quad x(t = 0) = X. \tag{2.8}$$

We will assume that:

$$p_\tau \coloneqq \frac{\mathrm{d}p}{\mathrm{d}\tau} < 0, \quad p_{\tau\tau} > 0. \tag{2.9}$$

Notice that the first condition $p_\tau < 0$ is the hyperbolicity condition for p-system, and is equivalent to $p_\rho > 0$. Fig. 2.1 shows a sketch of the pressure $p(\tau)$. The

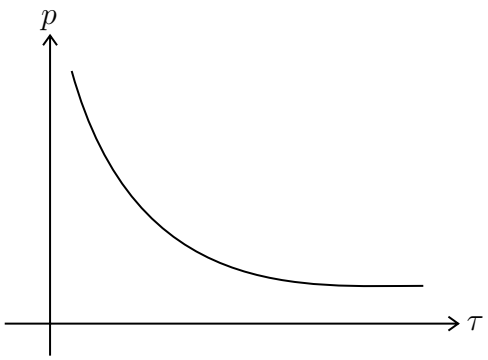

Figure 2.1. – Sketch of the pressure $p(\tau)$ in p-system

equation of energy E of the p-system is,

$$E_t + (up)_x = 0, \tag{2.10}$$

where $E(\tau, u) \coloneqq e(\tau) + \dfrac{1}{2}u^2$, and $\dfrac{\mathrm{d}e}{\mathrm{d}\tau} = -p$. By the definition of the energy $E(\tau, u)$ we have the corresponding Hessian matrix:

$$E'' = \begin{bmatrix} e_{\tau\tau} & 0 \\ 0 & 1 \end{bmatrix}.$$

Since $e_{\tau\tau} = -p_\tau > 0$, the energy is convex, which means that the p-system is a hyperbolic system. Notice that, since $\dfrac{\mathrm{d}e}{\mathrm{d}\tau} = -p$, the condition Eqn. (2.9) is equivalent to:

$$\begin{aligned} p_\tau < 0 &\Leftrightarrow e_{\tau\tau} > 0, \\ p_{\tau\tau} > 0 &\Leftrightarrow e_{\tau\tau\tau} < 0. \end{aligned}$$

The two eigenvalues of the p-system are:

$$\lambda_1 = -\sqrt{-p_\tau}, \quad \lambda_2 = \sqrt{-p_\tau}, \tag{2.11}$$

with the corresponding right eigenvectors given as:

$$r_1 = (1, -\lambda_1)^T, \quad r_2 = (1, -\lambda_2)^T. \tag{2.12}$$

It is easy to check that both characteristic fields are genuinely nonlinear:

$$\begin{aligned} \nabla\lambda_1 \cdot r_1 = \lambda_{1\tau} &= \frac{1}{2\sqrt{-p_\tau}} p_{\tau\tau} > 0, \\ \nabla\lambda_2 \cdot r_2 = \lambda_{2\tau} &= \frac{-1}{2\sqrt{-p_\tau}} p_{\tau\tau} < 0. \end{aligned}$$

The Rankine-Hugoniot jump relations Eqn. (2.4) of the p-system are:

$$\begin{cases} \tilde{D}[\tau] + [u] = 0, \\ -\tilde{D}[u] + [p] = 0. \end{cases} \tag{2.13}$$

Here, since the mass Lagrangian coordinates is used, instead of the velocity D of the discontinuity, $\tilde{D} \coloneqq \dfrac{\mathrm{d}q}{\mathrm{d}t}$ denotes the mass flux. Therefore we have the relation:

$$\frac{[p]}{[\tau]} = \frac{p^+ - p^-}{\tau^+ - \tau^-} = -\tilde{D}^2,$$

which provides, $\tilde{D} = \pm\sqrt{-[p(\tau)]/[\tau]}$. Since p is strictly convex ($p_{\tau\tau} > 0$) and $p_\tau < 0$, we have:

$$(\tilde{D}^2 + p_\tau^+)(\tilde{D}^2 + p_\tau^-) < 0. \tag{2.14}$$

Here p_τ^-, p_τ^+ are limits value of p_τ at discontinuity. First, consider the case $\tilde{D} = \sqrt{[p(\tau)]/[\tau]} > 0$. The Lax stability condition takes the form:

$$\sqrt{-p_\tau^+} = \lambda_2^+ < \tilde{D} < \lambda_2^- = \sqrt{-p_\tau^-}; \quad \tilde{D} > \lambda_1^+ > \lambda_1^-. \tag{2.15}$$

With the convexity of p, we have the relation: $\tau^+ > \tau^-$. On the contrary, when condition $\tau^+ > \tau^-$ is valid, and since p is strictly convex, then we have the relation:

$$\sqrt{-p_\tau^+} < \sqrt{-p_\tau^-}.$$

Combining with Eqn. (2.14), the Lax stability condition Eqn. (2.15) is valid. The Fig. 2.2 shows the illustration of the Lax condition Eqn. (2.15) on (q,t)-plane. It

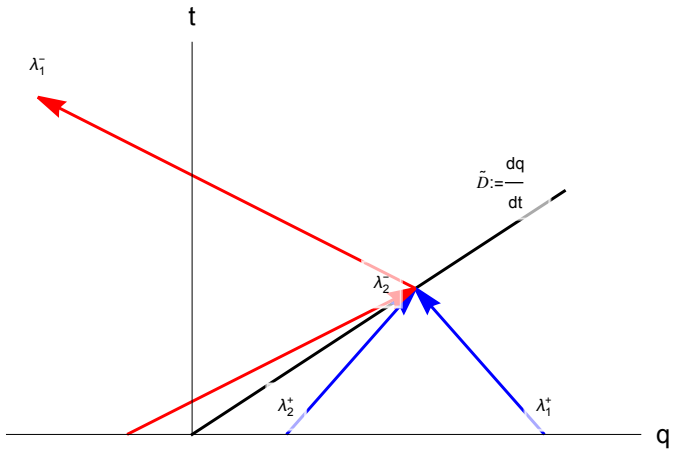

Figure 2.2. – Illustration of the Lax condition Eqn. (2.15) on (q,t)-plane

is similar for the case $\tilde{D} < 0$, the corresponding Lax stability condition takes the form:

$$\lambda_1^+ < \tilde{D} < \lambda_1^-; \quad \tilde{D} < \lambda_2^- < \lambda_2^+.$$

The "entropy" inequality (corresponds to the total energy decrease) of the system takes the form:

$$\mathcal{E} := -\tilde{D}[E] + [up], \tag{2.16}$$

with the energy is defined as: $E(\tau,u) := e(\tau) + \frac{1}{2}u^2$. The above "entropy" inequality equation above can be written in the form:

$$\mathcal{E} = -\tilde{D}\left(e^+ - e^- + \frac{1}{2}\left(u^{+2} - u^{-2}\right)\right) + \left(u^+p^+ - u^-p^-\right) \tag{2.17}$$

From the Rankine-Hugoniot jump relation of p-system Eqn. (2.13), we have:

$$\begin{cases} \tilde{D}\left(\tau^+ - \tau^-\right)\left(p^+ + p^-\right) = -\left(u^+ - u^-\right)\left(p^+ + p^-\right) = -u^+p^+ + u^-p^- - u^+p^- + u^-p^+, \\ \tilde{D}\left(u^+ - u^-\right)\left(u^+ + u^-\right) = \left(p^+ - p^-\right)\left(u^+ + u^-\right) = u^+p^+ - u^-p^- - u^+p^- + u^-p^+. \end{cases}$$

Therefore, finally, we have the relation:

$$\frac{\tilde{D}}{2}\left(u^{+2} - u^{-2}\right) - \frac{\tilde{D}}{2}\left(\tau^+ - \tau^-\right)\left(p^+ + p^-\right) = u^+p^+ - u^-p^- \tag{2.18}$$

The "entropy" inequality Eqn. (2.17) then takes the form,

$$\mathcal{E} = -\tilde{D}\left(e^+ - e^- + \frac{1}{2}\left(\tau^+ - \tau^-\right)\left(p^+ + p^-\right)\right). \tag{2.19}$$

Consider first when the " + " state is in the neighborhood of " − " state. Applying the Taylor series of p^+ and e^+ at p^- and e^- respectively,

$$p^+ = p^- + p^-_\tau\left(\tau^+ - \tau^-\right) + \frac{1}{2}p^-_{\tau\tau}\left(\tau^+ - \tau^-\right)^2 + \frac{1}{6}p^-_{\tau\tau\tau}\left(\tau^+ - \tau^-\right)^3 + \cdots \tag{2.20}$$

$$e^+ = e^- + e^-_\tau\left(\tau^+ - \tau^-\right) + \frac{1}{2}e^-_{\tau\tau}\left(\tau^+ - \tau^-\right)^2 + \frac{1}{6}e^-_{\tau\tau\tau}\left(\tau^+ - \tau^-\right)^3 + \cdots \tag{2.21}$$

With the fact that $e_\tau = -p$, the "entropy" equation finally takes the form:

$$\mathcal{E} = -\frac{\tilde{D}p^-_{\tau\tau}\left(\tau^+ - \tau^-\right)^3}{12} + O\left(\left(\tau^+ - \tau^-\right)^4\right). \tag{2.22}$$

To have a stable shock, with the convexity of the pressure p, namely $p_{\tau\tau} > 0$, for the case $\tilde{D} > 0$, it required $\tau^- < \tau^+$, therefore Eqn. (2.22) shows the "entropy" is decreasing, $\mathcal{E} < 0$. Similarly, for a stable shock with $\tilde{D} < 0$, it requires $\tau^- > \tau^+$, then $\mathcal{E} < 0$. In summary, in the vicinity of τ^-, the "entropy" inequality is satisfied. Now assume that at some point τ^+, $\mathcal{E} > 0$. Since $\mathcal{E}$ defined by Eqn. (2.17) is a smooth function, there exists a point $\tau^* \neq \tau^-$ such that, $\mathcal{E}(\tau^*, \tau^-) = 0$. More specifically, from Eqn. (2.19), at τ^*, we have:

$$e^* - e^- = -\frac{1}{2}\left(\tau^* - \tau^-\right)\left(p^* + p^-\right). \tag{2.23}$$

Since $e_\tau = -p$, the left hand side of Eqn. (2.23) can be expressed as:

$$e^* - e^- = -\int_{\tau^-}^{\tau^*} p(s)\mathrm{d}s. \tag{2.24}$$

For a shock when $\tilde{D} > 0$ and $\tau^- < \tau^*$, the above equation represents the red area in Fig.2.3. On the other hand, the left hand side of Eqn. (2.23) represents the area of the trapeze. Since p is a strictly convex function, the two areas are never equal. Similarly, when $\tilde{D} < 0$, it can also be checked in the same way. Therefore, the energy jump of the p-system is always negative.

Finally, this shows that for p-system the convexity of the energy and the Lax stability condition are equivalent if the eigenfields are genuinely nonlinear in the sense of Lax.

2.1.1.2. Oleinik-Liu condition for p-system

As mentioned above, when the fields are neither genuinely nonlinear nor linear degenerate, we need to apply the Oleinik-Liu condition to have a stable shock.

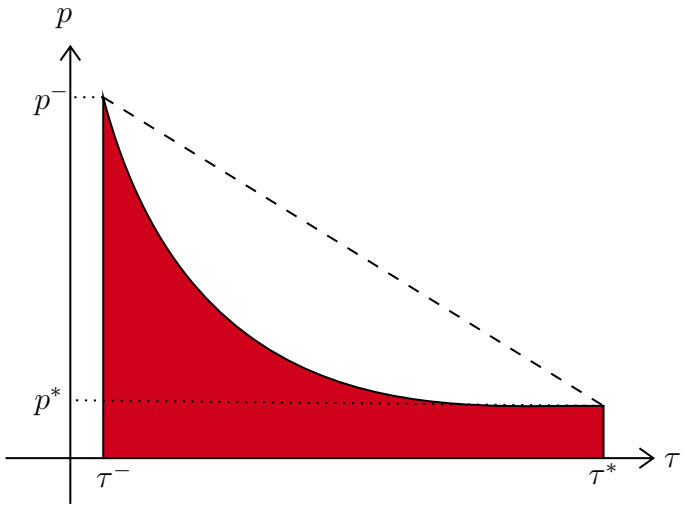

Figure 2.3. – Illustration of the function $p(\tau)$, for the right facing shock.

Consider again the p-system,

$$\begin{cases} \tau_t - u_q = 0, \\ u_t + (p(\tau))_q = 0. \end{cases} \tag{2.25}$$

In the case of $p_\tau < 0$ and $p_{\tau\tau} > 0$, a stable shock relating states " + " and " − " is shown in Fig. 2.4a, and a sketch of the solution to the system is shown in Fig. 2.4b. Consider now the pressure $p(\tau)$ as shown in Fig. 2.5a. A shock solution related

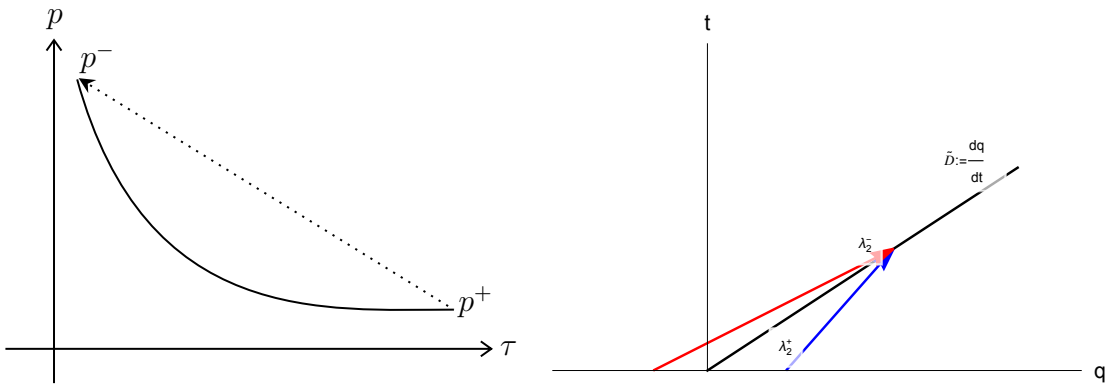

(a) Sketch of the pressure $p(\tau)$ of classic p-system.

(b) Sketch of the solution to the classic p-system

Figure 2.4. – p-system

states " + " and " − ", instead of passing directly along the red dashed line, it passes through the blue dashed line from state " + " to state " ∗ ", then the curve from state " ∗ " to state " ∗ ∗", finally the black dashed line from state " ∗ ∗" to state " − ". Here, the blue and black straight dashed lines are perpendicular to

the curve in the states " $*$ " and " $**$", respectively. A sketch of the solution to this p-system is shown in Fig. 2.5b. The thick blue line in Fig. 2.5b represents a shock from the state p^+ to p^*; the thick black line is a shock from the state p^{**} to p^-. The compression fan between two thick lines in Fig. 2.5b, represents the state going from p^* to p^{**} alone the curve.

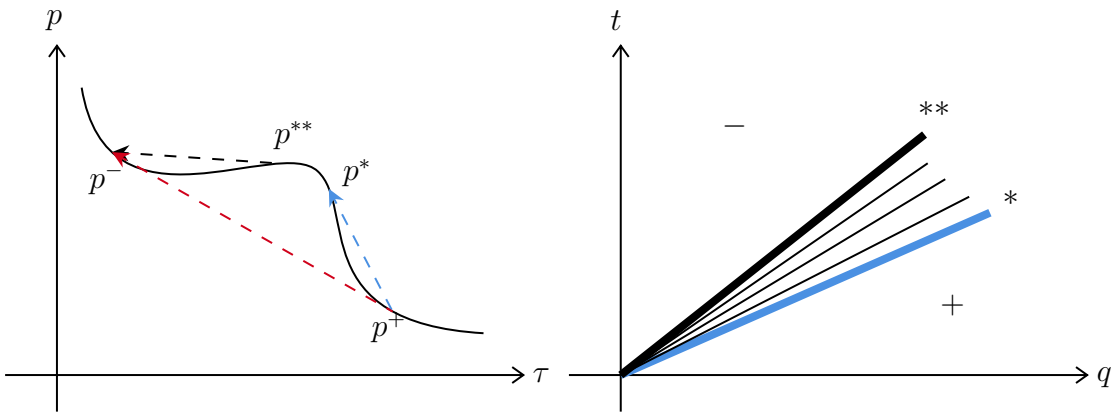

(a) Sketch of the function $p(\tau)$. (b) Sketch of the solution to the p-system

Figure 2.5. – p-system when the eigenfields are not genuinely nonlinear

2.1.2. Shallow water equations with piecewise linear velocity profiles

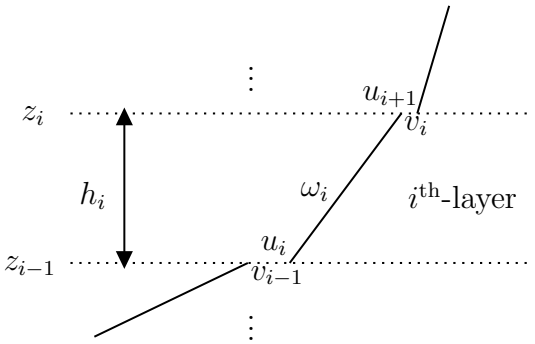

Figure 2.6. – Illustration of a piecewise linear velocity profile in $i^{\text{th}} -$ layer.

The Benney equations are a long-wave approximation of the Euler equations. They are:

$$u_t + uu_x + wu_z + gh_x = 0, \tag{2.26}$$

$$h_t + \left(\int_0^h u\mathrm{d}z\right)_x = 0, \quad w = -\int_0^z u_x(t,x,z')\mathrm{d}z'. \tag{2.27}$$

Here u and w are horizontal and vertical velocity, respectively, and h is the total water depth. Now, following the construction in Chesnokov, El, Gavrilyuk, and Pavlov 2017, a piecewise linear horizontal velocity profile is defined in the form:

$$u(t,x,z) = \omega_i(z - z_{i-1}) + u_i(t,x), \quad z \in (z_{i-1}, z_i), \quad i = 1, \ldots, N. \tag{2.28}$$

Here $u_i(t,x)$ is the velocity at the lower boundary of ith-layer, and ω_i is the constant vorticity. We introduce the following notations:

$$h_i(t,x) = z_i - z_{i-1}, \tag{2.29}$$
$$v_i(t,x) = \omega_i h_i + u_i, \tag{2.30}$$
$$\bar{u}_i(t,x) = \frac{v_i + u_i}{2} = u_i + \frac{\omega_i h_i}{2}. \tag{2.31}$$

Here h_i is the water depth of ith-layer, $v_i(t,x)$ is the velocity at the upper boundary of ith-layer, and $\bar{u}_i$ is the averaged velocity of the ith-layer. It is equal to the depth-averaged velocity of the ith-layer. The illustration of the piecewise linear velocity profiles is shown in Fig. 2.6. At the upper and lower boundaries of each layer the following kinematic conditions should be satisfied:

$$\frac{\partial z_i}{\partial t} + v_i \frac{\partial z_i}{\partial x} = w_i^+, \quad \frac{\partial z_{i-1}}{\partial t} + u_i \frac{\partial z_{i-1}}{\partial x} = w_i^-, \quad i = 1, \ldots, N. \tag{2.32}$$

With mass conservation $u_x + w_z = 0$, and kinematic condition, vertical velocity w can be expressed in the form:

$$w = -(z - z_{i-1})\left(\frac{\partial u_i}{\partial x} - \omega_i \frac{\partial z_{i-1}}{\partial x}\right) + \frac{\partial z_{i-1}}{\partial t} + u_i \frac{\partial z_{i-1}}{\partial x}, \quad z \in (z_{i-1}, z_i). \tag{2.33}$$

Calculating the difference $w_i^+ - w_i^-$ by using Eqn. (2.32) and Eqn. (2.33), we obtain:

$$\begin{aligned}
&\frac{\partial z_i}{\partial t} + v_i \frac{\partial z_i}{\partial x} - \frac{\partial z_{i-1}}{\partial t} - u_i \frac{\partial z_{i-1}}{\partial x} = -h_i\left(\frac{\partial u_i}{\partial x} - \omega_i \frac{\partial z_{i-1}}{\partial x}\right) \\
&\Rightarrow \frac{\partial h_i}{\partial t} + h_i \frac{\partial u_i}{\partial x} + v_i \frac{\partial h_i}{\partial x} + (v_i - u_i - \omega_i h_i)\frac{\partial z_{i-1}}{\partial x} \\
&= \frac{\partial h_i}{\partial t} + h_i \frac{\partial u_i}{\partial x} + u_i \frac{\partial h_i}{\partial x} + \omega_i h_i \frac{\partial h_i}{\partial x} \\
&= h_{it} + (\bar{u}_i h_i)_x = 0, \quad i = 1, \ldots, N.
\end{aligned} \tag{2.34}$$

Substitution of the velocities u and w given by formulas (2.28), (2.33) into Eqn. (2.26) yields

$$u_{it} + u_i u_{ix} + g h_x = 0, \quad i = 1, \ldots, N. \tag{2.35}$$

Combine the two equations above we get:

$$v_{it} + v_i v_{ix} + g h_x = u_{it} + u_i u_{ix} + g h_x + \omega_i [h_{it} + (\bar{u}_i h_i)_x] = 0, \quad i = 1, \ldots, N. \tag{2.36}$$

The system can be rewritten as:

$$h_{it} + (\overline{u}_i h_i)_x = 0, \quad \overline{u}_{it} + \left(\frac{\overline{u}_i^2}{2} + \frac{\omega_i^2 h_i^2}{8} + g h \right)_x = 0, \quad i = 1, \ldots N. \tag{2.37}$$

If the above system Eqn. (2.37) is hyperbolic, it can be written in the form:

$$R_{j_t} + \lambda_j R_{j_x} = 0, \quad j = 1, \ldots, 2N, \tag{2.38}$$

where R_j are the Riemann invariants and λ_j are the corresponding eigenvalues. For a piecewise linear velocity profile Eqn. (2.37) the Riemann invariants are defined as (Chesnokov, El, Gavrilyuk, and Pavlov 2017):

$$R_j = \lambda_j - \sum_{i=1}^{N} \frac{g}{\omega_i} \ln \left| \frac{v_i - \lambda_j}{u_i - \lambda_j} \right|, \tag{2.39}$$

where $\lambda_j(t, x)$ are the eigenvalues of the system and are the roots of the equation

$$1 + g \sum_{i=1}^{N} \frac{1}{\omega_i} \left(\frac{1}{v_i - \lambda_j} - \frac{1}{u_i - \lambda_j} \right) = 0. \tag{2.40}$$

Moreover, we further consider a piecewise linear continuous velocity profile for $N-$layer homogeneous fluid, where $u_i = v_{i-1}$, and the system Eqn. (2.37) becomes:

$$h_{it} + (\overline{u}_i h_i)_x = 0, \quad i = 1, \ldots, N \tag{2.41}$$

$$v_{0t} + v_0 v_{0x} + g h_x = 0. \tag{2.42}$$

The unknowns for these $N + 1$ equations are the height of each layer h_i and the velocity v_0 at the bottom $z = 0$. Here $\overline{u}_i$ denotes the averaged velocity in each layer and defined as:

$$\overline{u}_i = v_i - \frac{\omega_i h_i}{2}, \quad v_i = v_0 + \sum_{k=1}^{i} \omega_k h_k. \tag{2.43}$$

2.2. Two-layer stratified flow with continuous velocity profile

In this section, the system of 2-layer flow with a continuous velocity profile Eqn. (2.41) and Eqn. (2.42) is considered. The two-layer system is always hyperbolic, while in the case $n > 2$ one can have an elliptic-hyperbolic system. The illustrations

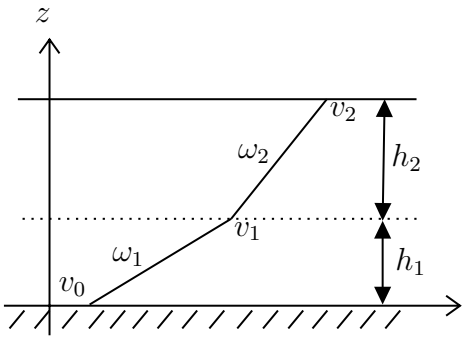

Figure 2.7. – Illustration of two-layer stratified flow with continuous velocity profile

are shown in Fig. 2.7. h_1, h_2 and ω_1, ω_2 are the water depths and the constant vorticities in two layers, respectively, v_0 is the bottom velocity; v_1 and v_2 are the velocities at the upper boundary of each layer. The system can be expressed as:

$$h_{1t} + (\overline{u}_1 h_1)_x = 0; \quad \overline{u}_1 = v_0 + \frac{\omega_1 h_1}{2}, \tag{2.44}$$

$$h_{2t} + (\overline{u}_2 h_2)_x = 0; \quad \overline{u}_2 = v_0 + \omega_1 h_1 + \frac{\omega_2 h_2}{2}, \tag{2.45}$$

$$v_{0t} + v_0 v_{0x} + g h_x = 0; \quad h = h_1 + h_2. \tag{2.46}$$

Here, $\overline{u}_1$, $\overline{u}_2$ represent the averaged velocities in two layers, respectively. Eqn. (2.44), Eqn. (2.45), and Eqn. (2.46) is a closed system of quasi-linear equations for three unknown variables (h_1, h_2, v_0). For getting conservation laws, it is convenient to write the equations for averaged velocity:

$$\overline{u}_{1t} + \left(\frac{\overline{u}_1^2}{2} + \frac{\omega_1^2 h_1^2}{8} + gh \right)_x = 0, \tag{2.47}$$

$$\overline{u}_{2t} + \left(\frac{\overline{u}_2^2}{2} + \frac{\omega_2^2 h_2^2}{8} + gh \right)_x = 0. \tag{2.48}$$

2.2.1. Total momentum equation

To obtain the momentum conservation equation, we use the water depth equations in each layer, Eqn. (2.44) and Eqn. (2.45), and the average velocity equations in each layer, Eqn. (2.47) to Eqn. (2.48). Consider h_1·Eqn. (2.47)+$\overline{u}_1$· Eqn. (2.44), we have:

$$\begin{aligned} &(h_1\overline{u}_1)_t + \overline{u}_1(\overline{u}_1 h_1)_x + h_1 \left(\frac{\overline{u}_1^2}{2} + \frac{\omega_1^2 h_1^2}{8} + gh \right)_x \\ &= (h_1\overline{u}_1)_t + (h_1\overline{u}_1^2)_x + \left(\frac{\omega_1^2 h_1^3}{12} \right)_x + h_1 (gh)_x = 0. \end{aligned}$$

Again, the averaged velocities in the each layer $\overline{u}_1$ and $\overline{u}_2$ are given as: $\overline{u}_1 = u_1 + \dfrac{\omega_1 h_1}{2}$ and $\overline{u}_2 = u_2 + \dfrac{\omega_2 h_2}{2}$, and the total water depth $h = h_1 + h_2$. Therefore, momentum equation takes the form:

$$(h_1\overline{u}_1 + h_2\overline{u}_2)_t + \left(h_1\overline{u}_1^2 + h_2\overline{u}_2^2 + \frac{\omega_1^2 h_1^3}{12} + \frac{\omega_1^2 h_2^3}{12} + \frac{gh^2}{2}\right)_x = 0. \tag{2.49}$$

Now we define the average velocity over the total water depth, $U \coloneqq \dfrac{h_1\overline{u}_1 + h_2\overline{u}_2}{h}$; averaged vorticity, $\Omega \coloneqq \dfrac{h_1\omega_1 + h_2\omega_2}{h}$; and the modified pressure for the system, $p \coloneqq \dfrac{1}{2}gh^2 + f_1$, where $f_1 = \dfrac{h_1 h_2 h\Omega^2}{4} + \dfrac{\omega_1^2 h_1^3}{12} + \dfrac{\omega_2^2 h_2^3}{12}$. Therefore the above momentum equation can be rewritten as:

$$(hU)_t + \left(hU^2 + p\right)_x = 0. \tag{2.50}$$

2.2.2. Vorticity equation

The conservation equation of vorticity can be obtained by applying $\omega_1\cdot$Eqn. (2.44) $+\omega_2\cdot$Eqn. (2.45),

$$(h_1\omega_1 + h_2\omega_2)_t + (\omega_1\overline{u}_1 h_1 + \omega_2\overline{u}_2 h_2)_x = 0. \tag{2.51}$$

Remark that the averaged vorticity is defined as: $\Omega = \dfrac{h_1\omega_1 + h_2\omega_2}{h}$, and the averaged velocity $U = \dfrac{h_1\overline{u}_1 + h_2\overline{u}_2}{h}$. Therefore, the above equation can be rewritten as

$$(h\Omega)_t + \left[hU\Omega + \frac{h_1 h_2 \Omega(\omega_2 - \omega_1)}{2}\right]_x = 0. \tag{2.52}$$

It is interesting to note that from the vorticity equation above, there are two special cases. First, when $\omega_1 = \omega_2 = \Omega$, the vorticity equation reduces to the mass equation, and the system reduces to one-layer the shallow water equations take the form:

$$\begin{aligned} h_t + (hU)_x &= 0, \\ (hU)_t + \left(hU^2 + \frac{gh^2}{2} + \frac{\Omega^2 h^3}{12}\right)_x &= 0. \end{aligned}$$

In the particular case of vanishing Ω, one obtains the classical shallow water equations discussed in appendix B. The second case is when the averaged vorticity is zero initially $\Omega(t = 0, x) = 0$. Then by Eqn. (2.52), Ω stays zero for all time. We call this particular case a potential-like flow. Since $\omega_i \neq 0$, the flow is not potential

in both layers. However, the average vorticity Ω remains zero, which corresponds to the analog of potential flow. This case will be discussed later.

2.2.3. Energy equation

Again we use the water depth equations in each layer, Eqn. (2.44) and Eqn. (2.45), and the average velocity equations in each layer, Eqn. (2.47) to Eqn. (2.48) to obtain the equation of energy. We first consider the part of horizontal momentum: $h_1\overline{u}_1\cdot$Eqn. (2.47) $+\left(\frac{\overline{u}_1^2}{2}+\frac{\omega_1^2h_1^2}{8}+gh\right)\cdot$Eqn. (2.44), then we get:

$$\left(\frac{\overline{u}_1^2}{2}+\frac{\omega_1^2h_1^2}{8}+gh\right)h_{1t}+h_1\overline{u}_1\overline{u}_{1t}+\left(\frac{\overline{u}_1^2}{2}+\frac{\omega_1^2h_1^2}{8}+gh\right)(\overline{u}_1h_1)_x+h_1\overline{u}_1\left(\frac{\overline{u}_1^2}{2}+\frac{\omega_1^2h_1^2}{8}+gh\right)_x$$
$$=\left[h_1\left(\frac{\overline{u}_1^2}{2}+\frac{\omega_1^2h_1^2}{24}\right)\right]_t+ghh_{1t}+\left[h_1\overline{u}_1\left(\frac{\overline{u}_1^2}{2}+\frac{\omega_1^2h_1^2}{8}+gh\right)\right]_x=0.$$

Therefore, the energy equation can be rewritten as:

$$\left[h_1\left(\frac{\overline{u}_1^2}{2}+\frac{\omega_1^2h_1^2}{24}\right)+h_2\left(\frac{\overline{u}_2^2}{2}+\frac{\omega_2^2h_2^2}{24}\right)+g\frac{h^2}{2}\right]_t+$$
$$\left[h_1\overline{u}_1\left(\frac{\overline{u}_1^2}{2}+\frac{\omega_1^2h_1^2}{8}+gh\right)+h_2\overline{u}_2\left(\frac{\overline{u}_2^2}{2}+\frac{\omega_2^2h_2^2}{8}+gh\right)\right]_x=0. \tag{2.53}$$

Now we define the modified averaged energy for the system, $e=\frac{1}{2}U^2+\frac{1}{2}gh+\frac{f_1}{2h}$, and $f_2=\frac{h_1^2h_2^2\Omega^2(\omega_2-\omega_1)}{8}$. The energy equation can be written in form:

$$(he)_t+(hUe+Up+f_2)_x=0. \tag{2.54}$$

Again, p here is modified pressure, $p=\frac{1}{2}gh^2+f_1$, and $f_1=\frac{h_1h_2h\Omega^2}{4}+\frac{\omega_1^2h_1^3}{12}+\frac{\omega_2^2h_2^3}{12}$.

2.2.4. Riemann invariants and eigenvalues

From Eqn. (2.39), the Riemann invariants of a two-layer piecewise continuous linear velocity profile with $\omega_1\neq\omega_2$ are:

$$R_j=\lambda_j-\frac{g}{\omega_1}\ln\left|\frac{v_1-\lambda_j}{v_0-\lambda_j}\right|-\frac{g}{\omega_2}\ln\left|\frac{v_2-\lambda_j}{v_1-\lambda_j}\right|,\quad j=1,2,3, \tag{2.55}$$

here $v_1 = v_0 + \omega_1 h_1$, $v_2 = v_0 + \omega_1 h_1 + \omega_2 h_2$ and the eigenvalues $\lambda_j(t,x)$ are the roots of the cubic function:

$$1 + \frac{g}{\omega_1}\left(\frac{1}{v_1 - \lambda_j} - \frac{1}{v_0 - \lambda_j}\right) + \frac{g}{\omega_2}\left(\frac{1}{v_2 - \lambda_j} - \frac{1}{v_1 - \lambda_j}\right) = 0, \quad j = 1,2,3. \tag{2.56}$$

Since the above equation is a cubic function, its real roots λ_j can be expressed explicitly (Viète 1646, Nickalls 2006, Miura 1980, Zwillinger 2002),

$$\lambda_j = v_0 - 2\sqrt{-\frac{\xi}{3}}\cos\left[\frac{1}{3}\arccos\left(\frac{3\zeta}{2\xi}\sqrt{-\frac{3}{\xi}}\right) - \frac{2\pi(j-1)}{3}\right] + \frac{a}{3}; \quad j = 1,2,3, \tag{2.57}$$

with

$$\hat{a} = \omega_1 h_1; \quad \hat{b} = \omega_1 h_1 + \omega_2 h_2;$$
$$a = \hat{a} + \hat{b}; \quad b = \hat{a}\hat{b} - gh; \quad c = -gh_1\hat{b};$$
$$\xi = \frac{3b - a^2}{3}; \quad \zeta = \frac{2a^3 - 9ab + 27c}{27}.$$

Here, the eigenvalues are ordered: $\lambda_1 < \lambda_2 < \lambda_3$. The time derivative of Riemann invariants take the form:

$$\begin{aligned} R_{j_t} &= \lambda_{j_t} - \frac{g}{\omega_1}\left[\frac{(v_1 - \lambda_j)_t}{v_1 - \lambda_j} - \frac{(v_0 - \lambda_j)_t}{v_0 - \lambda_j}\right] - \frac{g}{\omega_2}\left[\frac{(v_2 - \lambda_j)_t}{v_2 - \lambda_j} - \frac{(v_1 - \lambda_j)_t}{v_1 - \lambda_j}\right] \\ &= \lambda_{j_t}\left\{1 - \frac{g}{\omega_1}\left[\frac{-1}{v_1 - \lambda_j} - \frac{-1}{v_0 - \lambda_j}\right] - \frac{g}{\omega_2}\left[\frac{-1}{v_2 - \lambda_j} - \frac{-1}{v_1 - \lambda_j}\right]\right\} \\ &\quad - \frac{g}{\omega_1}\left[\frac{v_{1t}}{v_1 - \lambda_j} - \frac{v_{0t}}{v_0 - \lambda_j}\right] - \frac{g}{\omega_2}\left[\frac{v_{2t}}{v_2 - \lambda_j} - \frac{v_{1t}}{v_1 - \lambda_j}\right] \\ &= -\frac{g}{\omega_1}\left[\frac{v_{1t}}{v_1 - \lambda_j} - \frac{v_{0t}}{v_0 - \lambda_j}\right] - \frac{g}{\omega_2}\left[\frac{v_{2t}}{v_2 - \lambda_j} - \frac{v_{1t}}{v_1 - \lambda_j}\right]. \end{aligned} \tag{2.58}$$

Similarly, we have:

$$\lambda_j R_{j_x} = -\frac{g}{\omega_1}\left[\frac{\lambda_j v_{1x}}{v_1 - \lambda_j} - \frac{\lambda_j v_{0x}}{v_0 - \lambda_j}\right] - \frac{g}{\omega_2}\left[\frac{\lambda_j v_{2x}}{v_2 - \lambda_j} - \frac{\lambda_j v_{1x}}{v_1 - \lambda_j}\right]. \tag{2.59}$$

Therefore,

$$R_{j_t} + \lambda_j R_{j_x} = -\frac{g}{\omega_1}\left[\frac{v_{1t} + \lambda_j v_{1x}}{v_1 - \lambda_j} - \frac{v_{0t} + \lambda_j v_{0x}}{v_0 - \lambda_j}\right] - \frac{g}{\omega_2}\left[\frac{v_{1t} + \lambda_j v_{2x}}{v_2 - \lambda_j} - \frac{v_{1t} + \lambda_j v_{1x}}{v_1 - \lambda_j}\right], \quad j = 1,2,3.$$

On the other hand, from Eqn. (2.36):

$$v_{1t} + v_i v_{1x} + g h_x = 0, \quad v_{2t} + v_i v_{2x} + g h_x = 0.$$

Finally, we get the result:

$$\begin{aligned} R_{j_t} + \lambda_j R_{j_x} &= -\frac{g}{\omega_1}\left[\frac{(\lambda_j - v_1)v_{1x} - gh_x}{v_1 - \lambda_j} - \frac{(\lambda_j - v_0)v_{0x} - gh_x}{v_0 - \lambda_j}\right] \\ &\quad -\frac{g}{\omega_2}\left[\frac{(\lambda_j - v_2)v_{2x} - gh_x}{v_2 - \lambda_j} - \frac{(\lambda_j - v_1)v_{1x} - gh_x}{v_1 - \lambda_j}\right] \\ &= \frac{g}{\omega_1}(v_{1x} - u_{1x}) + \frac{g}{\omega_2}(v_{2x} - u_{2x}) \\ &\quad +gh_x\left\{\frac{g}{\omega_1}\left[\frac{1}{v_1 - \lambda_j} - \frac{1}{v_0 - \lambda_j}\right] + \frac{g}{\omega_2}\left[\frac{1}{v_2 - \lambda_j} - \frac{1}{v_1 - \lambda_j}\right]\right\} \\ &= gh_{1x} + gh_{2x} + gh_x\{-1\} = 0. \end{aligned} \tag{2.60}$$

Which means that the system of a two-layer piecewise linear velocity profile is hyperbolic. On the other hand, the corresponding right eigen vectors can be expressed as, $\mathbf{r}_j = (a_j, b_j, c_j)^T$, and $j = 1, 2, 3$, where

$$\begin{aligned} a_j &= -gh_1, \\ b_j &= -(v_0 - \lambda_j)(v_0 + \omega_1 h_1 - \lambda_j) + gh_1, \\ c_j &= g(v_0 + \omega_1 h_1 - \lambda_j). \end{aligned} \tag{2.61}$$

2.3. System study

Since the eigenvalues are ordered $\lambda_3 > \lambda_2 > \lambda_1$, the third characteristic field is called the fast characteristic field, contrarily, the first characteristic field is called the slow characteristic field. The second characteristic field (intermediate characteristic) corresponds to the propagation of vorticity

2.3.1. Study of $\nabla\lambda_j \cdot \mathbf{r}_j$

We show that the values of $\nabla\lambda_j \cdot \mathbf{r}_j$ is independent on the choice of unknowns. Consider a system written in $\mathbf{V}$-variables in non-conservative form:

$$\mathbf{V}_t + A_{\mathbf{V}}\mathbf{V}_x = 0, \tag{2.62}$$

Let $A_{\mathbf{V}}$ has an eigenvalue λ and a right eigenvector $\mathbf{r}_{\mathbf{V}}$. Now we change the variables from $\mathbf{V}$ to $\mathbf{U}$. The system can be expressed as:

$$\mathbf{U}_t + A_{\mathbf{U}}\mathbf{U}_x = J_{\mathbf{U}}\mathbf{V}_t + A_{\mathbf{U}}J_{\mathbf{U}}\mathbf{V}_x = 0, \tag{2.63}$$

where the Jacobian matrix is defined as: $J_{\mathbf{U}} \coloneqq \dfrac{\partial \mathbf{U}}{\partial \mathbf{V}}$. Assuming the determinant of the Jacobian matrix is never zero, $\det(J_{\mathbf{U}}) \neq 0$, we get:

$$\mathbf{V}_t + \left(J_{\mathbf{U}}^{-1} A_{\mathbf{U}} J_{\mathbf{U}}\right) \mathbf{V}_x = 0. \tag{2.64}$$

Therefore, we have the relation: $A_{\mathbf{V}} = J_{\mathbf{U}}^{-1} A_{\mathbf{U}} J_{\mathbf{U}}$. Since λ is the eigenvalue of $A_{\mathbf{V}}$, we know that $\det(A_{\mathbf{V}} - \lambda \mathbf{I}) = 0$. Here, $\mathbf{I}$ is the identical matrix. Moreover, we have:

$$\begin{aligned}
\det(A_{\mathbf{V}} - \lambda \mathbf{I}) &= \det\left(J_{\mathbf{U}}^{-1} A_{\mathbf{U}} J_{\mathbf{U}} - \lambda \mathbf{I}\right) = \det\left(J_{\mathbf{U}}^{-1} A_{\mathbf{U}} J_{\mathbf{U}} - \lambda J_{\mathbf{U}}^{-1} J_{\mathbf{U}}\right) \\
&= \det\left(J_{\mathbf{U}}^{-1} (A_{\mathbf{U}} - \lambda \mathbf{I}) J_{\mathbf{U}}\right) = \det\left(J_{\mathbf{U}}^{-1}\right) \det(A_{\mathbf{U}} - \lambda \mathbf{I}) \det\left(J_{\mathbf{U}}\right) \\
&= \det(A_{\mathbf{U}} - \lambda \mathbf{I}) = 0.
\end{aligned}$$

Therefore, the two matrices $A_{\mathbf{V}}$ and $A_{\mathbf{U}}$ share the same eigenvalue λ.
Furthermore,

$$A_{\mathbf{V}} \mathbf{r}_{\mathbf{V}} = J_{\mathbf{U}}^{-1} A_{\mathbf{U}} J_{\mathbf{U}} \mathbf{r}_{\mathbf{V}} = \lambda \mathbf{r}_{\mathbf{V}}. \tag{2.65}$$

Or:

$$A_{\mathbf{U}} J_{\mathbf{U}} \mathbf{r}_{\mathbf{V}} = \lambda J_{\mathbf{U}} \mathbf{r}_{\mathbf{V}}. \tag{2.66}$$

Now the right eigenvector of the matrix $A_{\mathbf{U}}$ can be written as:

$$\mathbf{r}_{\mathbf{U}} = J_{\mathbf{U}} \mathbf{r}_{\mathbf{V}}. \tag{2.67}$$

Since

$$\frac{\partial \lambda}{\partial \mathbf{V}} = \frac{\partial \lambda}{\partial \mathbf{U}} \frac{\partial \mathbf{U}}{\partial \mathbf{V}}, \tag{2.68}$$

we get:

$$(\nabla_{\mathbf{V}} \cdot \lambda) \mathbf{r}_{\mathbf{V}} = (\nabla_{\mathbf{U}} \cdot \lambda) J_{\mathbf{U}} (J_{\mathbf{U}}^{-1} \mathbf{r}_{\mathbf{U}}) = (\nabla_{\mathbf{U}} \cdot \lambda) \mathbf{r}_{\mathbf{U}} \tag{2.69}$$

The quantity doesn't depend on the choice of unknown, if we choose the right eigenvectors as $\mathbf{r}_{\mathbf{U}} = J_{\mathbf{U}} \mathbf{r}_{\mathbf{V}}$.

2.3.1.1. Region where 3 characteristic fields are all genuinely nonlinear

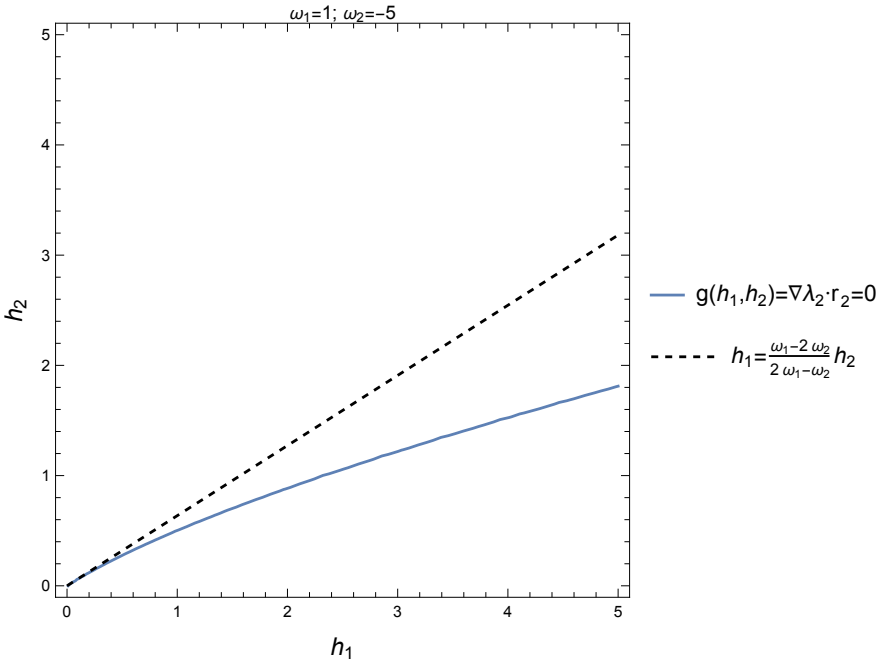

(a) $\omega_1 = 1$; and $\omega_2 = -5$

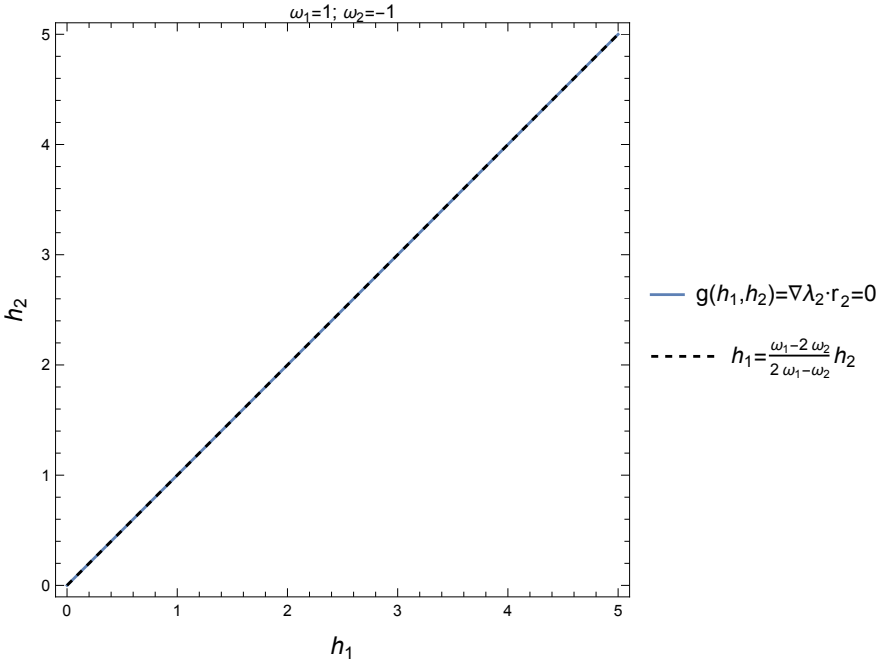

(b) $\omega_1 = 1$; and $\omega_2 = -1$

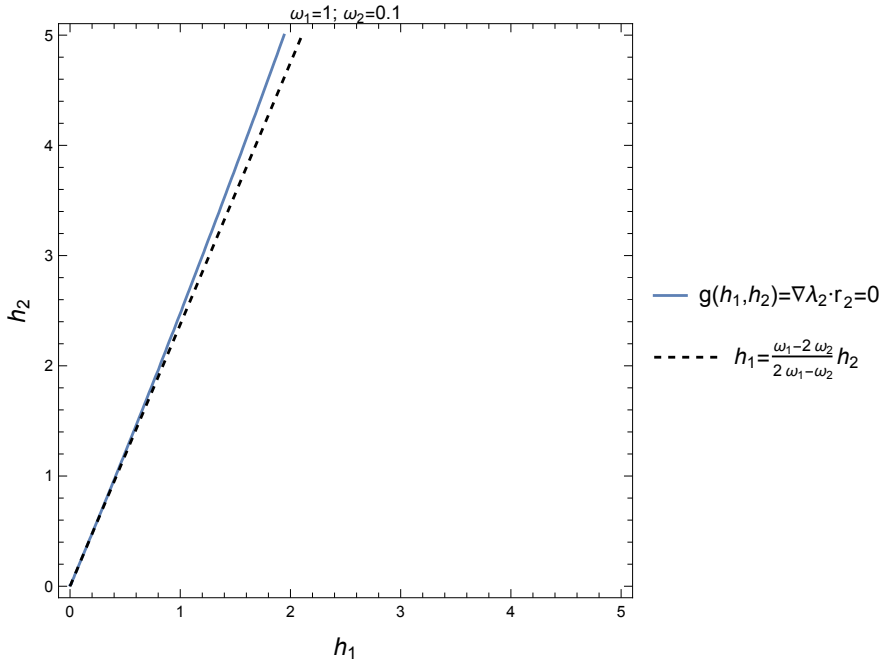

(c) $\omega_1 = 1$; and $\omega_2 = 0.1$

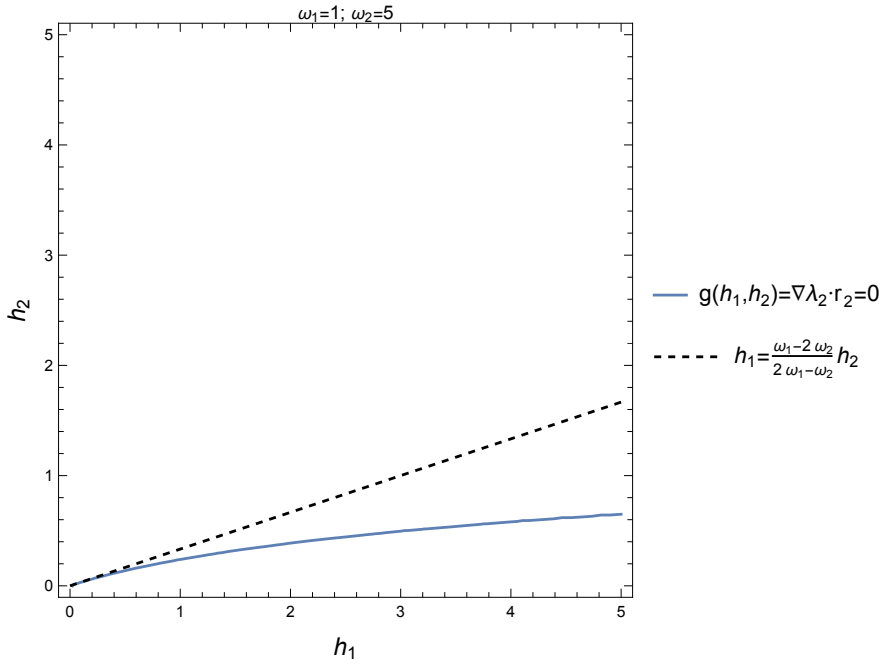

(d) $\omega_1 = 1$; and $\omega_2 = 5$

Figure 2.8. – The blue continuous curves are level sets of $g(h_1, h_2) = \nabla\lambda_2 \cdot \mathbf{r}_2 = 0$; The dashed black lines are the tangent lines to $g = 0$ at $h_1 = h_2 = 0$, The expression of the tangent lines is: $h_1 = \dfrac{\omega_1 - 2\omega_2}{2\omega_1 - \omega_2} h_2$

$\nabla\lambda_j$ and $\mathbf{r}_j$ are both independent of v_0. Thus we use only the plane (h_1, h_2). The fast and slow characteristic fields are observed always genuinely nonlinear, $\nabla\lambda_j \cdot \mathbf{r}_j \neq 0$, $j = 1, 3$. However, the second characteristic field is neither genuinely nonlinear nor linear degenerate. Therefore the scalar-valued function,

$$g(h_1, h_2) \coloneqq \nabla\lambda_2(h_1, h_2) \cdot \mathbf{r}_2(h_1, h_2) \tag{2.70}$$

can vanish. Since $g(h_1, h_2)$ is only depends on h_1 and h_2, the contour plot of $g(h_1, h_2) = 0$ can be drawn on (h_1, h_2)-plane. In Fig. 2.8 four example cases are shown, in which $\omega_1 = 1$ is fixed, and $\omega_2 = -5, -1, 0.1, 5$ respectively. The contour plot $g(h_1, h_2) = 0$ is shown in blue in Fig. 2.8. To understand the behavior of the curve, the tangent lines to the continuous curves at $h_1 = h_2 = 0$ are studied. By using Wolfram Mathematica, the tangent lines can be simplified to:

$$h_1 = \gamma h_2; \quad \gamma = \frac{\omega_1 - 2\omega_2}{2\omega_1 - \omega_2}. \tag{2.71}$$

This tangent line is shown as the dashed line in Fig. 2.8. If $\omega_1 = -\omega_2$, the curve $g(h_1, h_2) = 0$ becomes the straight line $h_1 = h_2$ (see Fig. 2.8b). This line will also be the Rankine-Hugoniot curve of a potential-like flow ($\Omega = 0$). To have the second characteristic field neither genuinely nonlinear nor linear degenerate, in positive h_1 and h_2 domain, we required $\gamma > 0$. Therefore, for $\omega_2 \neq 0$, when $\dfrac{|\omega_1|}{|\omega_2|} < \dfrac{1}{2}$ or $\dfrac{|\omega_1|}{|\omega_2|} > 2$, the second characteristic field is neither genuinely nonlinear nor linear degenerate. In other words, when $\dfrac{1}{2} \leq \dfrac{|\omega_1|}{|\omega_2|} \leq 2$, the three characteristic fields are genuinely nonlinear. The red region in Fig. 2.9, is the region where the all characteristic fields are genuinely nonlinear.

2.3.2. Convexity of energy

The total energy of the system is defined as $E \coloneqq he$. It depends on the water depth of the two layers h_1 and h_2 and the total flux, $Q \coloneqq hU$.

$$E(h_1, h_2, Q) = he = \frac{Q^2}{2h} + \frac{1}{2}gh^2 + \frac{1}{2}f_1; \quad f_1 = \frac{h_1 h_2 h \Omega^2}{4} + \frac{\omega_1^2 h_1^3}{12} + \frac{\omega_2^2 h_2^3}{12}. \tag{2.72}$$

The Hessian matrix of the total energy is,

$$E'' = \begin{bmatrix} E_{h_1h_1} & E_{h_1h_2} & E_{h_1Q} \\ E_{h_1h_2} & E_{h_2h_2} & E_{h_2Q} \\ E_{h_1Q} & E_{h_2Q} & E_{QQ} \end{bmatrix}, \tag{2.73}$$

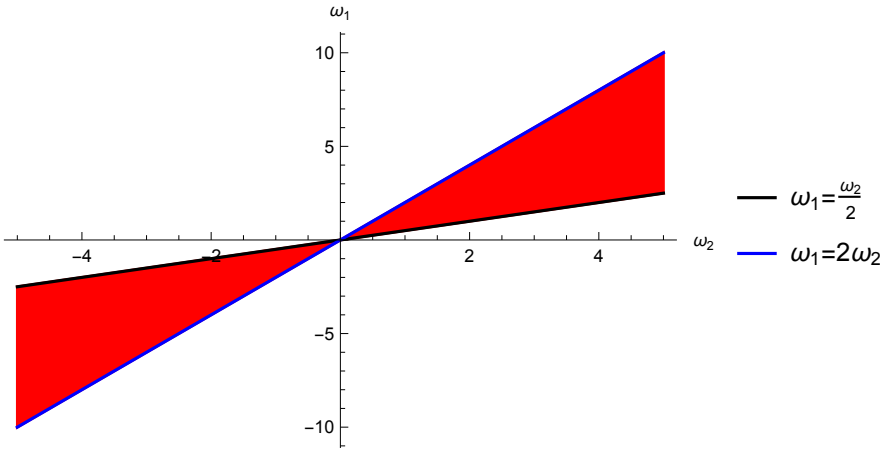

Figure 2.9. – The 3 characteristic fields are genuinely nonlinear in the red region $\frac{1}{2} \leq \frac{|\omega_1|}{|\omega_2|} \leq 2$

.

with

$$
\begin{aligned}
E_{h_1h_1} &= \frac{Q^2}{h^3} + g + \frac{1}{2}\frac{\partial^2 f_1}{\partial h_1^2}, \\
E_{h_1h_2} &= \frac{Q^2}{h^3} + g + \frac{1}{2}\frac{\partial^2 f_1}{\partial h_1 \partial h_2}, \\
E_{h_2h_2} &= \frac{Q^2}{h^3} + g + \frac{1}{2}\frac{\partial^2 f_1}{\partial h_2^2}, \\
E_{h_1Q} = -\frac{Q}{h^2}, \quad E_{h_2Q} &= -\frac{Q}{h^2}, \quad E_{QQ} = \frac{1}{h}, \\
\frac{\partial^2 f_1}{\partial h_1^2} &= \frac{\omega_1 h_1 + \Omega h_2}{2}\left(\omega_1 + \frac{h_2^2}{h^2}(\omega_1 - \omega_2)\right), \\
\frac{\partial^2 f_1}{\partial h_2^2} &= \frac{\omega_2 h_2 + \Omega h_1}{2}\left(\omega_2 + \frac{h_1^2}{h^2}(\omega_2 - \omega_1)\right), \\
\frac{\partial^2 f_1}{\partial h_1 \partial h_2} &= \frac{1}{2h}(\omega_1 h_1 + \Omega h_2)(\omega_2 h_2 + \Omega h_1).
\end{aligned}
$$

The first principal minor is $E_{h_1h_1}$. Consider a special case when $Q = 0$, and $\omega_1 = 0$, then the principal minor of the Hessian matrix of total energy E'' takes the form:

$$
E_{h_1h_1} = g + \frac{\omega_2 h_2^2}{4h}\left(-\frac{h_2^2}{h^2}\right) = g - \frac{\omega_2 h_2^4}{4h^3}. \tag{2.74}
$$

Therefore, as long as $4gh^3 < \omega_2 h_2^4$, $E_{h_1h_1}$ is negative. Then the Hessian matrix of the total energy E'' is not positive definite. In other words, the total energy E is not a convex function.

2.3.2.1. Study of convexity of energy when all characteristic fields are genuinely nonlinear

Consider the special case where all characteristic fields are genuinely nonlinear (the red region in Fig. 2.9). If we define $\alpha \coloneqq \dfrac{\omega_1}{\omega_2}$, then in this region, we have:

$$\frac{1}{2} < \alpha < 2. \tag{2.75}$$

Therefore, we can have the following relations:

$$\begin{aligned}
\omega_1 h_1 + \Omega h_2 &= \alpha\omega_2 h_1 + (\alpha\omega_2 h_1 + \omega_2 h_2)\frac{h_2}{h} \\
&= \frac{\omega_2}{h}\left(\alpha h_1^2 + 2\alpha h_1 h_2 + h_2^2\right) = \frac{\omega_2}{h}\left(\alpha h^2 + (1-\alpha)h_2^2\right), \\
\omega_2 h_2 + \Omega h_1 &= \frac{\omega_2}{h}\left(h^2 - (1-\alpha)h_1^2\right), \\
\omega_1 + \frac{h_2^2}{h^2}(\omega_1 - \omega_2) &= \frac{\omega_2}{h^2}\left(\alpha h^2 - (1-\alpha)h_2^2\right), \\
\omega_2 + \frac{h_1^2}{h^2}(\omega_2 - \omega_1) &= \frac{\omega_2}{h^2}\left(h^2 + (1-\alpha)h_1^2\right).
\end{aligned}$$

First principal minor of E''

The first principal minor is just $E_{h_1h_1}$,

$$E_{h_1h_1} = \frac{Q^2}{h^3} + g + \frac{1}{2}\frac{\partial^2 f_1}{\partial h_1^2}.$$

Notice that $\dfrac{Q^2}{h^3}$, and g are both non-negative terms, and with the above relations, the last term $\dfrac{\partial^2 f_1}{\partial h_1^2}$ can be further simplified:

$$\begin{aligned}
\frac{\partial^2 f_1}{\partial h_1^2} &= \frac{\omega_1 h_1 + \Omega h_2}{2}\left(\omega_1 + \frac{h_2^2}{h^2}(\omega_1 - \omega_2)\right) \\
&= \frac{\omega_2^2}{2h^3}\left(\alpha h^2 + (1-\alpha)h_2^2\right)\left(\alpha h^2 - (1-\alpha)h_2^2\right) \\
&= \frac{\omega_2^2}{2h^3}\left(\alpha^2 h^4 - (1-\alpha)^2 h_2^4\right) \\
&> \frac{\omega_2^2 h_2^4}{2h^3}\left(\alpha^2 - (1-\alpha)^2\right) = \frac{\omega_2^2 h_2^4}{2h^3}(2\alpha - 1).
\end{aligned}$$

Since $\dfrac{1}{2} < \alpha < 2$, then $\dfrac{\partial^2 f_1}{\partial h_1^2} > 0$. Therefore, the first principal minor, $E_{h_1h_1} > 0$.

Second principal minor of E''

The second principal minor is the determinant of the following matrix:

$$\det\left(\begin{bmatrix} E_{h_1h_1} & E_{h_1h_2} \\ E_{h_1h_2} & E_{h_2h_2} \end{bmatrix}\right) = \frac{1}{2}\left(\frac{Q^2}{h^3} + g\right)A + \frac{1}{4}B,$$

$$A = \frac{\partial^2 f_1}{\partial h_1^2} + \frac{\partial^2 f_1}{\partial h_2^2} - 2\frac{\partial^2 f_1}{\partial h_1 h_2}, \tag{2.76}$$

$$B = \frac{\partial^2 f_1}{\partial h_1^2}\frac{\partial^2 f_1}{\partial h_2^2} - \left(\frac{\partial^2 f_1}{\partial h_1 h_2}\right)^2. \tag{2.77}$$

Since the coefficients of the terms A and B are both positive, it is necessary to know if there is a region that makes both terms A and B negative. In fact, such a region exists, indicating that the second principal minor of E'' can be negative, or, in other words, the total energy E is not a convex function. The following shows a way to find such a region. With the definition of $\alpha \coloneqq \frac{\omega_1}{\omega_2}$, the term A can be simplified:

$$\begin{aligned}
\frac{\partial^2 f_1}{\partial h_1^2} + \frac{\partial^2 f_1}{\partial h_2^2} - 2\frac{\partial^2 f_1}{\partial h_1 h_2} &= \frac{\omega_2^2}{2h^3}\Big\{\alpha^2 h^4 - (1-\alpha)^2 h_2^4 + h^4 - (1-\alpha)^2 h_1^4 - \\
&\qquad 2\left(\alpha h^2 + (1-\alpha)h_2^2\right)\left(h^2 - (1-\alpha)h_1^2\right)\Big\} \\
&= \frac{\omega_2^2}{2h^3}\Big\{(1-\alpha)^2 h^4 - (1-\alpha)^2\left(h_1^4 + h_2^4\right) + \\
&\qquad 2(1-\alpha)^2 h_1^2 h_2^2 - 2(1-\alpha)h^2 h_2^2 + 2\alpha(1-\alpha)h^2 h_1^2\Big\} \\
&= \frac{\omega_2^2}{2h^3}\Big\{(1-\alpha)^2 h^4 - (1-\alpha)^2\left(h_1^2 - h_2^2\right)^2 - \\
&\qquad 2(1-\alpha)h^2 h_2^2 + 2\alpha(1-\alpha)h^2 h_1^2\Big\} \\
&= \frac{\omega_2^2}{h}(1-\alpha)\left\{2(1-\alpha)h_1 h_2 - h_2^2 + \alpha h_1^2\right\}
\end{aligned} \tag{2.78}$$

Further assuming that $h_2 = \alpha\beta h_1$, where β is a positive number. The term A can be further simplified:

$$\begin{aligned}
\frac{\partial^2 f_1}{\partial h_1^2} + \frac{\partial^2 f_1}{\partial h_2^2} - 2\frac{\partial^2 f_1}{\partial h_1 h_2} &= \frac{\omega_2^2 h_1^2}{h}\alpha(1-\alpha)\left\{2(1-\alpha)\beta - \alpha\beta^2 + 1\right\} \\
&= \frac{\omega_2^2 h_1^2}{h}\alpha(1-\alpha)\left\{2\beta + 1 - \beta(2+\beta)\alpha\right\}
\end{aligned} \tag{2.79}$$

Since $\frac{\omega_2^2 h_1^2}{h}\alpha$ is positive, term A can be negative if and only if the rest of the term is negative. And since we know $\frac{1}{2} < \alpha < 2$, the term A can be studied in two cases:

1. $1-\alpha < 0 \Leftrightarrow 1 < \alpha < 2$
   To have $A < 0$, we require $2\beta + 1 - \beta(2+\beta)\alpha > 0$, which means, $\alpha\beta^2 + 2(\alpha - 1)\beta - 1 < 0$, therefore,

$$0 < \beta < \frac{(1-\alpha) + \sqrt{2\alpha^2 - 2\alpha + 1}}{\alpha^2}$$

2. $1-\alpha > 0 \Leftrightarrow \frac{1}{2} < \alpha < 1$
   To have $A < 0$, we require $2\beta + 1 - \beta(2+\beta)\alpha < 0$, which means, $\alpha\beta^2 + 2(\alpha - 1)\beta - 1 > 0$, therefore,

$$\beta > \frac{(1-\alpha) + \sqrt{2\alpha^2 - 2\alpha + 1}}{\alpha^2}$$

The term B with the definition of α can be written and simplified as:

$$\begin{aligned}
\frac{\partial^2 f_1}{\partial h_1^2}\frac{\partial^2 f_1}{\partial h_2^2} - \left(\frac{\partial^2 f_1}{\partial h_1 h_2}\right)^2 &= \frac{\omega_2^4}{4h^6}\left(\alpha h^2 + (1-\alpha)h_2^2\right)\left(\alpha h^2 - (1-\alpha)h_2^2\right) \times \\
&\qquad \left(h^2 + (1-\alpha)h_1^2\right)\left(h^2 - (1-\alpha)h_1^2\right) \\
&\quad - \frac{\omega_2^4}{4h^6}\left(\alpha h^2 + (1-\alpha)h_2^2\right)^2\left(h^2 - (1-\alpha)h_1^2\right)^2 \\
&= \frac{\omega_2^4}{4h^6}\left(\alpha h^2 + (1-\alpha)h_2^2\right)\left(h^2 - (1-\alpha)h_1^2\right) \times \\
&\qquad \Big\{\left(\alpha h^2 - (1-\alpha)h_2^2\right)\left(h^2 + (1-\alpha)h_1^2\right) \\
&\qquad\quad - \left(\alpha h^2 + (1-\alpha)h_2^2\right)\left(h^2 - (1-\alpha)h_1^2\right)\Big\} \\
&= \frac{\omega_2^4}{2h^4}\left(\alpha h^2 + (1-\alpha)h_2^2\right)\left(h^2 - (1-\alpha)h_1^2\right)\left\{(1-\alpha)\left(\alpha h_1^2 - h_2^2\right)\right\}.
\end{aligned}$$

Notice that $\alpha h^2 + (1-\alpha)h_2^2 > \alpha h_2^2 + (1-\alpha)h_2^2 = h_2^2 > 0$, and $h^2 - (1-\alpha)h_1^2 > h_1^2 - (1-\alpha)h_1^2 = \alpha h_1^2 > 0$. Again, letting $h_2 = \alpha\beta h_1$, the term B can also be studied in two cases:

1. $1-\alpha < 0 \Leftrightarrow 1 < \alpha < 2$
   To have $B < 0$, we require $1 - \beta^2\alpha > 0$, which means,

$$0 < \beta < \frac{1}{\sqrt{\alpha}}$$

2. $1-\alpha > 0 \Leftrightarrow \frac{1}{2} < \alpha < 1$

To have $B < 0$, we require $1 - \beta^2\alpha < 0$, which means,

$$\beta > \frac{1}{\sqrt{\alpha}}$$

Combined with both cases and with both coefficients of the term A and B being positive, therefore, the region where the second principal minor of E'' is negative can be defined, which is shown in red in Fig. 2.10. In other words, the Hessian matrix of total energy E'' is not always positive definite (it can be negative in the red region). This means that the total energy is not a convex function in the region where the vorticity field is genuinely nonlinear.

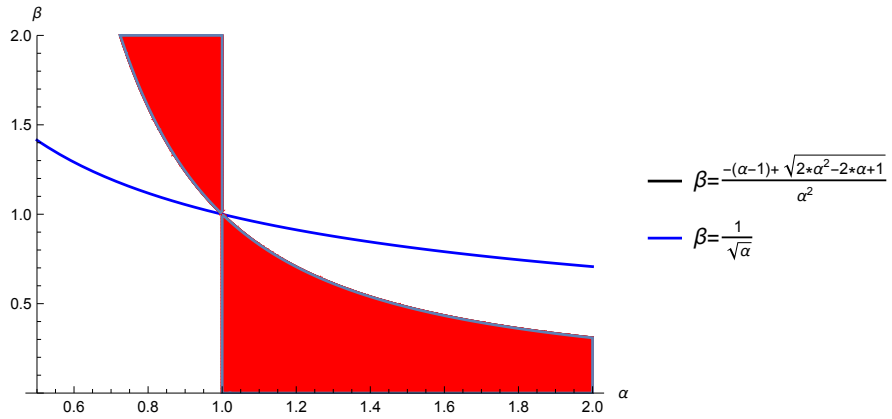

Figure 2.10. – The second principal minor of E'' is negative in the red region, which implies the total energy is not a convex function. The black line is where the term $A = 0$; and the blue line is where the term $B = 0$.

Third principal minor of E''

The third principal minor of E'' is the determinant of the matrix E'' itself. With the case $Q = 0$, the Hessian matrix E'', Eqn. (2.73) would reduce to:

$$E''(h_1, h_2, Q = 0) = \begin{bmatrix} E_{h_1h_1} & E_{h_1h_2} & 0 \\ E_{h_1h_2} & E_{h_2h_2} & 0 \\ 0 & 0 & \frac{1}{h} \end{bmatrix}. \tag{2.80}$$

which share the same condition as the second principal minor of E''.

In summary, the total energy E is not a convex function, which means that the system cannot be symmetrized using the Godunov, Friedrichs, and Lax method.

2.3.3. Rankine-Hugoniot locus and "entropy" inequality

It is convenient to use the mass conservation equations in both two layers (Eqn. (2.44), Eqn. (2.45)), and the momentum equation (Eqn. (2.50)) to derive the jump relations of a two-layer flow with continuous velocity profile.

$$h_{1t} + (\overline{u}_1 h_1)_x = 0; \quad \overline{u}_1 = v_0 + \frac{\omega_1 h_1}{2}, \tag{2.81}$$

$$h_{2t} + (\overline{u}_2 h_2)_x = 0; \quad \overline{u}_2 = v_0 + \omega_1 h_1 + \frac{\omega_2 h_2}{2}, \tag{2.82}$$

$$(hU)_t + \left(hU^2 + p\right)_x = 0. \quad h = h_1 + h_2. \tag{2.83}$$

Here, the average velocity is defined as: $U \coloneqq \dfrac{h_1\overline{u}_1 + h_2\overline{u}_2}{h}$; the average vorticity is: $\Omega \coloneqq \dfrac{h_1\omega_1 + h_2\omega_2}{h}$; and the modified pressure for the system $p \coloneqq \dfrac{1}{2}gh^2 + f_1$, where $f_1 = \dfrac{h_1 h_2 h\Omega^2}{4} + \dfrac{\omega_1^2 h_1^3}{12} + \dfrac{\omega_2^2 h_2^3}{12}$. The energy equation for the system can be written:

$$(he)_t + (hUe + Up + f_2)_x = 0, \tag{2.84}$$

where $e = \dfrac{1}{2}U^2 + \dfrac{1}{2}gh + \dfrac{f_1}{2h}$, and $f_2 = \dfrac{h_1^2 h_2^2 \Omega^2(\omega_2 - \omega_1)}{8}$.

2.3.3.1. Rankine-Hugoniot locus

Apply the Rankine-Hugoniot conditions Eqn. (2.4) to the above system, the jump relations of two-layer stratified flow with continuous velocity profile across a shock with the velocity of the shock $D \coloneqq \dfrac{x}{t}$ are given as follows:

$$[h_1(\bar{u}_1 - D)] = 0 \tag{2.85}$$

$$[h_2(\bar{u}_2 - D)] = 0 \tag{2.86}$$

$$[hU(U - D) + p] = 0 \Leftrightarrow [p] + m^2[\tau] = 0, \tag{2.87}$$

where mass flux through the shock is defined as before, $m = h^+(U^+ - D) = h^-(U^- - D)$, which is a non-zero constant. Here, h^+ and U^+ are water depth and average velocity before the shock; and h^- and U^- are water depth and averaged velocity after the shock.

Given the state before the shock $\mathbf{U}^+ = (h_1^+, h_2^+, U^+)^T$, the constant vorticities in both layers ω_1, ω_2, and the mass flux m, we can have a unique solution to the system of two layers flow with unknown variable $\mathbf{U}^- = (h_1^-, h_2^-, U^-)^T$. Therefore, with a fixed state before the shock $\mathbf{U}^+ = (h_1^+, h_2^+, U^+)^T$, and changing the value of mass flux m, the Rankine-Hugoniot locus $\mathcal{H}(h_1^-, h_2^-)$ defined by Eqn.(2.85) to Eqn. (2.87) can be constructed on (h_1^-, h_2^-)-plane.

2.3.3.2. "Entropy" inequality

The "entropy" inequality of the system takes the form,

$$
\begin{aligned}
\mathcal{E} &:= -D[he] + [hUe + Up + f_2] \\
&= [he(U-D) + up + f_2] \\
&= \left[\frac{1}{2}U^2 h(U-D) + p\tau h(U-D) - \frac{1}{2}f_1\tau h(U-D) + p\tau h(U-D) + Dp + f_2\right] \\
&= \left[\frac{1}{2}h(U-D)^3 + 2p\tau h(U-D) - \frac{1}{2}f_1\tau h(U-D) + f_2\right] \\
&= m\left[\frac{1}{2}m^2\tau^2 + 2p\tau - \frac{1}{2}f_1\tau + \frac{f_2}{m}\right] \\
&= m\left[-\frac{1}{2}p(\tau^+ + \tau^-) + 2p\tau - \frac{1}{2}f_1\tau + \frac{f_2}{m}\right] \qquad (2.88) \\
&= -\frac{mg[h]^3}{4h^+h^-} + m\left[-\frac{1}{2}f_1(\tau^+ + \tau^-) + 2f_1\tau - \frac{1}{2}f_1\tau + \frac{f_2}{m}\right] \\
&= -\frac{mg[h]^3}{4h^+h^-} + m\left[-\frac{1}{2}f_1(\tau^+ + \tau^-) + \frac{3}{2}f_1\tau + \frac{f_2}{m}\right]. \qquad (2.89)
\end{aligned}
$$

On the other hand, from the jump relation of momentum equation Eqn. (2.87), the mass flux can be transformed in:

$$
m = \pm\sqrt{\frac{-[p]}{[\tau]}}. \qquad (2.90)
$$

For a right-facing shock, the mass flux is negative through the shock, therefore the " $-$ " sign is picked, For a left-facing shock, the " $+$ " sign is picked. Substitute the above relation into the "entropy" inequality $\mathcal{E}$, with given constant vorticities in both layers ω_1, ω_2, and a fixed state before the shock, h_1^+ and h_2^+. Therefore, the "entropy" inequality is now only depends on the state after the shock $\mathcal{E} = \mathcal{E}(h_1^-, h_2^-)$. Finally, a curve $\mathcal{E}(h_1^-, h_2^-) = 0$ can also be plotted on (h_1^-, h_2^-)-plane (see Fig.2.11 for different value of ω_2).

2.4. Numerical results

The following numerical study involves solving the system Eqn. (2.81) to Eqn. (2.83) numerically. The numerical study is based on the HLL method; a brief introduction is presented in the appendix C. For a given state before the shock, $\mathbf{U}^+ = (h_1^+, h_2^+, U^+)^T$, combined with the given constant vorticities in both layers ω_1, ω_2, the curve $\mathcal{E}(h_1^-, h_2^-) = 0$ can be plotted on the (h_1^-, h_2^-)-plane. On the other hand, with the change in mass flux m, the Rankine-Hugoniot locus $\mathcal{H}(h_1^-, h_2^-)$ can also be constructed. The initial state after the shock is chosen from

the Rankine-Hugoniot relations. This means the solution satisfies the Rankine-Hugoniot condition initially. The shock solution is said to be stable when a single shock is presented numerically. Otherwise, the shock is unstable.

2.4.1. The fast characteristic field

For the fast characteristic field, the numerical results are studied with the given state before the shock, $\mathbf{V}^+ = (h_1^+, h_2^+, v_0^+)^T = (1, 2, 0)^T$. We fix the vorticity in the lower layer $\omega_1 = 1$ and change ω_2. Fig. 2.11 shows the evolutions of curves $\mathcal{E}(h_1^-, h_2^-) = 0$ and Rankine-Hugoniot locus $\mathcal{H}(h_1^-, h_2^-)$, with changing vorticity in the upper layer ω_2 from negative to positive numbers. Notice that the intersection of these two curves is the given state before the shock $\mathbf{V}^+ = (h_1^+, h_2^+, v_0^+)^T = (1, 2, 0)^T$, which is marked by " $*$ " in Fig. 2.11.
The curve $\mathcal{E}(h_1^-, h_2^-) = 0$ separates the unstable and stable parts of the Rankine-Hugoniot locus $\mathcal{H}(h_1^-, h_2^-)$.

Fig. 2.12 shows examples of stable and unstable cases. In these figures, the evolution of water depth is shown, the red dotted line represents the initial discontinuity, the solid lines are the total water depth, $h = h_1 + h_2$; the dashed lines are the water depth in the lower layer, h_1. The blue lines show the solution at time $t = 5$; the black lines show the solution at time $t = 10$. Fig. 2.12a and Fig. 2.12b show the stable and unstable cases, respectively, when $\omega_1 = 1$ and $\omega_2 = -2$, the corresponding initial states after the shock are marked as "$\bullet$" and "$\circ$" in Fig. 2.11a. Similarly, Fig. 2.12c and Fig. 2.12d show the stable and unstable cases, respectively, when $\omega_1 = 1$ and $\omega_2 = 2$, the corresponding initial states after the shock are marked as "$\blacksquare$" and "$\square$" in Fig. 2.11h.

In conclusion, as expected, the stability criterion $\mathcal{E} < 0$ for genuinely nonlinear eigenfields guarantees the stability property even in the case of non-convex total energy.

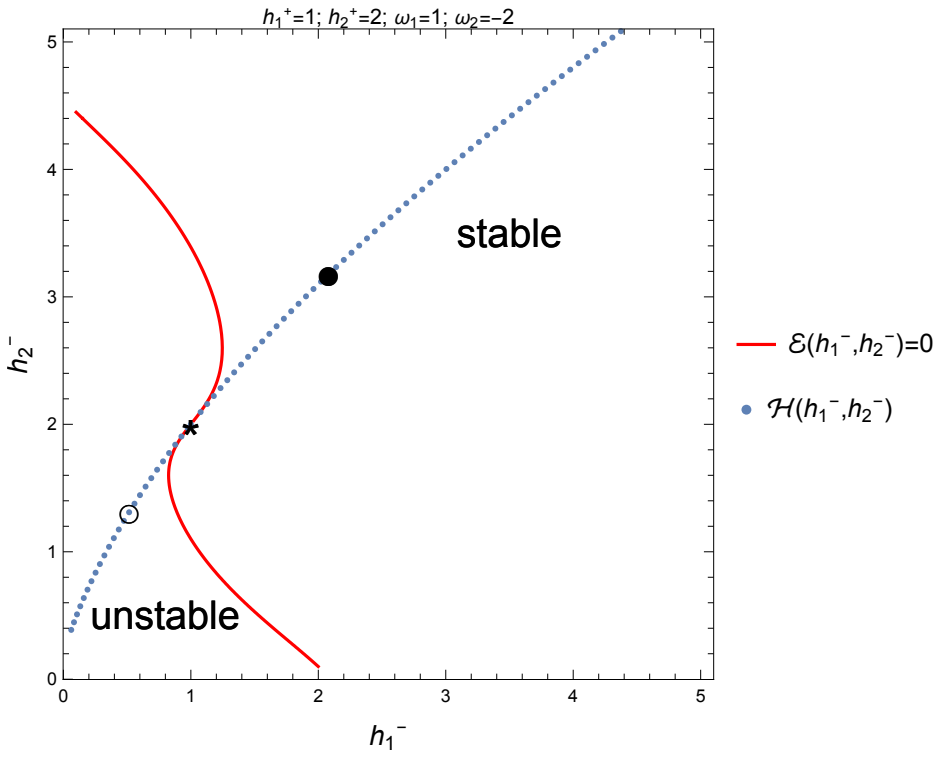

(a) $\omega_2 = -2.0$

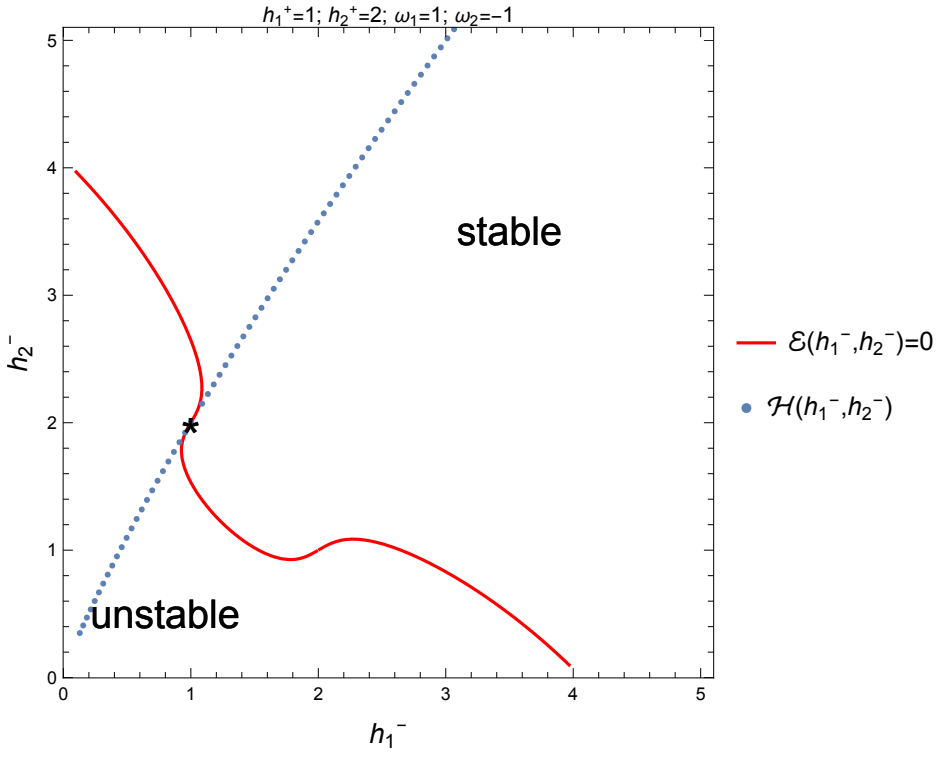

(b) $\omega_2 = -1.0$

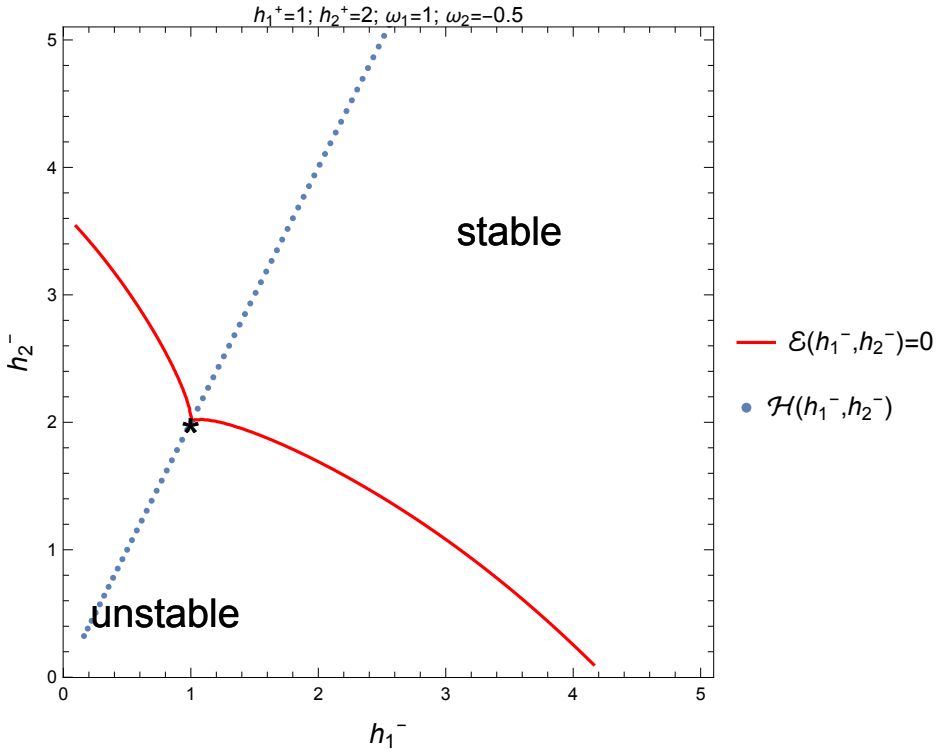

(c) $\omega_2 = -0.5$

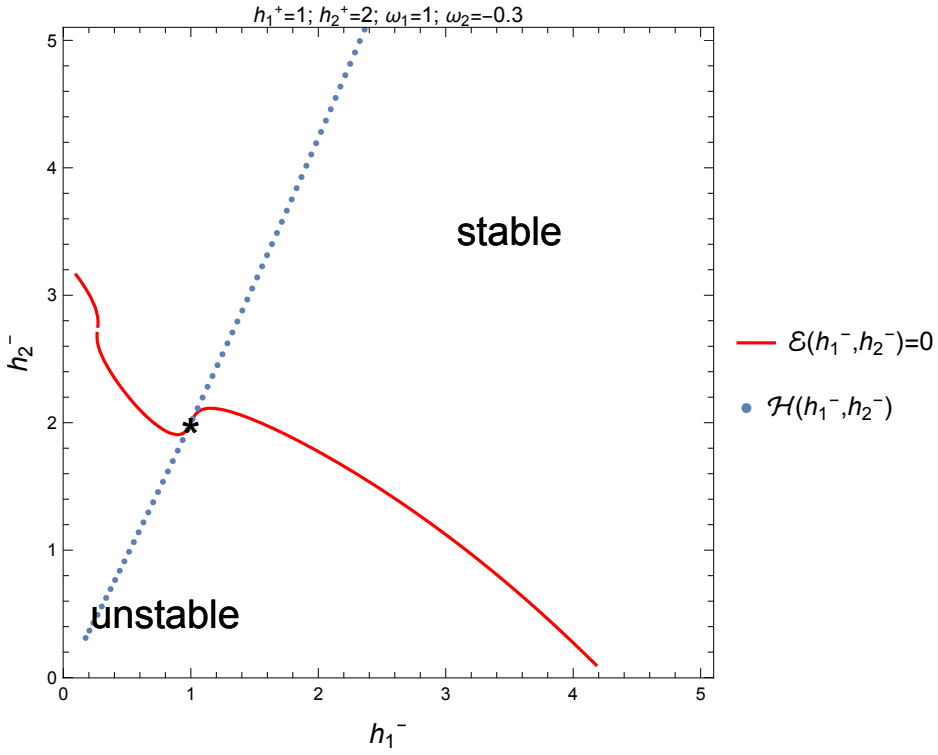

(d) $\omega_2 = -0.3$

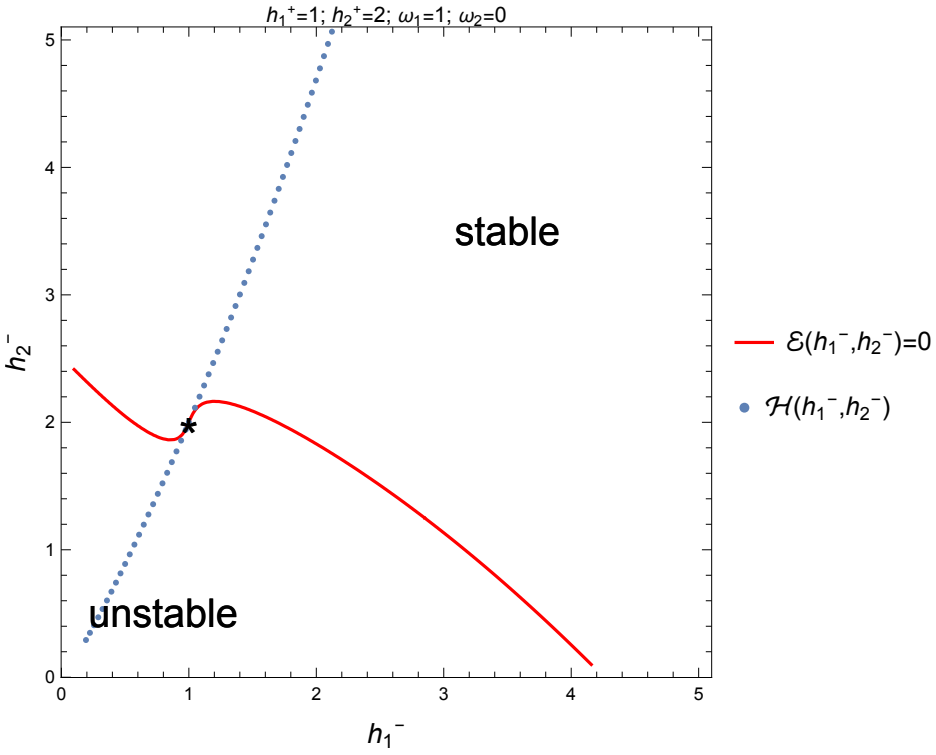

(e) $\omega_2 = 0.0$

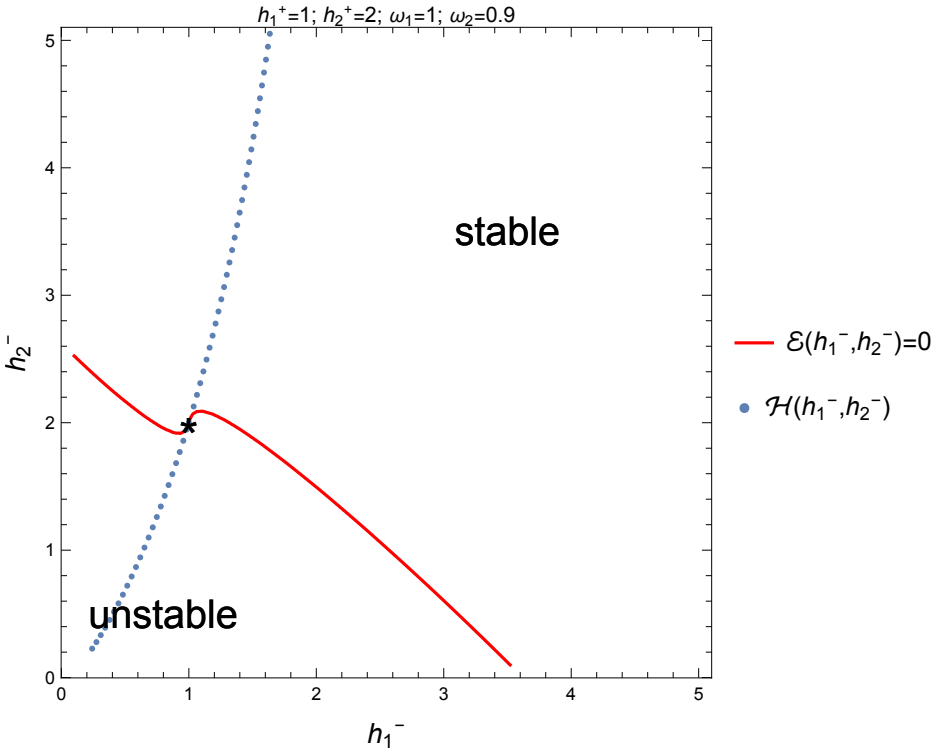

(f) $\omega_2 = 0.9$

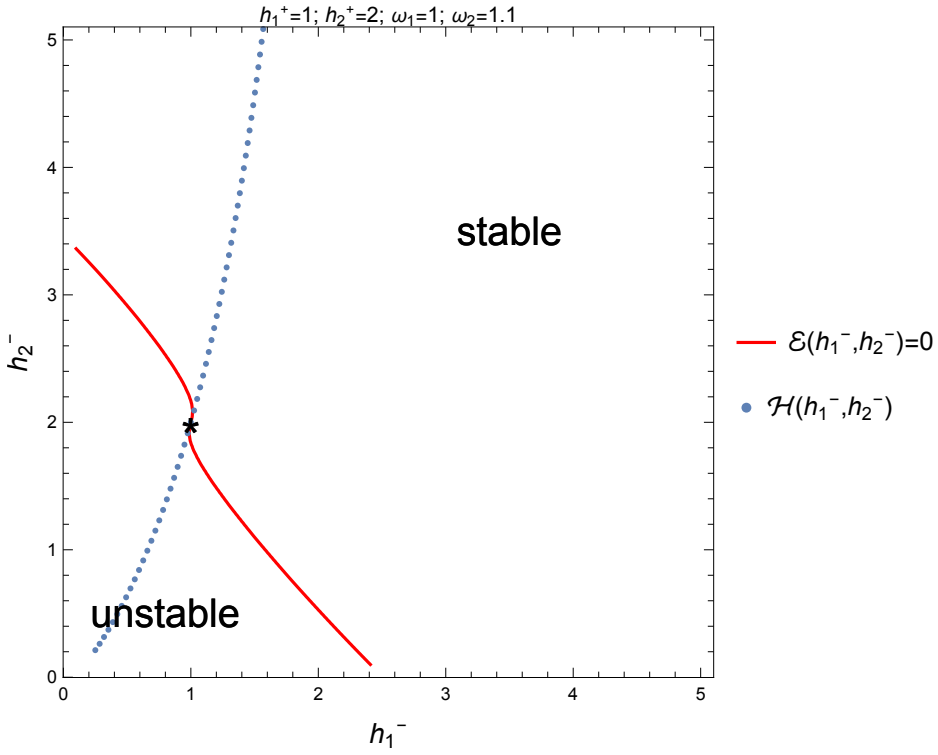

(g) $\omega_2 = 1.1$

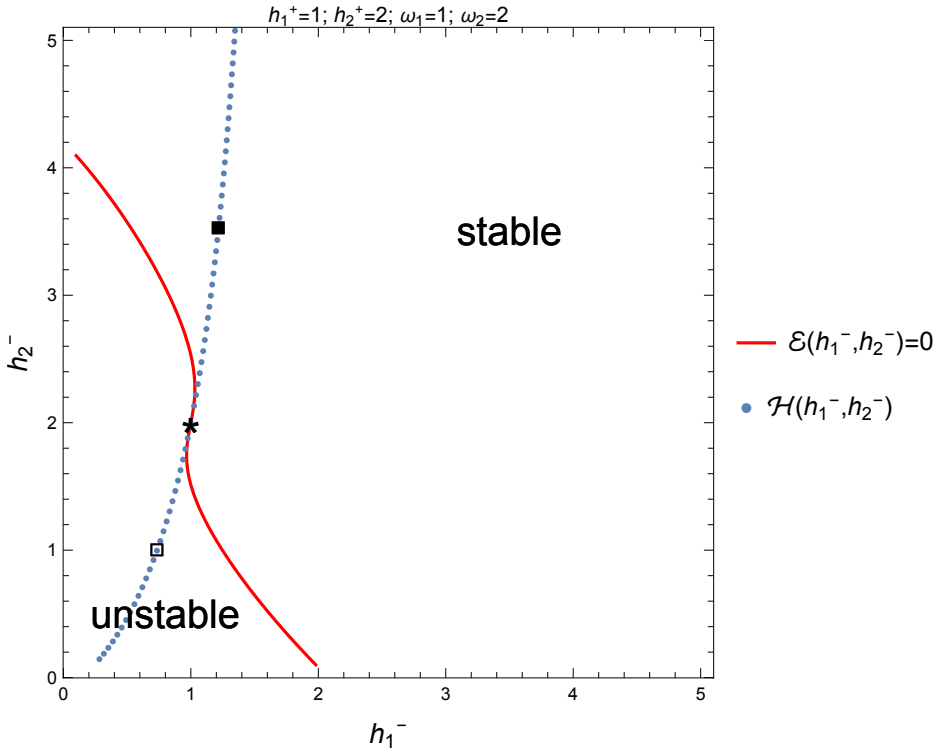

(h) $\omega_2 = 2.0$

Figure 2.11. – The evolutions of $\mathcal{E}(h_1^-, h_2^-) = 0$ and Rankine-Hugoniot locus $\mathcal{H}(h_1^-, h_2^-)$ varying the vorticity in the upper layer ω_2 from negative to positive.

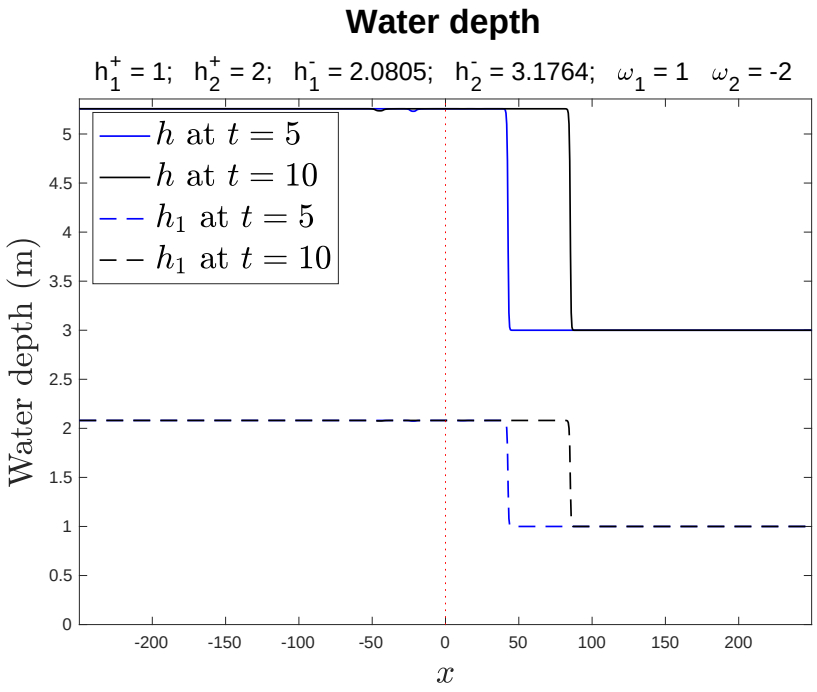

(a) The stable case when $\omega_1 = 1$, and $\omega_2 = -2.0$, the initial state is marked as " • " in Fig. 2.11a

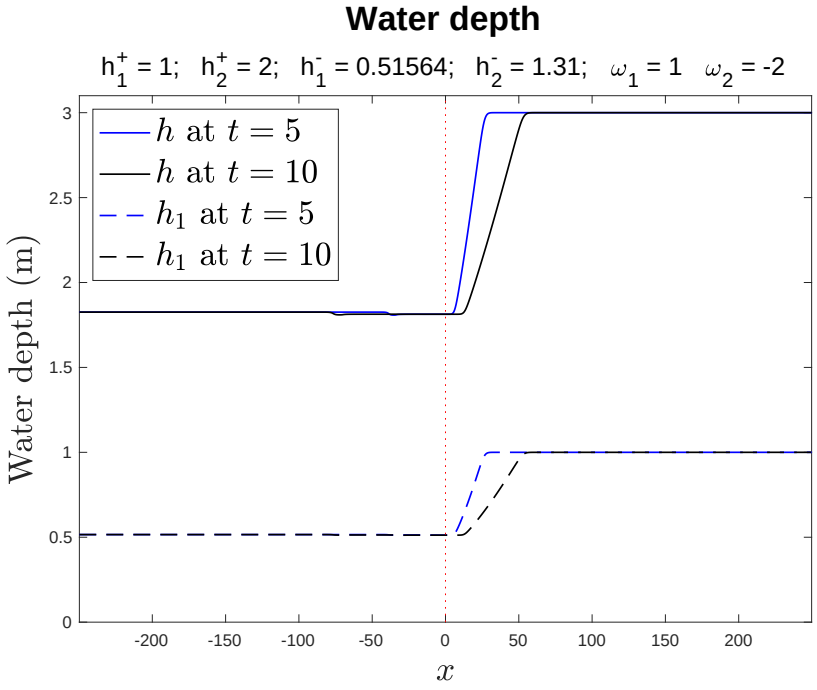

(b) The unstable case when $\omega_1 = 1$, and $\omega_2 = -2.0$, the initial state is marked as " ∘ " in Fig. 2.11a

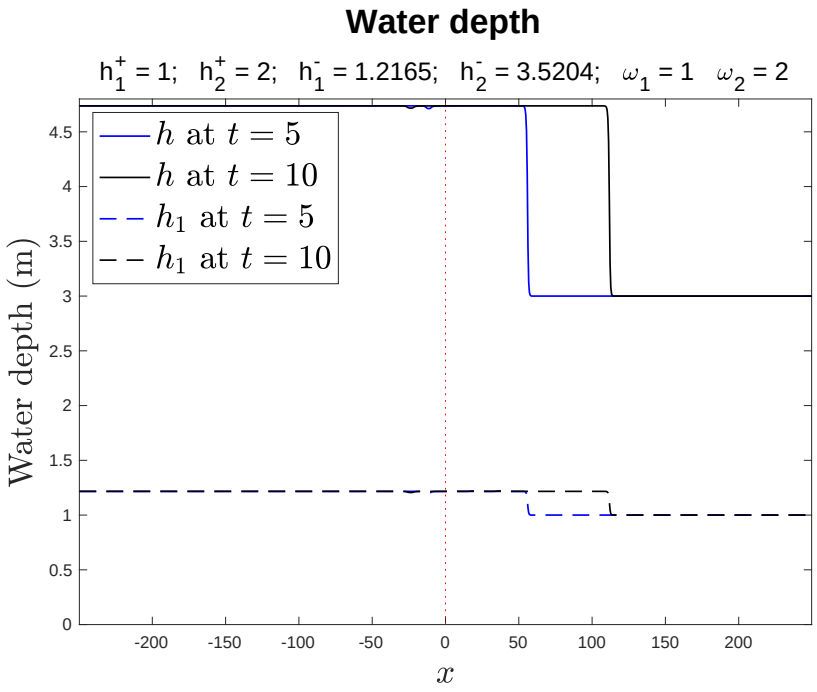

(c) The stable case when $\omega_1 = 1$, and $\omega_2 = 2.0$, the initial state is marked as "■" in Fig. 2.11h

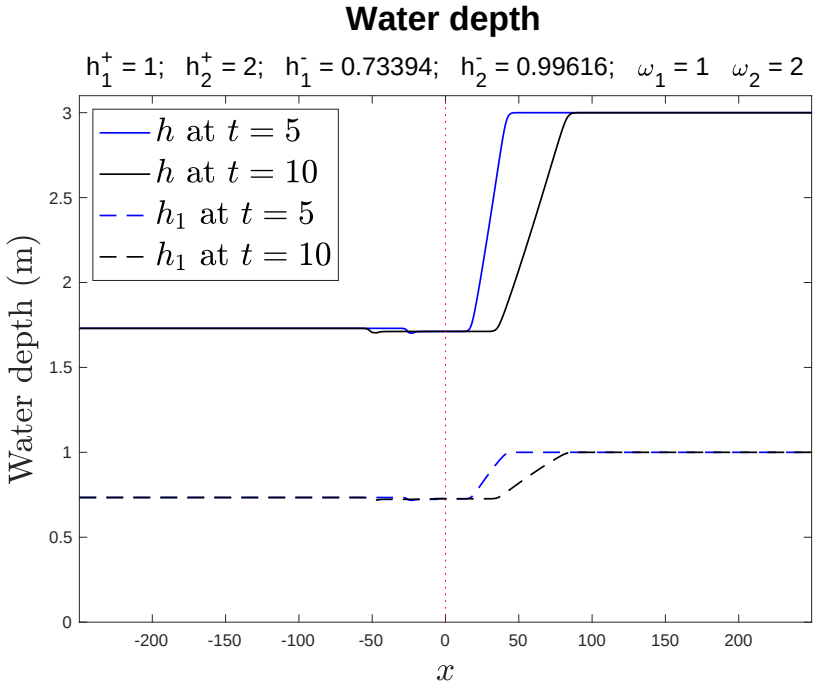

(d) The unstable case when $\omega_1 = 1$, and $\omega_2 = 2.0$, the initial state is marked as "□" in Fig. 2.11h

Figure 2.12. – Numerical results of the points marked in Fig. 2.11.

2.4.1.1. Potential-like flow $\Omega = 0$

As mentioned in section 2.2.2, a particular case refers to the averaged vorticity is zero for all the time, namely the potential-like flow. Thus the relation between h_1 and h_2 can be obtained directly from:

$$\Omega = \frac{h_1\omega_1 + h_2\omega_2}{h} \equiv 0.$$

This implies the relation between h_1 and h_2 is always a straight line: $h_2 = -\frac{\omega_1}{\omega_2}h_1$. The equation of Ω, Eqn. (2.52), is the linear combination of the mass equations in each layer. Thus the Rankine-Hugoniot relation for Ω is a consequence of the Rankine-Hugoniot relation for the mass equations in each layer. This means that $h_2 = -\frac{\omega_1}{\omega_2}h_1$ is also the Rankine-Hugoniot locus $\mathcal{H}(h_1^-, h_2^-)$. On the other hand, from Eqn. (2.88), $\mathcal{E}(h_1^-, h_2^-) = 0$ is a smooth function. Consider $\mathcal{E}$ along the straight line $h_2 = -\frac{\omega_1}{\omega_2}h_1$, the function $\mathcal{E}(h_1^-, h_2^-)$ can be written in the form:

$$\mathcal{E}\left(h_1^-, -\frac{\omega_1}{\omega_2}h_1^-\right) = \tilde{\mathcal{E}}(h_1^-). \tag{2.91}$$

Take the derivative of the above equation, we have the following relation:

$$\mathcal{E}_1 - \frac{\omega_1}{\omega_2}\mathcal{E}_2 = \tilde{\mathcal{E}}', \tag{2.92}$$

$$\mathcal{E}_{11} - 2\frac{\omega_1}{\omega_2}\mathcal{E}_{12} + \left(\frac{\omega_1}{\omega_2}\right)^2 \mathcal{E}_{22} = \tilde{\mathcal{E}}''. \tag{2.93}$$

Here $\mathcal{E}_i \coloneqq \dfrac{\partial \mathcal{E}}{\partial h_i^-}$, $\mathcal{E}_{ij} \coloneqq \dfrac{\partial^2 \mathcal{E}}{\partial h_i^- \partial h_j^-}$, $i = 1, 2$; and $\tilde{\mathcal{E}}' \coloneqq \dfrac{\mathrm{d}\tilde{\mathcal{E}}}{\mathrm{d}h_1^-}$, $\tilde{\mathcal{E}}'' \coloneqq \dfrac{\mathrm{d}^2\tilde{\mathcal{E}}}{\mathrm{d}{h_1^-}^2}$ Define a vector $\mathbf{a} \coloneqq \left(1, -\dfrac{\omega_1}{\omega_2}\right)^T$. The above relations can be written in vector form:

$$\mathbf{a}^T \nabla \mathcal{E} = \tilde{\mathcal{E}}', \tag{2.94}$$

$$\mathbf{a}^T \mathcal{E}'' \mathbf{a} = \tilde{\mathcal{E}}''. \tag{2.95}$$

Here, $\nabla = \left(\dfrac{\partial}{\partial h_1^-}, \dfrac{\partial}{\partial h_2^-}\right)^T$, and $\mathcal{E}''$ is the Hessian matrix of $\mathcal{E}$:

$$\mathcal{E}'' \coloneqq \begin{bmatrix} \mathcal{E}_{11} & \mathcal{E}_{12} \\ \mathcal{E}_{12} & \mathcal{E}_{22} \end{bmatrix}.$$

Along the line $\Omega \equiv 0$, we have the following relations:

$$h_2 = -\frac{\omega_1}{\omega_2} h_1, \tag{2.96}$$

$$f_2 = \frac{h_1^2 h_2^2 \Omega^2 (\omega_2 - \omega_1)}{8} = 0, \tag{2.97}$$

$$f_1 = \frac{h_1 h_2 h \Omega^2}{4} + \frac{\omega_1^2 h_1^3}{12} + \frac{\omega_2^2 h_2^3}{12} = \frac{\omega_1^2 h_1^2}{12} h. \tag{2.98}$$

The total water depth h can also be expressed as a function of h_1, $h = (1-\alpha)h_1 = \left(1 - \frac{\omega_1}{\omega_2}\right) h_1$. Moreover, the mass flux can also be simplified along the line $\Omega \equiv 0$:

$$m = -\sqrt{-\frac{[p]}{[\tau]}} = -\sqrt{-\frac{\left[\frac{1}{2}h^2 + f_1\right]}{[\tau]}} \tag{2.99}$$

$$= -\sqrt{\frac{\frac{(1-\alpha)^2}{2}\left(h_1^{+2} - h_1^{-2}\right) + \frac{(1-\alpha)\omega_1^2}{12}\left(h_1^{+3} - h_1^{-3}\right)}{\frac{h_1^+ - h_1^-}{(1-\alpha)h_1^+ h_1^-}}} \tag{2.100}$$

$$= -(1-\alpha)\sqrt{\frac{h_1^+ h_1^-}{2}\left\{(1-\alpha)\left(h_1^+ + h_1^-\right) + \frac{\omega_1^2}{6}\left(h_1^{+2} + h_1^+ h_1^- + h_1^{-2}\right)\right\}} \tag{2.101}$$

Therefore, m is a smooth function without singularity along the line $\Omega \equiv 0$. With Eqn. (2.89), $\tilde{\mathcal{E}}$ can be expressed as:

$$\begin{aligned}
\tilde{\mathcal{E}}(h_1^-) &= -\frac{mg[h]^3}{4h^+h^-} + m\left[-\frac{1}{2}f_1(\tau^+ + \tau^-) + \frac{3}{2}f_1\tau + \frac{f_2}{m}\right] \\
&= \frac{m}{2}\left\{-\frac{g[h]^3}{2h^+h^-} + \left[3f_1\tau - f_1(\tau^+ + \tau^-)\right]\right\} \\
&= \frac{m}{4}\left\{-\frac{(1-\alpha)g\left(h_1^+ - h_1^-\right)^3}{h_1^+ h_1^-} + \frac{\omega_1^2}{6}\left\{3\left(h_1^{+2} - h_1^{-2}\right) - \left(h_1^{+3} - h_1^{-3}\right)\left(\frac{h_1^+ + h_1^-}{h_1^+ h_1^-}\right)\right\}\right\} \\
&= -\frac{m\left(h_1^+ - h_1^-\right)^3}{4h_1^+ h_1^-}\left\{(1-\alpha)g + \frac{\omega_1^2\left(h_1^+ + h_1^-\right)}{6}\right\}
\end{aligned} \tag{2.102}$$

Because of the term, $\left(h_1^+ - h_1^-\right)^3$, the first and second derivatives of $\tilde{\mathcal{E}}(h_1)$ would vanish at $h_1^- = h_1^+$. Due to Eqn. (2.94) and Eqn. (2.94), this will imply:

$$\mathbf{a}^T \nabla \mathcal{E} = 0, \tag{2.103}$$

$$\mathbf{a}^T \mathcal{E}'' \mathbf{a} = 0, \tag{2.104}$$

at $h_1^- = h_1^+$, $h_2^- = h_2^+$. The first derivative of Eqn. (2.103) takes the form:

$$\mathcal{E}_1 - \frac{\omega_1}{\omega_2}\mathcal{E}_2 = 0.$$

One can check that $\mathcal{E}_1(h_1^- = h_1^+, h_2^- = h_2^+) = 0$. Therefore we get:

$$\nabla\mathcal{E}(h_1^- = h_1^+, h_2^- = h_2^+) = 0. \tag{2.105}$$

On the other hand, from Eqn. (2.104), since the vector $\mathbf{a} := \left(1, -\frac{\omega_1}{\omega_2}\right)^T$, is not a zero vector, then:

$$\det(\mathcal{E}'') \equiv 0, \tag{2.106}$$

at $h_1^- = h_1^+$, $h_2^- = h_2^+$. From the above two relations, Eqn. (2.105) and Eqn. (2.106), we know the curve $\mathcal{E} = 0$ is a cusp. Furthermore, by numerical results, we observed that the angle of the cusp is 0, which be shown in Fig. 2.13.

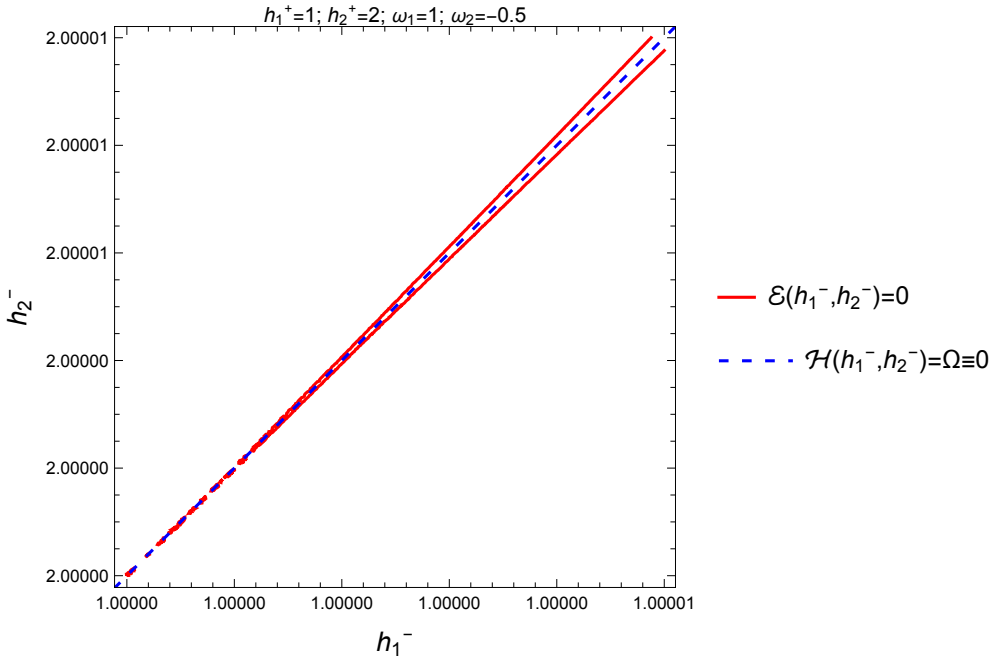

(a) $h_1 = 1; h_2 = 2; \omega_1 = 1; \omega_2 = -0.5$

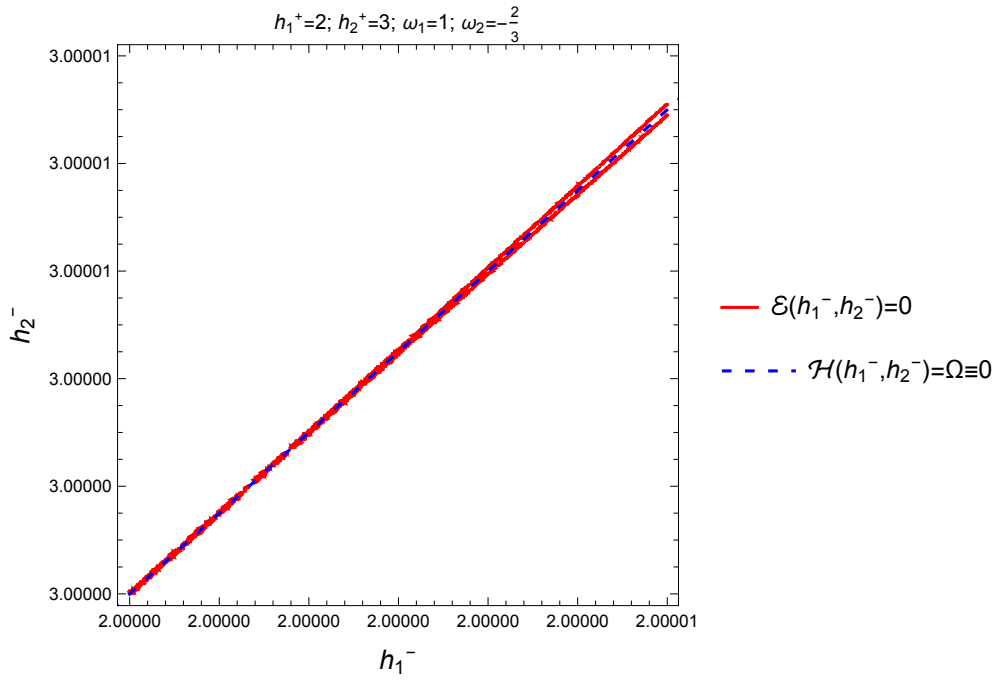

(b) $h_1 = 2; h_2 = 3; \omega_1 = 1; \omega_2 = -\frac{2}{3}$

Figure 2.13. – Numerical results of observing the angle of the cusp when the averaged vorticity is zero $\Omega \equiv 0$.

Moreover, Eqn. (2.106) shows that, the Hessian matrix $\mathcal{E}''$ is a matrix with linearly dependent rows, therefore we can always write $\mathcal{E}_{11} = b\mathcal{E}_{12}$ and $\mathcal{E}_{12} = b\mathcal{E}_{22}$, where b is a constant, when $h_1^- = h_1^+$, $h_2^- = h_2^+$. Therefore, the Hessian matrix $\mathcal{E}''$ can be simplified at $h_1^- = h_1^+$, $h_2^- = h_2^+$ as:

$$\mathcal{E}'' = \begin{bmatrix} \mathcal{E}_{11} & \mathcal{E}_{12} \\ \mathcal{E}_{12} & \mathcal{E}_{22} \end{bmatrix} = \mathcal{E}_{11} \begin{bmatrix} 1 & b \\ b & b^2 \end{bmatrix}. \tag{2.107}$$

Applying it back to Eqn. (2.104), we get:

$$\mathbf{a}^T \mathcal{E}'' \mathbf{a} = \mathcal{E}_{11} - 2\frac{\omega_1}{\omega_2}\mathcal{E}_{12} + \left(\frac{\omega_1}{\omega_2}\right)^2 \mathcal{E}_{22} = \mathcal{E}_{11}\left(1 - \frac{\omega_1}{\omega_2} b\right)^2 = 0. \tag{2.108}$$

One can check that $\mathcal{E}_{11} \neq 0$, thus, $b = \dfrac{\omega_2}{\omega_1}$. Therefore, we have:

$$\mathcal{E}''\mathbf{a} = \mathcal{E}_{11} \begin{bmatrix} 1 & b \\ b & b^2 \end{bmatrix} \begin{bmatrix} 1 \\ -\frac{\omega_1}{\omega_2} \end{bmatrix} = 0. \tag{2.109}$$

This indicated that the vector $\mathbf{a} \coloneqq \left(1, -\dfrac{\omega_1}{\omega_2}\right)^T$, is an eigenvector of $\mathcal{E}''$ with 0 eigenvalue at $h_1^- = h_1^+$, $h_2^- = h_2^+$. The second eigenvalue would be: $\lambda \coloneqq \mathcal{E}_{11}(b^2 + 1)$,

and the corresponding eigenvector is: $\mathbf{b} \coloneqq (1, b)^T$. This is a vector perpendicular to the other eigenvector $\mathbf{a}$. Remark that the eigenvector $\mathbf{a}$ also represents the straight line $\Omega \equiv 0$ and the Rankine-Hugoniot locus $\mathcal{H}(h_1^-, h_2^-)$. Since $\mathcal{E}''$ is a symmetric matrix, the spectral decomposition of it takes the form:

$$\mathcal{E}'' = \lambda \hat{\mathbf{b}} \otimes \hat{\mathbf{b}}; \quad \hat{\mathbf{b}} \coloneqq \frac{\mathbf{b}}{\|\mathbf{b}\|}. \tag{2.110}$$

Therefore $\mathcal{E}$ can be approximated as:

$$\begin{aligned} \mathcal{E} &\approx \frac{1}{2} (\mathbf{h} - \mathbf{h}_0)^T \mathcal{E}_0'' (\mathbf{h} - \mathbf{h}_0) + \mathcal{O}\left(\|\mathbf{h} - \mathbf{h}_0\|^3\right) \\ &= \frac{\lambda \| (\mathbf{h} - \mathbf{h}_0)^T \hat{\mathbf{b}}\|^2}{2}, + \mathcal{O}\left(\|\mathbf{h} - \mathbf{h}_0\|^3\right) \end{aligned} \tag{2.111}$$

where $\mathbf{h}_0 = (h_1^+, h_2^+)^T$, $\mathbf{h} = (h_1^-, h_2^-)^T$, and $\mathcal{E}_0'' \coloneqq \mathcal{E}''(\mathbf{h} = \mathbf{h}_0)$.

2.4.2. The second characteristic field

In this section, numerical studies of the second characteristic field are studied. This corresponds to the pair $(\lambda_2, \mathbf{r}_2)$. Since the second characteristic field can be neither genuinely nonlinear nor linear degenerate in the region when $\frac{|\omega_1|}{|\omega_2|} < \frac{1}{2}$ or $\frac{|\omega_1|}{|\omega_2|} > 2$, the contour plot of the scalar-valued function:

$$g(h_1, h_2) \coloneqq \nabla \lambda_2(h_1, h_2) \cdot \mathbf{r}_2(h_1, h_2) = 0, \tag{2.112}$$

can be drawn on (h_1^-, h_2^-)-plane with given ω_1 and ω_2. Choose a point $\mathbf{V}^+ = (h_1^+, h_2^+, v_0^+)^T$ on curve $g(h_1, h_2) = 0$. Fig. 2.14 shows two examples, with $\omega_1 = 1$ in both cases, and $\omega_2 = -2$ and $\omega_2 = -3$, respectively. The solid black line is the curve $g(h_1, h_2) = 0$; and, as in the previous section, the value given before the shock, $\mathbf{V}^+$ is shown by $'*'$. The solid red line is the curve $\mathcal{E}(h_1^-, h_2^-) = 0$. The Rankine-Hugoniot locus corresponding to the second characteristic field does not necessarily pass through $\mathbf{V}^+$. However, we can still construct a Rankine-Hugoniot locus that satisfies the Lax condition for the characteristic λ_2. Choose a state $\mathbf{V}^-$ from the Rankine-Hugoniot relation and belongs to the "unstable region" $\mathcal{E} > 0$, which is indicated by " $\diamond$ " in Fig. 2.14. However, the corresponding shock is stable (see Fig.2.15) This means that the stability criteria should be formulated in a more precise way for the characteristic field corresponding to the vortex waves. In the case where $\frac{1}{2} \leq \frac{\omega_1}{\omega_2} \leq 2$ the criterion $\mathcal{E} < 0$ is always valid.

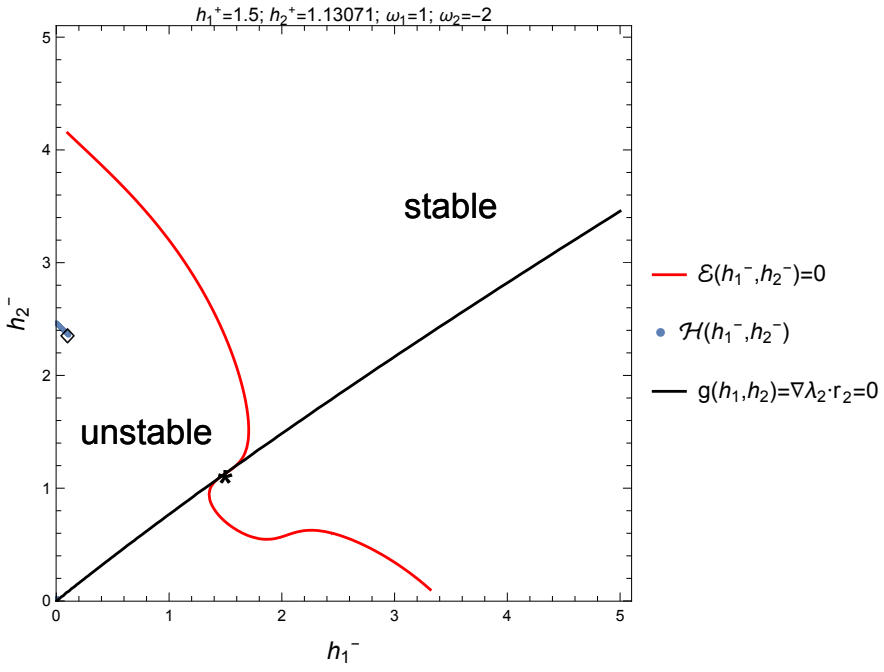

(a) $\omega_2 = -2.0$

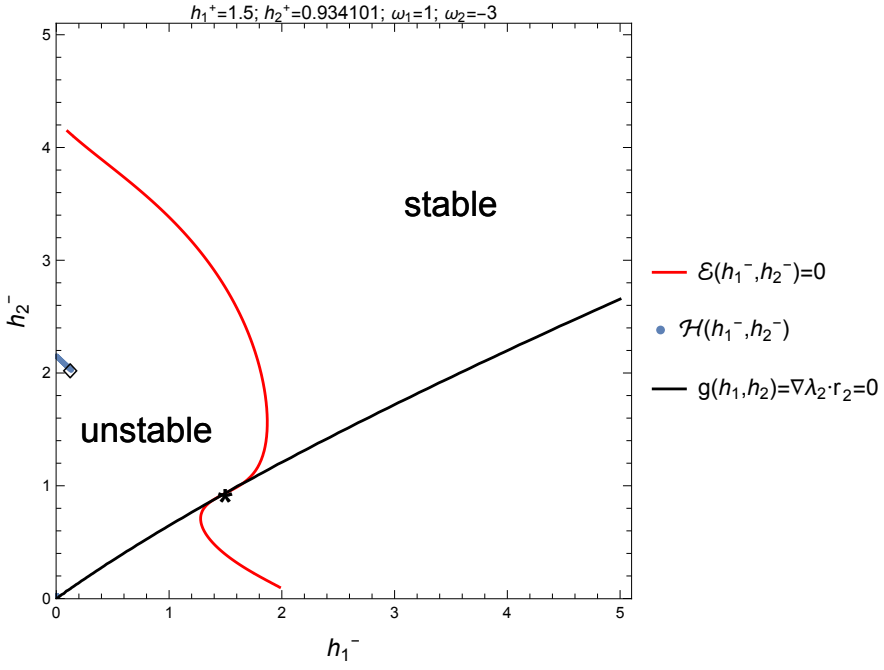

(b) $\omega_2 = -3.0$

Figure 2.14. – Two examples of the second characteristic field of $g(h_1, h_2) = 0$, $\mathcal{E}(h_1^-, h_2^-) = 0$, and the Rankine-Hugoniot locus $\mathcal{H}(h_1^-, h_2^-)$ on (h_1^-, h_2^-)-plane.

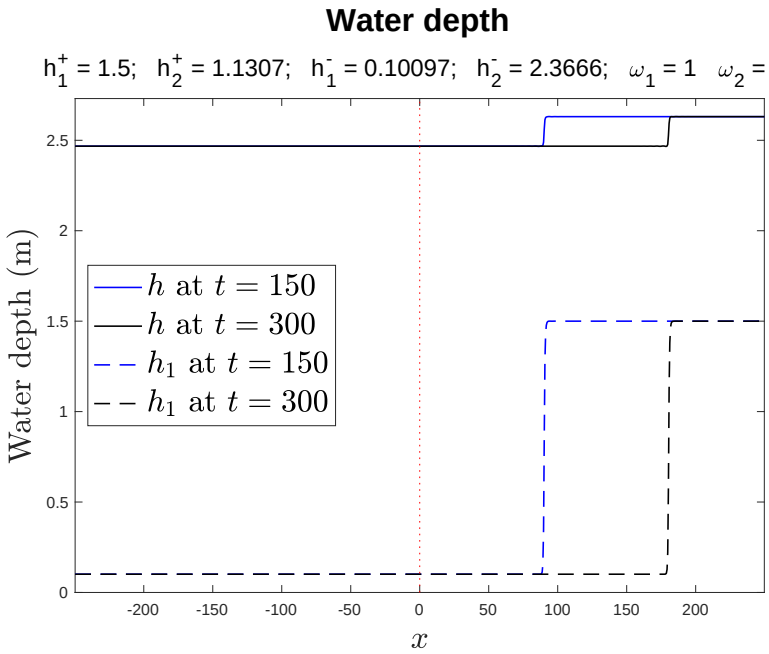

(a) A stable case of the second characteristic field when $\omega_1 = 1$, and $\omega_2 = -2.0$, with the initial state is located in the unstable region, which is marked as " $\diamond$ " in Fig. 2.14a

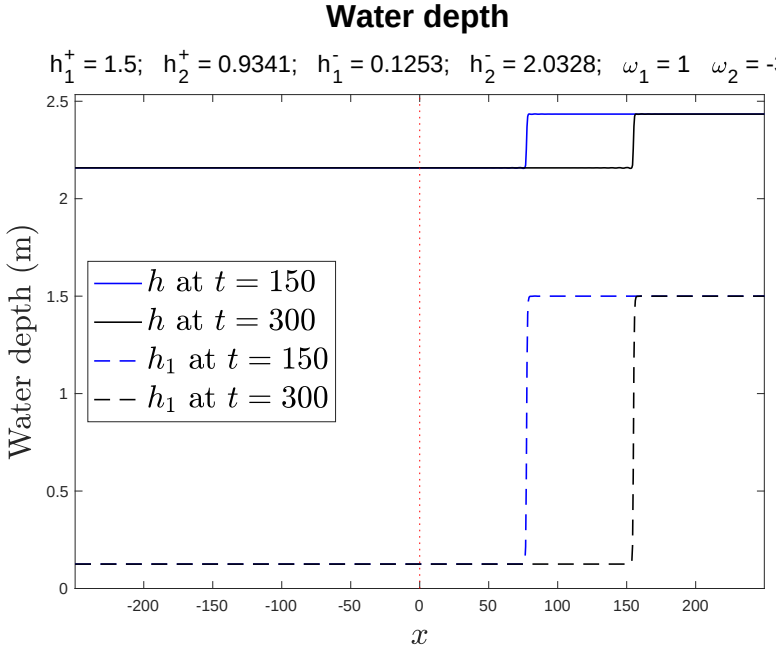

(b) A stable case of the second characteristic field when $\omega_1 = 1$, and $\omega_2 = -3.0$, with the initial state is located in the unstable region, which is marked as " $\diamond$ " in Fig. 2.14b

Figure 2.15. – Numerical results showing two stable shocks in unstable region

2.5. Conclusion

A two-layer flow of an ideal homogeneous fluid described by the Benney equations with a continuous piecewise linear velocity profile is studied. The total energy of this system E is not convex. However, the system is hyperbolic and the Riemann invariants of this system can be found explicitly. Therefore, a study of the eigenfields can be done. We found that, in general, the second characteristic field can be neither genuinely nonlinear nor linear degenerate. The region of parameters (ω_1, ω_2) is found where all three eigenfields are genuinely nonlinear. In this case, the stability criterion $\mathcal{E} < 0$ guarantees the shock stability for all fields. However, when the second characteristic field is neither genuinely nonlinear nor linear degenerate, a stable shock exists even when $\mathcal{E} > 0$. This unphysical result ($\mathcal{E} > 0$) could be due to the strong assumption of constant vorticities in both layers, $\omega_1 = \text{const.}$ and $\omega_2 = \text{const.}$ These vorticities are assumed not to change through the shock. This assumption can be released in the work of Richard and Gavrilyuk 2013, where the vorticity in the one-layer system is allowed to change after the hydraulic jump. Probably a new two-layer flow model should be derived where the vorticity in both layers can change through the shock.

APPENDIX

B. Recall on shallow water equations

We consider now a particular case of p-system written in the Eulerian coordinates as follows:

$$\begin{cases} h_t + (uh)_x = 0, \\ (hu)_t + (hu^2 + p)_x = 0, \end{cases} \tag{2.113}$$

and the energy equation of this system,

$$(he)_t + (hue + up)_x = 0. \tag{2.114}$$

Here, h is the water depth, u represents the horizontal velocity, p and e are the pressure and energy of the shallow water system, respectively. p and e are defined as follows:

$$p = \frac{1}{2}gh^2, \tag{2.115}$$

$$e = \frac{1}{2}u^2 + \frac{1}{2}gh = \frac{1}{2}u^2 + \frac{p}{h}. \tag{2.116}$$

The total energy of this system is defined as: $E(h, V = hu) \coloneqq he = \dfrac{V^2}{2h} + p$. The corresponding Hessian matrix:

$$E'' = \begin{bmatrix} \frac{1}{h} & \frac{-V}{h^2} \\ \frac{-V}{h^2} & g + \frac{V^2}{h^3} \end{bmatrix}.$$

Even if, formally, the shallow water equations are a particular case of p-system, we again present all computations because of the importance of this particular system. It is a sort of reference system for the two-layer Benney equations.

We know that $\dfrac{1}{h} > 0$ and $\det(E'') = \dfrac{g}{h} > 0$, therefore the shallow water equations are a hyperbolic system. The two eigenvalues of the system are:

$$\lambda_1 = u - C, \quad \lambda_2 = u + C; \quad C^2 = \frac{\mathrm{d}p}{\mathrm{d}h} = gh, \tag{2.117}$$

with the corresponding right eigenvectors are,

$$r_1 = (h, -C)^T, \quad r_2 = (h, C)^T \tag{2.118}$$

Therefore, we can obtain:

$$\nabla\lambda_1 \cdot r_1 = -hC_h - C = -\frac{3C}{2} = -\frac{3\sqrt{gh}}{2} < 0,$$
$$\nabla\lambda_2 \cdot r_2 = hC_h + C = \frac{3C}{2} = \frac{3\sqrt{gh}}{2} > 0,$$

here $\nabla = (\frac{\partial}{\partial h}, \frac{\partial}{\partial u})^T$. Since $h > 0$, both characteristic fields are genuinely nonlinear. From the Rankine-Hugoniot conditions Eqn. (2.4) we find the jump relations of the shallow water equations Eqn. (2.113) across a shock with the velocity of the shock $D \coloneqq \frac{x}{t}$ are given as follows:

$$\begin{cases} [h(u-D)] = 0, \\ [hu(u-D) + p] = 0. \end{cases} \tag{2.119}$$

Now we define the mass flux from the mass equation shown above $m = h^+(u^+ - D) = h^-(u^- - D)$, which is a non-zero constant. We consider the case, the shock propagate to the right, which mean $m < 0$. In terms of the mass flow m, one can write the second equation as:

$$[hu(u-D) + p] = 0 \Leftrightarrow [h(u-D)^2 + p] = 0 \Leftrightarrow [m^2\tau + p] = 0, \tag{2.120}$$

where $\tau = 1/h$. Finally, the momentum equation can be expressed as:

$$[p] = -m^2[\tau]. \tag{2.121}$$

Moreover, the "entropy" inequality of the shallow water equations takes the form,

$$\begin{aligned} \mathcal{E} &\coloneqq -D[he] + [hue + up] \\ &= [h(u-D)e + up] \\ &= \left[\frac{1}{2}u^2 h(u-D) + p\tau h(u-D) + h\tau(u-D)p + Dp\right] \\ &= \left[\frac{1}{2}(u^2 + D^2)h(u-D) + 2h\tau(u-D)p + Dp\right] \\ &= \left[\frac{1}{2}h(u-D)^3 + 2h\tau(u-D)p\right] \\ &= m\left[\frac{1}{2}m^2\tau^2 + 2p\tau\right]. \end{aligned}$$

Since $[\tau^2] = [\tau](\tau^+ + \tau^-)$, and $[p] = -m^2[\tau]$, the above equation can be further

expressed as,

$$\mathcal{E} \coloneqq -D[he] + [hue + up] = m\left[\frac{1}{2}m^2\tau^2 + 2p\tau\right] \tag{2.122}$$

$$\begin{aligned}
&= m\left[-\frac{1}{2}p(\tau^+ + \tau^-) + 2p\tau\right] \\
&= m\left[-\frac{1}{4}g\left(h^{+^2} - h^{-^2}\right)\left(\frac{h^+ + h^-}{h^+h^-}\right) + g\left(h^+ - h^-\right)\right] \\
&= mg[h]\left\{-\frac{(h^+ + h^-)^2}{4h^+h^-} + 1\right\} \\
&= -\frac{mg[h]^3}{4h^+h^-}
\end{aligned} \tag{2.123}$$

Compare to Eqn. (2.22), the cubic term in the right-hand side is now exact. As mentioned above, we consider the shock propagate to the right, which means $m < 0$. Then $\mathcal{E} < 0$ if and only if $[h] = h^+ - h^- < 0$. Furthermore, from Eqn. (2.121) the mass flow can be written as:

$$m^2 = -\frac{[p]}{[\tau]} = -\frac{p^+ - p^-}{\tau^+ - \tau^-}. \tag{2.124}$$

Again, when τ^+ and close to τ^-, then $m^2 = -\dfrac{[p]}{[\tau]} \approx -p_\tau$. Here one can express the pressure p in the terms of τ, $p = \dfrac{g}{2\tau^2}$, which is a hyperbola function, and its derivative takes the form:

$$\frac{\mathrm{d}p}{\mathrm{d}\tau} = \frac{\mathrm{d}p}{\mathrm{d}h}h_\tau = -\frac{\mathrm{d}p}{\mathrm{d}h}h^2. \tag{2.125}$$

Since p is a hyperbola function in terms of τ, and additionally with the condition $[h] = h^+ - h^- < 0$, we have the relation,

$$\left(\frac{\mathrm{d}p}{\mathrm{d}\tau}\right)^+ = -\left(\frac{\mathrm{d}p}{\mathrm{d}h}h^2\right)^+ > -m^2 > -\left(\frac{\mathrm{d}p}{\mathrm{d}h}h^2\right)^- = \left(\frac{\mathrm{d}p}{\mathrm{d}\tau}\right)^-$$

Then we obtain,

$$\left(gh^3\right)^+ = \left(\frac{\mathrm{d}p}{\mathrm{d}h}h^2\right)^+ < \left[h^+(u^+ - D)\right]^2 = m^2 = \left[h^-(u^- - D)\right]^2 < \left(\frac{\mathrm{d}p}{\mathrm{d}h}h^2\right)^- = \left(gh^3\right)^- \tag{2.126}$$

Finally, since we consider the case that the shock propagate to the right ($m < 0$), we have the Lax condition:

$$u^- + \sqrt{gh^-} = \lambda_2^- > D > \lambda_2^+ = u^+ + \sqrt{gh^+}. \tag{2.127}$$

On the other hand, one can also prove that if the Lax condition is valid, then $[h] = h^+ - h^- < 0$. Now we have the Lax condition,

$$u^- + C^- = \lambda_2^- > D > \lambda_2^+ = u^+ + C^+; \quad C = \sqrt{gh} \tag{2.128}$$

From the definition of the mass flow $m = h^+(u^+ - D) = h^-(u^- - D)$, the shock velocity can be expressed

$$D = \frac{h^+u^+ - h^-u^-}{h^+ - h^-} \tag{2.129}$$

From Lax stability condition we have the relation,

$$D - u^+ = \frac{u^+ - u^-}{h^+ - h^-}h^- > C^+ = \sqrt{gh^+} > 0. \tag{2.130}$$

Therefore, we know $[u] = u^+ - u^-$ and $[h] = h^+ - h^-$ share the same sign. Combine with the Lax stability condition Eqn. (2.130), we have the result: $[u] = u^+ - u^- < 0$ and $[h] = h^+ - h^- < 0$.

C. Recall on the basic algorithms for finite volume methods

Here, a short recall is presented; for more details, see Toro 2013 and LeVeque 1992. Consider the following general Cauchy problem:

$$\begin{aligned} \text{PDE} &: \mathbf{U}_t + \mathbf{F}(\mathbf{U})_x = 0, \\ \text{IC} &: \mathbf{U}(x,0) = \mathbf{U}_0(x), \end{aligned} \tag{2.131}$$

in the domain $x_L \leq x \leq x_R$. Here, $\mathbf{U}$ is an unknown vector and $\mathbf{F}(\mathbf{U})$ is the flux vector. The spatial control volumes are in the center of x_i, the boundaries of the cell x_i can be discretized as:

$$\begin{aligned} x_{i+\frac{1}{2}} = x_L + \frac{\Delta x}{2} + (i-1)\Delta x, \quad & i = 1, \cdots i_{\text{Max}}, \\ \Delta x = \frac{x_R - x_L}{i_{\text{Max}}}, \quad & x \in [x_L, x_R]. \end{aligned}$$

The temporal control volume is discretized as:

$$t^n = (n-1)\Delta t, \quad n = 1, \cdots n_{\text{Max}}.$$

The integral formulation over the space-time control volume $[x_{i-\frac{1}{2}}, x_{i+\frac{1}{2}}] \times [t^n, t^{n+1}]$ of the conservation law takes the form:

$$\int_{x_{i-\frac{1}{2}}}^{x_{i+\frac{1}{2}}} \left(\mathbf{U}(x, t^{n+1}) - \mathbf{U}(x, t^n)\right) \mathrm{d}x + \int_{t^n}^{t^{n+1}} \left(\mathbf{F}(\mathbf{U}(x_{i+\frac{1}{2}}, t)) - \mathbf{F}(\mathbf{U}(x_{i-\frac{1}{2}}, t))\right) \mathrm{d}t = 0. \tag{2.132}$$

The cell-averaged value computed at time t^n is defined as:

$$\mathbf{U}_i^n \coloneqq \frac{1}{\Delta x} \int_{x_{i-\frac{1}{2}}}^{x_{i+\frac{1}{2}}} \mathbf{U}(x, t^n) \mathrm{d}x. \tag{2.133}$$

Similarly, the time-averaged flux computed at the cell boundary $x_{i+\frac{1}{2}}$ is:

$$\mathbf{F}_{i+\frac{1}{2}} \coloneqq \frac{1}{\Delta t} \int_{t^n}^{t^{n+1}} \mathbf{F}(\mathbf{U}(x_{i+\frac{1}{2}}, t)) \mathrm{d}t. \tag{2.134}$$

Therefore, Eqn. (2.132) can be rewritten as:

$$\mathbf{U}_i^{n+1} = \mathbf{U}_i^n - \frac{\Delta t}{\Delta x} \left(\mathbf{F}_{i+\frac{1}{2}} - \mathbf{F}_{i-\frac{1}{2}}\right). \tag{2.135}$$

C.1. Godunov method

There are many ways to compute the numerical flux at the cell boundary $\mathbf{F}_{i+\frac{1}{2}}$ as a function of $\mathbf{U}_i^n$ or $\mathbf{U}(x, t^n)$. In this section, the Godunov flux (S. Godunov 1959), is introduced. To compute the numerical flux at the cell boundary $\mathbf{F}_{i+\frac{1}{2}}$, the unknown vector $\mathbf{U}$ should be first defined at the boundary $x_{i+\frac{1}{2}}$. The simplest way is assuming the unknown vector $\mathbf{U}$ is a piecewise constant vector in every cells $x_{i-\frac{1}{2}} < x < x_{i+\frac{1}{2}}$:

$$\mathbf{U}(x, t^n) = \mathbf{U}_i^n, \quad \forall x \in (x_{i-\frac{1}{2}}, x_{i+\frac{1}{2}}). \tag{2.136}$$

The Godunov flux (S. Godunov 1959) takes the form:

$$\mathbf{F}_{i+\frac{1}{2}}^{\mathrm{GOD}} = \mathbf{F}(\mathbf{U}_{i+\frac{1}{2}}^{\mathrm{GOD}}). \tag{2.137}$$

Here the Godunov state $\mathbf{U}_{i+\frac{1}{2}}^{\mathrm{GOD}}$ is the exact solution of the following local Riemann problem defined at the boundary $x_{i+\frac{1}{2}}$:

$$\mathbf{U}_t + \mathbf{F}(\mathbf{U})_{x'} = 0, \quad x' \coloneqq x - x_{i+\frac{1}{2}} \tag{2.138}$$

$$\mathbf{U}(x, t^n) = \begin{cases} \mathbf{U}_i^n, & x' \leq 0, \\ \mathbf{U}_{i+1}^n, & x' \geq 0. \end{cases} \tag{2.139}$$

Then finally the Godunov scheme takes the form:

$$\mathbf{U}_i^{n+1} = \mathbf{U}_i^n - \frac{\Delta t}{\Delta x}\left(\mathbf{F}_{i+\frac{1}{2}}^{\mathrm{GOD}} - \mathbf{F}_{i-\frac{1}{2}}^{\mathrm{GOD}}\right). \tag{2.140}$$

C.2. The HLL approximate Riemann solver

Instead of directly calculating the Godunov flux, which is a complex way, Harten, Lax, and van Leer (Harten, Lax, and Leer 1983) provided an approximate method for computing the Godunov flux. The main idea is to assume the solution that consists of two waves that separate three piecewise constant states (see Fig. 2.16). In region R_0, the unknown vector is set as the initial state $\mathbf{U}_L$; in region R_2, we

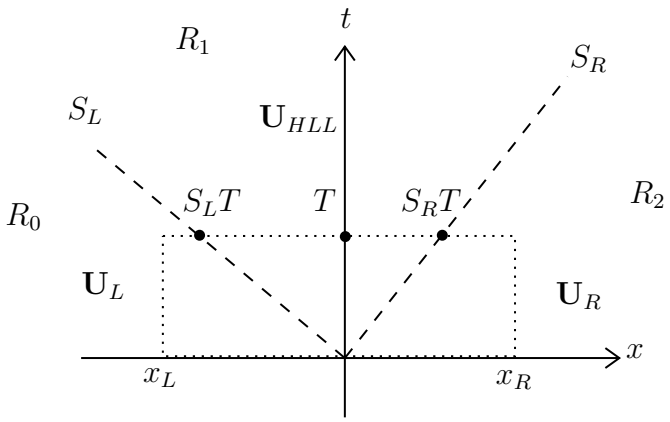

Figure 2.16. – Illustration of HLL method

have the initial state $\mathbf{U}_R$; and in region R_1, the unknown vector is set as the intermediate state $\mathbf{U}_{HLL}$. Here S_L and S_R are fixed wave speeds, suppose the eigenvalues of the system are ordered, $\lambda_1 \leq \lambda_2 \leq \cdots \leq \lambda_m$, Davis (Davis 1988) suggests a simple choice:

$$S_L = \min(0, \lambda_1(\mathbf{U}_L), \lambda_1(\mathbf{U}_R)); \quad S_R = \max(0, \lambda_m(\mathbf{U}_L), \lambda_m(\mathbf{U}_R)). \tag{2.141}$$

Starting from the conservation laws:

$$\mathbf{U}_t + \mathbf{F}(\mathbf{U})_x = 0.$$

The integral form of the conservation laws in the control volume $[x_L, x_R] \times [0, T]$ (dotted box in Fig. 2.16) reads:

$$\int_{x_L}^{x_R} (\mathbf{U}(x,T) - \mathbf{U}(x,0))\,\mathrm{d}x + \int_0^T (\mathbf{F}(\mathbf{U}(x_R,t)) - \mathbf{F}(\mathbf{U}(x_L,t)))\,\mathrm{d}t = 0, \tag{2.142}$$

which results in:

$$\mathbf{U}_L S_L + \mathbf{U}_{HLL}(S_R - S_L) - \mathbf{U}_R S_R + \mathbf{F}(\mathbf{U}_R) - \mathbf{F}(\mathbf{U}_L) = 0.$$

Finally, the approximate intermediate state $\mathbf{U}_{HLL}$ takes the form:

$$\mathbf{U}_{HLL} = \frac{S_R \mathbf{U}_R - S_L \mathbf{U}_L + \mathbf{F}(\mathbf{U}_R) - \mathbf{F}(\mathbf{U}_L)}{S_R - S_L}. \tag{2.143}$$

In the HLL method, instead of assuming the intermediate flux as: $\mathbf{F}^{HLL}_{i+\frac{1}{2}} = \mathbf{F}(\mathbf{U}_{HLL})$, the intermediate flux $\mathbf{F}^{HLL}_{i+\frac{1}{2}}$ must be calculated by the integral form of the conservation laws in the control volume $[0, x_R] \times [0, T]$:

$$\int_0^{x_R} (\mathbf{U}(x,T) - \mathbf{U}(x,0))\,\mathrm{d}x + \int_0^T (\mathbf{F}(\mathbf{U}(x_R,t)) - \mathbf{F}(\mathbf{U}(0,t)))\,\mathrm{d}t = 0. \tag{2.144}$$

This leads to the numerical flux $\mathbf{F}^{HLL}_{i+\frac{1}{2}}$ takes the form:

$$\mathbf{F}^{HLL}_{i+\frac{1}{2}} = \mathbf{F}(\mathbf{U}_R) + S_R(\mathbf{U}_{HLL} - \mathbf{U}_R) = \frac{S_R \mathbf{F}(\mathbf{U}_L) - S_L \mathbf{F}(\mathbf{U}_R) + S_L S_R (\mathbf{U}_R - \mathbf{U}_L)}{S_R - S_L}.$$

Finally, the HLL scheme takes the form:

$$\mathbf{U}_i^{n+1} = \mathbf{U}_i^n - \frac{\Delta t}{\Delta x}\left(\mathbf{F}^{\mathrm{HLL}}_{i+\frac{1}{2}} - \mathbf{F}^{\mathrm{HLL}}_{i-\frac{1}{2}}\right). \tag{2.145}$$

3. Modelling of the Euler equations with arbitrary vorticity over variable topography in semi-Lagrangian coordinates

Table of Content

3.1 Introduction . . . 95
3.2 Two-dimensional Euler equations in semi-Lagrangian coordinates . . 96
3.3 Equation for the pressure . . . 98
3.3.1 Boundary condition for the pressure on the bottom . . . 99
3.3.1.1 Curvature of a plane curve . . . 101
3.3.2 Bottom boundary condition of the pressure in semi-Lagrangian coordinates . . . 102
3.4 Equation for Energy . . . 103
3.5 Three-dimensional Euler equations in semi-Lagrangian coordinates . 104
3.5.1 Divergence operator . . . 104
3.5.2 Laplacian operator of pressure . . . 106
3.5.3 Reduction from 3D to 2D . . . 106
3.5.3.1 Mass equation . . . 106
3.5.3.2 Momentum equation . . . 107
3.5.3.3 Energy equation . . . 107
3.5.3.4 Pressure equation . . . 108
3.6 Numerical scheme . . . 108
3.6.1 Overview of the numerical solution strategy . . . 108
3.6.2 Discretizations . . . 109
3.6.3 Partial numerical results . . . 112
3.7 Conclusion . . . 119

3.1. Introduction

Consider a two-dimensional domain $\mathfrak{D}_{\mathbf{x}}$ described by the Euler equations $\mathfrak{D}_{\mathbf{x}} = \{(x,z)|b(x) \leq z \leq \eta(x)\}$. The Euler equations in (x,z) coordinates take the form:

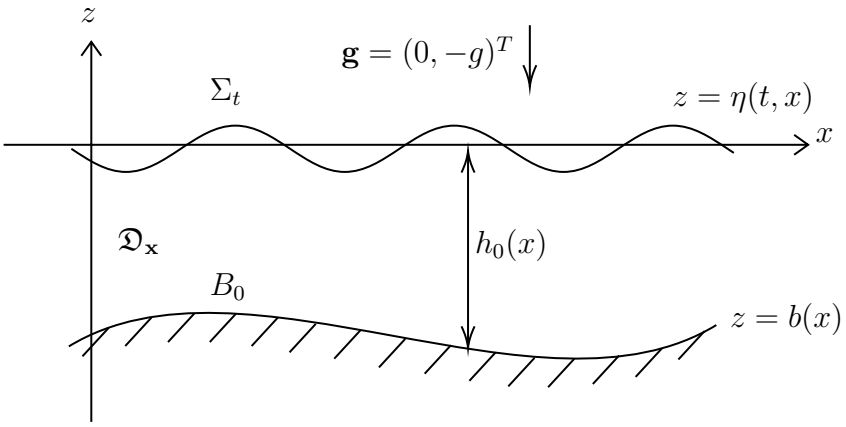

Figure 3.1. – Two-dimensional domain $\mathfrak{D}_{\mathbf{x}}$ in Eulerian coordinates

$$u_x + w_z = 0, \tag{3.1}$$

$$\begin{cases} u_t + uu_x + wu_z + \dfrac{1}{\rho}p_x = 0, \\ w_t + uw_x + ww_z + \dfrac{1}{\rho}p_z = -g. \end{cases} \tag{3.2}$$

The boundary conditions the free surface Σ_t:

$$\eta_t + u_s\eta_x = w_s, \quad z = \eta(t,x), \tag{3.3}$$

$$p_s = 0, \quad z = \eta(t,x). \tag{3.4}$$

On the bottom B_0, the boundary condition is:

$$u_b b_x = w_b, \quad z = b(x). \tag{3.5}$$

The free surface Euler equations lead to a moving boundary problem. It is necessary to map the moving domain into a fixed domain with flat boundaries. Instead of using a classical method, namely σ-transformation, we follow the idea of Zakharov 1980: the semi-Lagrangian coordinates (x,λ), are used. The Lagrangian coordinate λ belongs to $(0,1)$. The free surface $z = \eta(t,x)$ corresponds to the value $\lambda = 1$; and the bottom $z = b(x)$ corresponds to the value $\lambda = 0$. The mapping function of the changing variables $(x,z) \to (x,\lambda)$ is:

$$z = \Phi(t,x,\lambda), \tag{3.6}$$

where $\Phi(t, x, \lambda)$ is the solution of the equation

$$\Phi_t + \tilde{u}\Phi_x = \tilde{w}. \tag{3.7}$$

The initial condition for Φ is:

$$\Phi|_{t=0} = (1-\lambda)b(x) + \lambda\eta_0(x) = b(x) + \lambda h_0(x), \quad h_0(x) = \eta_0(x) - b(x),$$

where the subscript "0" represents the initial value of the corresponding variables. In fact, this is a consequence of the boundary condition for the vertical velocity w in Eulerian coordinates. Thus, this change of variables corresponds to the foliation of the moving domain by the surface $\lambda = \text{const}$.

3.2. Two-dimensional Euler equations in semi-Lagrangian coordinates

Denote the fixed domain in semi-Lagrangian coordinates by $\mathfrak{D}_{\mathbf{\Lambda}} \coloneqq \{(x, \lambda) | 0 \leq \lambda \leq 1\}$. For any physical variable in $\mathfrak{D}_{\mathbf{x}}$, $F(t, x, z)$, the corresponding physical variable in $\mathfrak{D}_{\lambda}$, $\tilde{F}(t, x, \lambda)$, can be expressed as:

$$F(t, x, z) = F(t, x, \Phi(t, x, \lambda)) = \tilde{F}(t, x, \lambda).$$

Taking the partial derivative of any physical variable with respect to t, x, and λ the following relation can be obtained:

$$F_t + F_z\Phi_t = \tilde{F}_t; \quad F_x + F_z\Phi_x = \tilde{F}_x; \quad F_z\Phi_\lambda = \tilde{F}_\lambda.$$

Therefore, the term of vertical velocity in the material derivative would vanish in semi-Lagrangian coordinates. By using the above relation, the Euler equations can be written in (x, λ) coordinates:

$$\tilde{u}_x - \frac{\Phi_x}{\Phi_\lambda}\tilde{u}_\lambda + \frac{\tilde{w}_\lambda}{\Phi_\lambda} = 0, \tag{3.8}$$

$$\begin{cases} \tilde{u}_t + \tilde{u}\tilde{u}_x + \dfrac{1}{\rho}\left(\tilde{p}_x - \tilde{p}_\lambda\dfrac{\Phi_x}{\Phi_\lambda}\right) = 0, \\ \tilde{w}_t + \tilde{u}\tilde{w}_x + \dfrac{1}{\rho}\left(\tilde{p}_\lambda\dfrac{1}{\Phi_\lambda}\right) = -g. \end{cases} \tag{3.9}$$

The boundary condition at the free surface, $\Sigma_t^\Lambda \coloneqq \{(x, \lambda) | \lambda = 1\}$, would become:

$$\tilde{p}_s = 0, \quad \lambda = 1. \tag{3.10}$$

On the bottom, $B_0^\Lambda \coloneqq \{(x,\lambda)|\lambda = 0\}$, the boundary condition is:

$$\tilde{u}_b b_x = \tilde{w}_b, \quad \lambda = 0. \tag{3.11}$$

Notice that the kinematic free surface boundary condition Eqn. (3.3) is replaced by the additional condition Eqn. (3.7):

$$\Phi_t + \tilde{u}\Phi_x = \tilde{w}, \tag{3.12}$$

with the initial condition:

$$\Phi|_{t=0} = b(x) + \lambda h_0(x). \tag{3.13}$$

The incompressible condition of the Euler system can be further rewritten in the conservative form,

$$\begin{aligned}\Phi_\lambda \tilde{u}_x - \Phi_x \tilde{u}_\lambda + \tilde{w}_\lambda &= \Phi_\lambda \tilde{u}_x - \Phi_x \tilde{u}_\lambda + \frac{\partial}{\partial \lambda}\left(\frac{\tilde{\mathrm{d}}\Phi}{\tilde{\mathrm{d}}t}\right) \\ &= \Phi_\lambda \tilde{u}_x - \Phi_x \tilde{u}_\lambda + (\Phi_t)_\lambda + (\tilde{u}\Phi_x)_\lambda \\ &= (\Phi_\lambda)_t + (\tilde{u}\Phi_\lambda)_x = 0.\end{aligned} \tag{3.14}$$

To write the momentum equations in conservative form, the following relation for any physical variables $\tilde{F}$ is needed:

$$\begin{aligned}(\Phi_\lambda \tilde{F})_t + (\tilde{u}\Phi_\lambda \tilde{F})_x &= \tilde{F}(\Phi_\lambda)_t + \Phi_\lambda \tilde{F}_t + \tilde{F}(\tilde{u}\Phi_\lambda)_x + \tilde{u}\Phi_\lambda \tilde{F}_x \\ &= \Phi_\lambda \tilde{F}_t + \tilde{u}\Phi_\lambda \tilde{F}_x = \Phi_\lambda \frac{\tilde{\mathrm{d}}\tilde{F}}{\tilde{\mathrm{d}}t}.\end{aligned} \tag{3.15}$$

Therefore, the Euler equations written in semi-Lagrangian coordinates take the form:

$$\Phi_t + \tilde{u}\Phi_x = \tilde{w}, \tag{3.16}$$

$$(\Phi_\lambda)_t + (\tilde{u}\Phi_\lambda)_x = 0, \tag{3.17}$$

$$\begin{cases}(\rho\Phi_\lambda \tilde{u})_t + (\rho\tilde{u}\tilde{u}\Phi_\lambda + \Phi_\lambda \tilde{p})_x - (\Phi_x \tilde{p})_\lambda = 0 \\ (\rho\Phi_\lambda \tilde{w})_t + (\rho\tilde{u}\tilde{w}\Phi_\lambda)_x + (\tilde{p} + \rho g\Phi)_\lambda = 0.\end{cases} \tag{3.18}$$

In this system, the unknown variables are Φ, $\tilde{u}$, $\tilde{w}$, and $\tilde{p}$. However, Eqn. (3.16) and Eqn. (3.17) are both equations for Φ. Therefore, we replace Eqn. (3.16) with the equation for pressure.

3.3. Equation for the pressure

The classical way to obtain the equation of pressure is to take the divergence of the momentum equations. Starting with the Euler equations in Eulerian coordinates:

$$\mathbf{u}_t + \frac{\partial \mathbf{u}}{\partial \mathbf{x}}\mathbf{u} + \frac{1}{\rho}\nabla_{\mathbf{x}} p = \mathbf{g}. \tag{3.19}$$

Taking the divergence of the above equations, the Poisson's equation for the pressure p is obtained:

$$\frac{1}{\rho}\Delta_{\mathbf{x}} p = \operatorname{div}_{\mathbf{x}}\left(\mathbf{g} - \frac{\partial \mathbf{u}}{\partial \mathbf{x}}\mathbf{u}\right) = -\operatorname{div}_{\mathbf{x}}\left(\frac{\partial \mathbf{u}}{\partial \mathbf{x}}\mathbf{u}\right). \tag{3.20}$$

Here $\Delta_{\mathbf{x}}$ denote the Laplace operator on the domain $\mathfrak{D}_{\mathbf{x}}$; and $\operatorname{div}_{\mathbf{x}}$ being the divergence operator on the domain $\mathfrak{D}_{\mathbf{x}}$. Using the following relation of derivative to map the Poisson's equation for the pressure to semi-Lagrangian coordinates:

$$F_x + F_z\Phi_x = \tilde{F}_x; \quad F_z\Phi_\lambda = \tilde{F}_\lambda.$$

And the second-order derivatives take the form:

$$\begin{aligned}
(F_z\Phi_\lambda)_\lambda &= F_{zz}\Phi_\lambda^2 + F_z\Phi_{\lambda\lambda} = \tilde{F}_{\lambda\lambda},\\
(F_z\Phi_\lambda)_x &= F_{xz}\Phi_\lambda + F_{zz}\Phi_x\Phi_\lambda + F_z\Phi_{x\lambda} = \tilde{F}_{x\lambda},\\
(F_x + F_z\Phi_x)_x &= F_{xx} + 2F_{xz}\Phi_x + F_{zz}\Phi_x^2 + F_z\Phi_{xx} = \tilde{F}_{xx}.
\end{aligned}$$

With these relation, the Laplace pressure at the left hand side of Eqn. (3.20) can be transformed in semi-Lagrangian coordinates as:

$$\Delta_{\mathbf{\Lambda}} p = \tilde{p}_{xx} - 2\frac{\Phi_x}{\Phi_\lambda}\tilde{p}_{x\lambda} + \frac{1+\Phi_x^2}{\Phi_\lambda^2}\tilde{p}_{\lambda\lambda} - \frac{\Phi_{\lambda\lambda}(1+\Phi_x^2) - 2\Phi_x\Phi_{x\lambda}\Phi_\lambda + \Phi_\lambda^2\Phi_{xx}}{\Phi_\lambda^3}\tilde{p}_\lambda. \tag{3.21}$$

On the other hand, the right-hand side of Eqn. (3.20) becomes:

$$\begin{aligned}
\nabla_{\mathbf{x}} \cdot \left(\frac{\partial \mathbf{u}}{\partial \mathbf{x}}\mathbf{u}\right) &= (uu_x + wu_z)_x + (uw_x + ww_z)_z\\
&= 2(w_z^2 + u_z w_x) \qquad (3.22)\\
&= 2\left[\frac{\tilde{w}_\lambda^2}{\Phi_\lambda^2} + \frac{\tilde{u}_\lambda}{\Phi_\lambda}\left(\tilde{w}_x - \tilde{w}_\lambda\frac{\Phi_x}{\Phi_\lambda}\right)\right]\\
&= 2\frac{1}{\Phi_\lambda}(-\tilde{w}_\lambda\tilde{u}_x + \tilde{u}_\lambda\tilde{w}_x) \qquad (3.23)
\end{aligned}$$

Combining everything together, Poisson's equation for pressure in semi-Lagrangian coordinates takes the form:

$$\tilde{p}_{xx}-2\frac{\Phi_x}{\Phi_\lambda}\tilde{p}_{x\lambda}+\frac{1+\Phi_x^2}{\Phi_\lambda^2}\tilde{p}_{\lambda\lambda}-\frac{\Phi_{\lambda\lambda}(1+\Phi_x^2)-2\Phi_x\Phi_{x\lambda}\Phi_\lambda+\Phi_\lambda^2\Phi_{xx}}{\Phi_\lambda^3}\tilde{p}_\lambda=-\frac{2\rho}{\Phi_\lambda}(-\tilde{w}_\lambda\tilde{u}_x+\tilde{u}_\lambda\tilde{w}_x) \tag{3.24}$$

And can also be written in conservative form:

$$\frac{1}{\Phi_\lambda}\left[(\Phi_\lambda\tilde{p}_x-\Phi_x\tilde{p}_\lambda+2\rho\tilde{u}_\lambda\tilde{w})_x+\left(-\Phi_x\tilde{p}_x+\frac{1+\Phi_x^2}{\Phi_\lambda}\tilde{p}_\lambda-2\rho\tilde{u}_x\tilde{w}\right)_\lambda\right]=0. \tag{3.25}$$

To solve the above Poisson's equation for pressure, only the free surface boundary condition $\tilde{p}_s=0$ is not enough. Therefore, an additional boundary condition on the bottom is needed.

3.3.1. Boundary condition for the pressure on the bottom

Define the unit tangential vector $\boldsymbol{\tau}_b$ and the unit normal vector $\mathbf{n}_b$ on $B_0 \coloneqq \{(x,z)|z=b(x)\}$, in which, $\boldsymbol{\tau}_b$ and $\mathbf{n}_b$ is pointing to negative $x-$direction and outward the fluid domain respectively, so that the basis $(\boldsymbol{\tau}_b, \mathbf{n}_b)$ has the same orientation as the standard Cartesian basis (see Fig. 3.3). The two unit vectors can be expressed as follows,

$$\mathbf{n}_b=\frac{(b_x,-1)}{\sqrt{1+b_x^2}};\quad \boldsymbol{\tau}_b=\frac{(-1,-b_x)}{\sqrt{1+b_x^2}} \tag{3.26}$$

To construct the boundary condition for the pressure on B_0, we take inner product with the momentum equation and the unit normal vector $\mathbf{n}_b$,

$$\mathbf{n}_b\cdot\nabla_{\mathbf{x}}p=\rho\mathbf{n}_b\cdot\left(\mathbf{g}-\mathbf{u}_t-\frac{\partial\mathbf{u}}{\partial\mathbf{x}}\mathbf{u}\right). \tag{3.27}$$

Moreover, the velocity field $\mathbf{u}$ on B_0 can be expressed in the orthogonal basis $(\boldsymbol{\tau}_b, \mathbf{n}_b)$:

$$\mathbf{u}=u_\tau\boldsymbol{\tau}_b+u_n\mathbf{n}_b. \tag{3.28}$$

Since the velocity boundary condition: $\mathbf{u}\cdot\mathbf{n}_b=0$, the normal component of the velocity u_n should be zero on B_0. Therefore, the term $\mathbf{n}_b\cdot\mathbf{u}_t$ in Eqn. (3.27) vanishes.

The last term of Eqn. (3.27) can be simplified:

$$\begin{aligned}
-\rho\mathbf{n}_b \cdot \left(\frac{\partial \mathbf{u}}{\partial \mathbf{x}}\mathbf{u}\right) &= -\rho\left[\frac{\partial(\mathbf{n}_b \cdot \mathbf{u})}{\partial \mathbf{x}} \cdot \mathbf{u} - \mathbf{u} \cdot \left(\frac{\partial \mathbf{n}_b}{\partial \mathbf{x}}\mathbf{u}\right)\right] \\
&= -\rho\left[\frac{\partial(\mathbf{n}_b \cdot \mathbf{u})}{\partial \mathbf{x}} \cdot (u_\tau \boldsymbol{\tau}_b) - (u_\tau \boldsymbol{\tau}_b) \cdot \left(\frac{\partial \mathbf{n}_b}{\partial \mathbf{x}}(u_\tau \boldsymbol{\tau}_b)\right)\right] \\
&= \rho u_\tau^2 \boldsymbol{\tau}_b \cdot \left(\frac{\partial \mathbf{n}_b}{\partial \mathbf{x}}\boldsymbol{\tau}_b\right).
\end{aligned} \tag{3.29}$$

Here using the fact that the term $\dfrac{\partial(\mathbf{n}_b \cdot \mathbf{u})}{\partial \mathbf{x}} \cdot \boldsymbol{\tau}_b$ means the variation of $\mathbf{n}_b \cdot \mathbf{u}$ along $\boldsymbol{\tau}_b$, which is zero everywhere on B_0. Combine everything together, Eqn. (3.27) finally takes the form:

$$\frac{\partial p}{\partial n_b} - \rho u_\tau^2 \boldsymbol{\tau}_b \cdot \left(\frac{\partial \mathbf{n}_b}{\partial \mathbf{x}}\boldsymbol{\tau}_b\right) = \rho \mathbf{n}_b \cdot \mathbf{g}. \tag{3.30}$$

To understand Eqn. (3.30), introduce another definition of the normal vector:

$$\mathbf{n}_b = \nabla d(\mathbf{x}). \tag{3.31}$$

Here $d(\mathbf{x})$ is the signed distance function and is defined as:

$$d(\mathbf{x}) = \min \|\mathbf{x} - \boldsymbol{\xi}\|, \qquad \mathbf{x} \in \mathfrak{D}_\mathbf{x}, \quad \boldsymbol{\xi} \in B_0,$$

in which $\|\cdot\|$ denotes the norm of the corresponded vector. Notice that this normal vector $\mathbf{n}_b$ is not only defined at the bottom B_0, but also defined in the vicinity of B_0. Moreover, because the normal vector is a gradient of a scalar function, the matrix $\dfrac{\partial \mathbf{n}_b}{\partial \mathbf{x}}$ is symmetric. This means that it is diagonalizable in the orthonormal base of eigenvector. On the other hand, because of $\mathbf{n}_b \cdot \mathbf{n}_b = 1$, we have:

$$\frac{\partial \mathbf{n}_b}{\partial \mathbf{x}}\mathbf{n}_b = 0,$$

which indicates the matrix $\dfrac{\partial \mathbf{n}_b}{\partial \mathbf{x}}$ is singular: the corresponding eigenvalue of the eigenvector $\mathbf{n}_b$ is zero. Then $\boldsymbol{\tau}_b$ is another eigenvector. Therefore, the matrix can be rewritten in the basis $(\boldsymbol{\tau}_b, \mathbf{n}_b)$:

$$-\frac{\partial \mathbf{n}_b}{\partial \mathbf{x}} = \begin{bmatrix} \zeta & 0 \\ 0 & 0 \end{bmatrix}, \tag{3.32}$$

where ζ is the eigenvalue corresponding to the eigenvector $\boldsymbol{\tau}_b$, and would be determined later.

3.3.1.1. Curvature of a plane curve

The magnitude of the curvature of a plane curve $|\kappa|$ of B_0 is defined as:

$$|\kappa| = \left|\frac{\mathrm{d}\theta}{\mathrm{d}s}\right| = \frac{|b_{xx}|}{(1+b_x^2)^{\frac{3}{2}}}, \tag{3.33}$$

in which, θ is the angle between the tangent line and the positive $x-$axis, in other words, $\tan\theta = b_x$ (see Fig. 3.2); $\mathrm{d}s$ is the small arc-length of B_0, and is defined as, $\mathrm{d}s = \mathrm{d}x\sqrt{1+b_x^2}$. On the other hand, from Eqn. (3.26), the normal vector can also

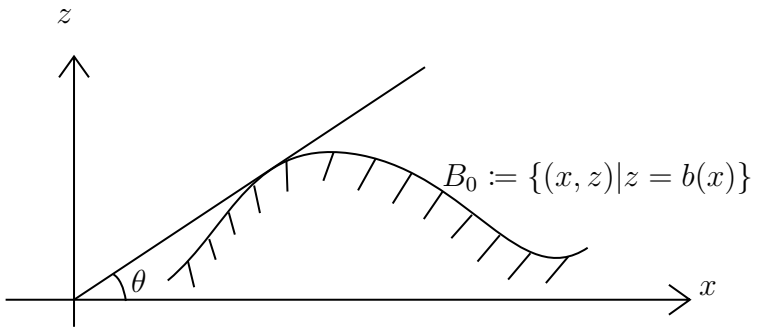

Figure 3.2. – Illustration of geometrical parameters

be expressed as:

$$\mathbf{n}_b = \frac{(b_x, -1)}{\sqrt{1+b_x^2}}.$$

Observe the derivative with respect to the x variable of the x component of the normal vector is:

$$\frac{\mathrm{d}}{\mathrm{d}x}\left(\frac{b_x}{\sqrt{1+b_x^2}}\right) = \frac{b_{xx}}{(1+b_x^2)^{\frac{3}{2}}}. \tag{3.34}$$

Compare Eqn. (3.33) and Eqn. (3.34), the sign of the curvature of a plan curve can be determinate:

$$\kappa = \frac{-b_{xx}}{(1+b_x^2)^{\frac{3}{2}}} = -\nabla_H \cdot \mathbf{n}_b, \tag{3.35}$$

where $\nabla_H \cdot$ denotes the horizontal divergence. Specifically, in the two-dimensional case, this derivative is only with respect to the horizontal variable x. Therefore, in the two-dimensional case, ζ in Eqn. (3.32) is exactly the curvature of a plan curve κ. Notice that, by this definition of curvature, when the curve $z = b(x)$ is convex, the curvature is negative, $\kappa < 0$; the curvature is positive when the curve is concave $\kappa > 0$. Therefore, the bottom boundary condition for pressure Eqn. (3.30) can be finally expressed as:

$$\frac{\partial p}{\partial n_b} + \rho\kappa u_\tau^2 = \rho\mathbf{n}_b \cdot \mathbf{g}. \tag{3.36}$$

Eqn. (3.36) shows that when the bottom topography is concave (there is a hill on the sea bed), κ is positive, and the pressure gradient along $\mathbf{n}_b$ would be smaller than when the bottom topography is flat.

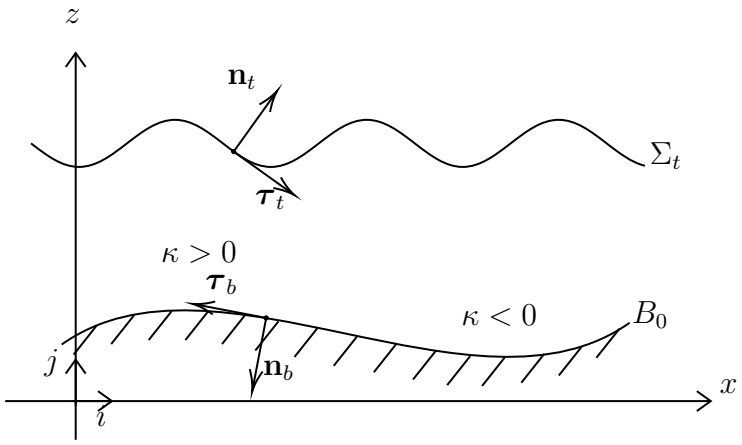

Figure 3.3. – Illustration of bottom boundary condition for pressure

3.3.2. Bottom boundary condition of the pressure in semi-Lagrangian coordinates

From Eqn. (3.26), the tangential velocity at the bottom takes the fore:

$$u_\tau = \frac{-(u + wb_x)}{\sqrt{1 + b_x^2}}. \tag{3.37}$$

Since $b(x)$, $\mathbf{n}_b(x)$, and $\kappa(x)$ depend only on x, these quantities remain of the same form in Euler and semi-Lagrangian coordinates. As before, using the relation between two coordinates systems for all physical parameters:

$$F_x + F_z\Phi_x = \tilde{F}_x; \quad F_z\Phi_\lambda = \tilde{F}_\lambda.$$

The pressure gradient along $\mathbf{n}_b(x)$ in semi-Lagrangian coordinates takes the form:

$$\begin{aligned}\frac{\partial \tilde{p}}{\partial n_b} &= \left(\tilde{p}_x - \tilde{p}_\lambda \frac{\Phi_x}{\Phi_\lambda}\right) \frac{b_x}{\sqrt{1 + b_x^2}} - \frac{\tilde{p}_\lambda}{\Phi_\lambda} \frac{1}{\sqrt{1 + b_x^2}} \\ &= \frac{b_x}{\sqrt{1 + b_x^2}} \tilde{p}_x - \frac{\sqrt{1 + b_x^2}}{\Phi_\lambda} \tilde{p}_\lambda \end{aligned} \tag{3.38}$$

Finally, Eqn. (3.36) becomes:

$$b_x\tilde{p}_x - \frac{1+b_x^2}{\Phi_\lambda}\tilde{p}_\lambda - \rho\frac{b_{xx}(\tilde{u}+\tilde{w}b_x)^2}{(1+b_x^2)^2} = \rho g. \tag{3.39}$$

It is interesting to note that for a flat bottom $b(x) = -H$, where H is a positive constant, the above bottom boundary condition Eqn. (3.39) reduces to the classic bottom boundary condition of hydrostatic pressure: $\dfrac{\partial p}{\partial \mathbf{n}} = \rho \mathbf{n}\cdot\mathbf{g}$.

3.4. Equation for Energy

We start with the momentum equations in semi-Lagrangian coordinates, Eqn. (3.9):

$$\begin{cases} \tilde{u}_t + \tilde{u}\tilde{u}_x + \dfrac{1}{\rho}\left(\tilde{p}_x - \tilde{p}_\lambda\dfrac{\Phi_x}{\Phi_\lambda}\right) = 0, \\ \tilde{w}_t + \tilde{u}\tilde{w}_x + \dfrac{1}{\rho}\left(\tilde{p}_\lambda\dfrac{1}{\Phi_\lambda}\right) = -g. \end{cases}$$

The energy equation in semi-Lagrangian coordinates, can be obtained by taking inner product of the momentum equations showing above and the velocity vector $\tilde{\mathbf{u}} = (\tilde{u}, \tilde{w})^T$,

$$\Phi_\lambda\left(\tilde{u}\tilde{u}_t + \tilde{w}\tilde{w}_t\right) + \Phi_\lambda\tilde{u}\left(\tilde{u}\tilde{u}_x + \tilde{w}\tilde{w}_x\right) + \frac{1}{\rho}\left[\tilde{u}\tilde{p}_x\Phi_\lambda + \tilde{p}_\lambda(\tilde{w} - \tilde{u}\Phi_x)\right] = -\tilde{w}g\Phi_\lambda.$$

With the mass conservation equation:

$$(\Phi_\lambda)_t + (\tilde{u}\Phi_\lambda)_x = 0,$$

and the definition of equation of Φ:

$$\Phi_t + \tilde{u}\Phi_x = \tilde{w}.$$

The above equation can be further simplified as:

$$\begin{aligned}\left(\frac{|\tilde{\mathbf{u}}|^2}{2}\Phi_\lambda\right)_t + \left(\frac{|\tilde{\mathbf{u}}|^2}{2}\Phi_\lambda\tilde{u}\right)_x + \frac{1}{\rho}\left(\tilde{p}\tilde{u}\Phi_\lambda\right)_x + \frac{1}{\rho}\left(\tilde{p}\Phi_t\right)_\lambda - \left(\frac{|\tilde{\mathbf{u}}|^2}{2} + \frac{1}{\rho}\tilde{p}\right)\left[(\Phi_\lambda)_t + (\tilde{u}\Phi_\lambda)_x\right] \\ = -\left(\Phi_t + \tilde{u}\Phi_x\right)g\Phi_\lambda = -\left[(\Phi_\lambda\Phi g)_t - \Phi g\left(\Phi_\lambda\right)_t + (\Phi_\lambda\tilde{u}\Phi g)_x - g\Phi\left(\tilde{u}\Phi_\lambda\right)_x\right].\end{aligned}$$

Finally, the conservative form of energy equation takes the form:

$$\left[\left(\frac{|\tilde{\mathbf{u}}|^2}{2} + g\Phi\right)\Phi_\lambda\right]_t + \left[\left(\frac{|\tilde{\mathbf{u}}|^2}{2} + g\Phi + \frac{\tilde{p}}{\rho}\right)\tilde{u}\Phi_\lambda\right]_x + \left[\frac{\tilde{p}}{\rho}\left(\tilde{w} - \tilde{u}\Phi_x\right)\right]_\lambda = 0. \tag{3.40}$$

3.5. Three-dimensional Euler equations in semi-Lagrangian coordinates

In this section, a general three-dimensional case is discussed. A method is presented to map the whole system from Cartesian coordinates $\mathfrak{D}_{\mathbf{x}} \coloneqq \{(x, y, z)|b(x, y) \leq z \leq \eta(x, y)\}$ to semi-Lagrangian coordinates $\mathfrak{D}_{\mathbf{\Lambda}} \coloneqq \{(x, y, \lambda)|0 \leq \lambda \leq 1\}$. The Jacobian matrix of the mapping is defined as:

$$\mathbf{J} \coloneqq \frac{\partial \mathbf{x}}{\partial \mathbf{\Lambda}} = \begin{bmatrix} 1 & 0 & 0 \\ 0 & 1 & 0 \\ \Phi_x & \Phi_y & \Phi_\lambda \end{bmatrix}, \tag{3.41}$$

where $\mathbf{x} \coloneqq (x, y, z)$, and $\mathbf{\Lambda} \coloneqq (x, y, \lambda)$, and the mapping function $\Phi(t, x, y, \lambda)$ is defined as before:

$$z \coloneqq \Phi(t, x, y, \lambda).$$

The determinant of the Jacobian matrix is: $J = \det \mathbf{J} = \Phi_\lambda$. Since the determinant of the Jacobian matrix $J = \Phi_\lambda$ is never zero, the inverse Jacobian matrix $\mathbf{J}^{-1}$ is exist. In order to map the whole system, including the Euler equations, Poisson's equation of pressure, and the energy equation, it is necessary to derive three vector operators, namely the gradient, the divergence, and the Laplacian. The gradient operator is obvious; f denotes a smooth scalar function in $\mathfrak{D}_{\mathbf{x}}$; and $\tilde{f}$ is the corresponding smooth scalar function in $\mathfrak{D}_{\mathbf{\Lambda}}$. Therefore, we have the following relation:

$$\frac{\partial \tilde{f}}{\partial \mathbf{\Lambda}} = \frac{\partial f}{\partial \mathbf{x}} \frac{\partial \mathbf{x}}{\partial \mathbf{\Lambda}}. \tag{3.42}$$

Here $\nabla_{\mathbf{x}} f$ and $\nabla_{\mathbf{\Lambda}} \tilde{f}$ denote the gradient in domain $\mathfrak{D}_{\mathbf{x}}$ and $\mathfrak{D}_{\mathbf{\Lambda}}$, respectively.

3.5.1. Divergence operator

The divergence operator in the domain $\mathfrak{D}_{\mathbf{x}}$ is denoted by $\mathrm{div}_{\mathbf{x}}$. If $\mathbf{F}$ is a continuously differentiable vector defined on $\mathfrak{D}_{\mathbf{x}}$, then it can be transformed to semi-Lagrangian coordinates using the determinant of the Jacobian matrix:

$$\int_{\mathfrak{D}_{\mathbf{x}}} (\mathrm{div}_{\mathbf{x}} \mathbf{F}) \mathbf{d}\mathfrak{D}_{\mathbf{x}} = \int_{\mathfrak{D}_{\mathbf{\Lambda}}} (\mathrm{div}_{\mathbf{x}} \mathbf{F} J) \, \mathbf{d}\mathfrak{D}_{\mathbf{\Lambda}}. \tag{3.43}$$

On the other hand, by Gauss's theorem, we also have the relation:

$$\int_{\mathfrak{D}_{\mathbf{x}}} (\mathrm{div}_{\mathbf{x}} \mathbf{F}) \mathrm{d}\mathfrak{D}_{\mathbf{x}} = \int_{S_{\mathbf{x}}} (\mathbf{F} \cdot \mathbf{n}) \mathrm{d}S_{\mathbf{x}}. \tag{3.44}$$

Here, $S_{\mathbf{x}}$ is the smooth boundary of the domain $\mathfrak{D}_{\mathbf{x}}$, and $\mathbf{n}$ is the unit normal vector pointing outward to the boundary $S_{\mathbf{x}}$. Assume that the smooth boundary can be parameterized by $\mathbf{r}(x_1, x_2)$, where x_1 and x_2 are two real variables. Then

the surface integral is defined as:

$$\int_{S_{\mathbf{x}}} f \mathrm{d}S_{\mathbf{x}} \coloneqq \int_{S_{\mathbf{x}}} f(\mathbf{r}(x_1, x_2)) \left\| \frac{\partial \mathbf{r}}{\partial x_1} \times \frac{\partial \mathbf{r}}{\partial x_2} \right\| \mathrm{d}x_1 \mathrm{d}x_2.$$

On the other hand, the unit normal vector is given by the cross product of the partial derivatives:

$$\mathbf{n} \coloneqq \frac{\frac{\partial \mathbf{r}}{\partial x_1} \times \frac{\partial \mathbf{r}}{\partial x_2}}{\left\| \frac{\partial \mathbf{r}}{\partial x_1} \times \frac{\partial \mathbf{r}}{\partial x_2} \right\|}. \tag{3.45}$$

Then Eqn. (3.44) can be rewritten as:

$$\begin{aligned} \int_{S_{\mathbf{x}}} (\mathbf{F} \cdot \mathbf{n}) \mathrm{d}S_{\mathbf{x}} &= \int_{S_{\mathbf{x}}} \mathbf{F} \cdot \left(\frac{\partial \mathbf{r}}{\partial x_1} \times \frac{\partial \mathbf{r}}{\partial x_2} \right) \mathrm{d}x_1 \mathrm{d}x_2 \\ &= \int_{S_{\mathbf{x}}} (\mathbf{F}, \mathrm{d}_1\mathbf{x}, \mathrm{d}_2\mathbf{x}) \end{aligned} \tag{3.46}$$

Here, $(\mathbf{F}, \mathrm{d}_1\mathbf{x}, \mathrm{d}_2\mathbf{x}) \coloneqq \det[\mathbf{F}, \mathrm{d}_1\mathbf{x}, \mathrm{d}_2\mathbf{x}]$ denotes the volume form by the three vectors. Therefore, it can be mapped to the smooth boundary $S_{\mathbf{\Lambda}}$ of the domain $\mathfrak{D}_{\mathbf{\Lambda}}$:

$$\int_{S_{\mathbf{x}}} (\mathbf{F}, \mathrm{d}_1\mathbf{x}, \mathrm{d}_2\mathbf{x}) = \int_{S_{\mathbf{\Lambda}}} (\tilde{\mathbf{F}}, \mathbf{J}\mathrm{d}_1\mathbf{\Lambda}, \mathbf{J}\mathrm{d}_2\mathbf{\Lambda}) = \int_{S_{\mathbf{\Lambda}}} \left(\mathbf{J}\mathbf{J}^{-1}\tilde{\mathbf{F}}, \mathbf{J}\mathrm{d}_1\mathbf{\Lambda}, \mathbf{J}\mathrm{d}_2\mathbf{\Lambda} \right) \tag{3.47}$$

Here, $\mathrm{d}_i\mathbf{\Lambda}$ is the corresponding vector of $\mathrm{d}_i\mathbf{x}$ in Domain $\mathfrak{D}_{\mathbf{\Lambda}}$. Since the determinant of a matrix product equals the product of their determinants, the above equation can be further transferred as:

$$\int_{S_{\mathbf{\Lambda}}} \left(\mathbf{J}\mathbf{J}^{-1}\tilde{\mathbf{F}}, \mathbf{J}\mathrm{d}_1\mathbf{\Lambda}, \mathbf{J}\mathrm{d}_2\mathbf{\Lambda} \right) = \int_{S_{\mathbf{\Lambda}}} J \left(\mathbf{J}^{-1}\tilde{\mathbf{F}}, \mathrm{d}_1\mathbf{\Lambda}, \mathrm{d}_2\mathbf{\Lambda} \right) = \int_{S_{\mathbf{\Lambda}}} J \left(\mathbf{J}^{-1}\tilde{\mathbf{F}} \cdot \tilde{\mathbf{n}} \right) \mathrm{d}S_{\mathbf{\Lambda}}$$

Here, $\tilde{\mathbf{n}}$ denotes the unit normal vector pointing outward on the boundary $S_{\mathbf{\Lambda}}$. Apply Gauss's theorem again, we get:

$$\int_{S_{\mathbf{\Lambda}}} J \left(\mathbf{J}^{-1}\tilde{\mathbf{F}} \cdot \tilde{\mathbf{n}} \right) \mathrm{d}S_{\mathbf{\Lambda}} = \int_{\mathfrak{D}_{\mathbf{\Lambda}}} \mathrm{div}_{\Lambda}(J\mathbf{J}^{-1}\tilde{\mathbf{F}}) \mathrm{d}\mathfrak{D}_{\Lambda}. \tag{3.48}$$

Similarly, $\mathrm{div}_{\mathbf{\Lambda}}$ denotes the divergence operator in the domain $\mathfrak{D}_{\mathbf{\Lambda}}$. Finally, combine Eqn. (3.43) and Eqn. (3.48), the mapping of the divergence operator takes the form:

$$\mathrm{div}_{\mathbf{x}} \mathbf{F} = \frac{1}{J} \mathrm{div}_{\Lambda}(J\mathbf{J}^{-1}\tilde{\mathbf{F}}). \tag{3.49}$$

3.5.2. Laplacian operator of pressure

Since the Laplacian operator is only applied to the pressure, we take the pressure field as the example directly. We know that the Laplacian operator is defined as:

$$\Delta_{\mathbf{x}} p = \mathrm{div}_{\mathbf{x}}(\nabla_{\mathbf{x}} p). \tag{3.50}$$

Now, let $\mathbf{F} = \nabla_{\mathbf{x}}$, and with the mapping relation of the gradient operator Eqn. (3.42), the corresponding $\tilde{\mathbf{F}}$ takes the form:

$$\tilde{\mathbf{F}} = \left((\nabla_{\mathbf{\Lambda}} \tilde{p})^T \mathbf{J}^{-1}\right)^T = \mathbf{J}^{-T}(\nabla_{\mathbf{\Lambda}} \tilde{p}). \tag{3.51}$$

Substituting it back to Eqn. (3.49), the Laplacian pressure can be obtained:

$$\begin{aligned} \Delta_{\mathbf{x}} p &= \frac{1}{J} \mathrm{div}_{\Lambda} \left(J \mathbf{J}^{-1} \mathbf{J}^{-T} (\nabla_{\mathbf{\Lambda}} \tilde{p}) \right) \\ &= \frac{1}{J} \mathrm{div}_{\Lambda} \left(J \left(\mathbf{J}^{-T} \mathbf{J} \right)^{-1} (\nabla_{\mathbf{\Lambda}} \tilde{p}) \right). \end{aligned} \tag{3.52}$$

3.5.3. Reduction from 3D to 2D

In the two-dimensional case, the Jacobian matrix takes the form:

$$\mathbf{J} \coloneqq \frac{\partial \mathbf{x}}{\partial \mathbf{\Lambda}} = \begin{bmatrix} 1 & 0 \\ \Phi_x & \Phi_\lambda \end{bmatrix}. \tag{3.53}$$

The determinant of the Jacobian matrix is: $J = \det \mathbf{J} = \Phi_\lambda$. The inverse Jacobian matrix is defined as:

$$\mathbf{J}^{-1} = \begin{bmatrix} 1 & 0 \\ -\frac{\Phi_x}{\Phi_\lambda} & \frac{1}{\Phi_\lambda} \end{bmatrix}. \tag{3.54}$$

3.5.3.1. Mass equation

Substitute $\mathbf{F} = (u, w)^T$ and $\tilde{\mathbf{F}} = (\tilde{u}, \tilde{w})^T$ as velocity vector in Eqn. (3.49), we have:

$$\begin{aligned} u_x + w_z = \frac{1}{J} \mathrm{div}_{\Lambda}(J \mathbf{J}^{-1} \tilde{\mathbf{F}}) &= \frac{1}{\Phi_\lambda} \mathrm{div}_{\Lambda} \left(\Phi_\lambda \begin{bmatrix} 1 & 0 \\ -\frac{\Phi_x}{\Phi_\lambda} & \frac{1}{\Phi_\lambda} \end{bmatrix} \begin{bmatrix} \tilde{u} \\ \tilde{w} \end{bmatrix} \right) \\ &= \frac{1}{\Phi_\lambda} ((\Phi_\lambda \tilde{u})_x + (-\Phi_x \tilde{u} + \tilde{w})_\lambda) \\ &= \tilde{u}_x - \frac{\Phi_x}{\Phi_\lambda} \tilde{u}_\lambda + \frac{\tilde{w}_\lambda}{\Phi_\lambda} = 0 \end{aligned} \tag{3.55}$$

This is consistent with the mass conservation equation Eqn. (3.8).

3.5.3.2. Momentum equation

The momentum equation in $\mathfrak{D}_{\mathbf{x}}$ takes the form:

$$\rho\frac{\mathrm{d}\mathbf{u}}{\mathrm{d}t}+\nabla_{\mathbf{x}}p=\rho\mathbf{g}. \tag{3.56}$$

The material derivative can be transferred directly, and the gradient of pressure can be mapped as mentioned above. Therefore, the momentum equations in $\mathfrak{D}_{\mathbf{\Lambda}}$ take the form:

$$\rho\frac{\tilde{\mathrm{d}}\tilde{\mathbf{u}}}{\tilde{\mathrm{d}}t}+\nabla_{\mathbf{\Lambda}}p\mathbf{J}^{-1}=\rho\mathbf{g}. \tag{3.57}$$

In other form, This is consistent with the momentum equation Eqn. (3.9):

$$\begin{cases}\tilde{u}_t+\tilde{u}\tilde{u}_x+\dfrac{1}{\rho}\left(\tilde{p}_x-\tilde{p}_\lambda\dfrac{\Phi_x}{\Phi_\lambda}\right)=0,\\ \tilde{w}_t+\tilde{u}\tilde{w}_x+\dfrac{1}{\rho}\left(\tilde{p}_\lambda\dfrac{1}{\Phi_\lambda}\right)=-g.\end{cases} \tag{3.58}$$

3.5.3.3. Energy equation

The energy equation in $\mathfrak{D}_{\mathbf{x}}$ takes the form:

$$\left(\frac{|\mathbf{u}|^2}{2}+gz\right)_t+\mathrm{div}_{\mathbf{x}}\left[\left(\frac{|\mathbf{u}|^2}{2}+gz+\frac{p}{\rho}\right)\mathbf{u}\right]=0. \tag{3.59}$$

Or we can write as:

$$\frac{\mathrm{d}}{\mathrm{d}t}\left(\frac{|\mathbf{u}|^2}{2}+gz\right)+\mathrm{div}_{\mathbf{x}}\left(\frac{p}{\rho}\mathbf{u}\right)=0. \tag{3.60}$$

Again, the material derivative can be transferred directly, and from the relation of the gradient operator, Eqn. (3.49), we obtain the energy equation in $\mathfrak{D}_{\mathbf{\Lambda}}$:

$$\begin{aligned}&\frac{\tilde{\mathrm{d}}}{\tilde{\mathrm{d}}t}\left(\frac{|\mathbf{u}|^2}{2}+g\Phi\right)+\frac{1}{\Phi_\lambda}\mathrm{div}_{\mathbf{\Lambda}}\left(\frac{\tilde{p}}{\rho}\begin{bmatrix}\Phi_\lambda & 0\\ -\Phi_x & 1\end{bmatrix}\begin{bmatrix}\tilde{u}\\ \tilde{w}\end{bmatrix}\right)\\ =&\frac{\tilde{\mathrm{d}}}{\tilde{\mathrm{d}}t}\left(\frac{|\mathbf{u}|^2}{2}+g\Phi\right)+\frac{1}{\Phi_\lambda}\left\{\left(\frac{\tilde{p}}{\rho}\tilde{u}\Phi_\lambda\right)_x+\left[(\tilde{w}-\tilde{u}\Phi_x)\frac{\tilde{p}}{\rho}\right]_\lambda\right\}=0.\end{aligned} \tag{3.61}$$

Multiply the above equation with Φ_λ, and with the integral form of the mass conservation equation, $(\Phi_\lambda)_t+(\tilde{u}\Phi_\lambda)_x=0$, we obtain:

$$\left[\left(\frac{|\tilde{\mathbf{u}}|^2}{2}+g\Phi\right)\Phi_\lambda\right]_t+\left[\left(\frac{|\tilde{\mathbf{u}}|^2}{2}+g\Phi+\frac{\tilde{p}}{\rho}\right)\tilde{u}\Phi_\lambda\right]_x+\left[\frac{\tilde{p}}{\rho}(\tilde{w}-\tilde{u}\Phi_x)\right]_\lambda=0, \tag{3.62}$$

this is consistent with the energy equation Eqn. (3.40).

3.5.3.4. Pressure equation

From Eqn. (3.52), the equation of pressure takes the form:

$$\begin{aligned}
\Delta_{\mathbf{x}} p &= \frac{1}{J}\,\mathrm{div}_\Lambda\left(J\left(\mathbf{J}^{-T}\mathbf{J}\right)^{-1}(\nabla_{\mathbf{\Lambda}}\tilde{p})^T\right)\\
&= \frac{1}{\Phi_\lambda}\,\mathrm{div}_\Lambda\left(\Phi_\lambda\left(\begin{bmatrix}1 & \Phi_x\\ 0 & \Phi_\lambda\end{bmatrix}\begin{bmatrix}1 & 0\\ \Phi_x & \Phi_\lambda\end{bmatrix}\right)^{-1}\begin{bmatrix}\tilde{p}_x\\ \tilde{p}_\lambda\end{bmatrix}\right)\\
&= \frac{1}{\Phi_\lambda}\,\mathrm{div}_\Lambda\left(\frac{1}{\Phi_\lambda}\begin{bmatrix}\Phi_\lambda^2 & -\Phi_x\Phi_\lambda\\ -\Phi_x\Phi_\lambda & 1+\Phi_x^2\end{bmatrix}\begin{bmatrix}\tilde{p}_x\\ \tilde{p}_\lambda\end{bmatrix}\right) = \frac{1}{\Phi_\lambda}\,\mathrm{div}_\Lambda\left(\begin{bmatrix}\Phi_\lambda\tilde{p}_x - \Phi_x\tilde{p}_\lambda\\ -\Phi_x\tilde{p}_x + \frac{1+\Phi_x^2}{\Phi_\lambda}\tilde{p}_\lambda\end{bmatrix}\right)\\
&= \frac{1}{\Phi_\lambda}\left[(\Phi_\lambda\tilde{p}_x - \Phi_x\tilde{p}_\lambda)_x + \left(-\Phi_x\tilde{p}_x + \frac{1+\Phi_x^2}{\Phi_\lambda}\tilde{p}_\lambda\right)_\lambda\right],
\end{aligned} \tag{3.63}$$

This is consistent with the energy equation Eqn. (3.25).

3.6. Numerical scheme

3.6.1. Overview of the numerical solution strategy

The unknown variables of this system are: the mapping function $\Phi(t,x,\lambda)$, the two velocity components $\tilde{u}(t,x,\lambda)$, $\tilde{w}(t,x,\lambda)$, and the total pressure $\tilde{p}(t,x,\lambda)$.

Instead of using the definition of the mapping function $\Phi_t + \tilde{u}\Phi_x = \tilde{w}$ to solve for Φ, the equivalent equation Eqn. (3.14) is used:

$$(\Phi_\lambda)_t + (\tilde{u}\Phi_\lambda)_x = 0.$$

Introduce $q(t,x,\lambda) \coloneqq \Phi_\lambda$ as an independent variable. In our scheme, Φ is obtained by numerical integration of q over λ.

Two velocity equations are solved with the momentum equations. Moreover, instead of using the total pressure $\tilde{p}$, the dynamic pressure is introduced:

$$Q(t,x,\lambda) \coloneqq \frac{\tilde{p}}{\rho} - g(\eta - \Phi). \tag{3.64}$$

Here $\eta(t,x)$ is the position of the free surface, and it is defined as:

$$\eta(t,x) \coloneqq \Phi(t,x,\lambda=1).$$

Then, the momentum equations Eqn. (3.9) can be rewritten as:

$$\begin{cases} \tilde{u}_t + \tilde{u}\tilde{u}_x + Q_x - Q_\lambda \dfrac{\Phi_x}{q} = -g\eta_x, \\ \tilde{w}_t + \tilde{u}\tilde{w}_x + \dfrac{Q_\lambda}{q} = 0. \end{cases} \tag{3.65}$$

The dynamic pressure is obtained by the projection method (Wesseling 2009). Moreover, instead of calculating the dynamic pressure at the next time-step t^{n+1} directly, for the purpose of accuracy, a new unknown variable is introduced:

$$\delta \coloneqq Q^{n+1} - Q^n, \tag{3.66}$$

which is the difference of the dynamic pressure between two time-steps. Here, the superscript n denotes the index of the time step.

Since the projection method is applied, several prediction steps appear for the velocity field. More precisely, there are two prediction steps for the horizontal velocity $\tilde{u}$, and one prediction step for the vertical velocity $\tilde{w}$.

Moreover, the vertical momentum equation is discretized with the Keller-box scheme (Stelling and Zijlema 2003). This scheme is more accurate than the common finite difference scheme with the same number of vertical grid points. Time discretization uses the $\theta-$scheme, where θ is an implication factor between the next timestep, t^{n+1}, and the current timestep, t^n. To make the scheme stable, we choose $\frac{1}{2} \leq \theta \leq 1$.

3.6.2. Discretizations

The vertical domain is discretized as:

$$\lambda_{k+\frac{1}{2}} \coloneqq k\Delta\lambda; \quad k = 0, 1, \cdots K; \quad \Delta\lambda \coloneqq \frac{1}{K}, \quad K \in \mathbb{N}, \tag{3.67}$$

with $\Delta\lambda$ represents the vertical length of the cell. Similarly, the horizontal domain is discretized as:

$$x_{i+\frac{1}{2}} \coloneqq i\Delta x; \quad i = 0, 1, \cdots I; \quad \Delta x \coloneqq \frac{L}{I}, \quad I \in \mathbb{N}, \tag{3.68}$$

with Δx as the horizontal length of the cell.

Finally, the time discretization is defined as: $\Delta t \coloneqq t^{n+1} - t^n$. In the current implementation, Δt is kept constant.

A staggered grid is applied, in which the velocity components $\tilde{u}$ and $\tilde{w}$ are located in the middle of the cell boundary, $\left(i + \frac{1}{2}, k\right)$ and $\left(i, k + \frac{1}{2}\right)$, respectively. However, the dynamic pressure component Q is located at the same location as $\tilde{w}$, $\left(i, k + \frac{1}{2}\right)$ due to the application of the Keller-box scheme. Fig. 3.4 shows the

locations of the unknown variables. Notice that, to have more accurate results of the horizontal velocity $\tilde{u}$ on the free surface and bottom, $\tilde{u}$ is also placed on $\left(i, K+\frac{1}{2}\right)$ and $\left(i, \frac{1}{2}\right)$, respectively.

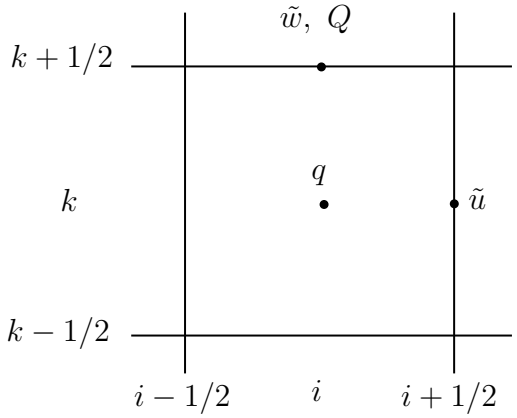

Figure 3.4. – Locations of the unknown variables in a staggered grid.

The first prediction of the horizontal velocity component is based on the forward Euler method, and it's calculated at the cell boundary $\left(i+\frac{1}{2}, k\right)$, which takes the form:

$$\frac{\tilde{u}^{**}-\tilde{u}^{n}}{\Delta t}+(\tilde{u}\tilde{u}_{x})^{n}+Q_{x}^{n}-\left(\frac{\Phi_{x}}{q}\right)^{n}Q_{\lambda}^{n}=-g\eta_{x}^{n}. \tag{3.69}$$

Here, the horizontal and vertical derivatives are obtained by the finite difference method. The reason of calculating this first predictor of $\tilde{u}$ is to construct a semi-implicit scheme of the unknown variable q at the center of the cell, (i,k):

$$\frac{q^{n+1}-q^{n}}{\Delta t}+(\tilde{u}^{**}q^{n+1})_{x}=0. \tag{3.70}$$

After obtaining q^{n+1}, the mapping function $\Phi(t^{n+1},x,\lambda)$ can be obtained by numerical integration of q^{n+1} from $\lambda=0$ to any λ, with the bottom boundary condition $\Phi(t^{n+1},x,\lambda=0)\equiv 0$.

The second prediction of the horizontal velocity component is a transitional step for the final step, which can calculated explicitly at the cell boundary $\left(i+\frac{1}{2}, k\right)$:

$$\frac{\tilde{u}^{*}-\tilde{u}^{**}}{\Delta t}+\theta\left(\frac{\Phi_{x}}{q}\right)^{n}Q_{\lambda}^{n}-\left(\frac{\Phi_{x}}{q}\right)^{n+1}Q_{\lambda}^{n}=-g\theta\left(\eta^{n+1}-\eta^{n}\right)_{x}. \tag{3.71}$$

The final step is not only the equation to obtain the horizontal velocity component in the next time step $\tilde{u}^{n+1}$, but also one of the equations to construct the Poisson equation for pressure. Therefore, this equation should be formulated from the unknown variable $\delta \coloneqq Q^{n+1}-Q^{n}$, and that is why the first predictor of horizontal

velocity $\tilde{u}^{**}$ is needed.

Finally, the equation for the horizontal velocity component at the next time step takes the form:

$$\frac{\tilde{u}^{n+1}-\tilde{u}^{*}}{\Delta t}+\theta\delta_x-\left(\frac{\Phi_x}{q}\right)^{n+1}\delta_\lambda=0. \tag{3.72}$$

The vertical momentum equation is discretized with the Keller-box scheme. The idea of this scheme is the following: instead of calculating the vertical momentum equation at the boundary of the cell where $\tilde{w}$ is located, we calculate the vertical momentum equation at the middle of the cell, (i,k), by taking the average of the vertical momentum equation at both the upper and lower boundaries of the cell, $\left(i,k+\frac{1}{2}\right)$ and $\left(i,k-\frac{1}{2}\right)$, respectively.

Therefore, the predictor of the vertical velocity component takes the form:

$$\frac{\tilde{w}_{+}^{*}-\tilde{w}_{+}^{n}}{\Delta t}+\frac{\tilde{w}_{-}^{*}-\tilde{w}_{-}^{n}}{\Delta t}+(\tilde{u}\tilde{w}_x)_{+}^{n}+(\tilde{u}\tilde{w}_x)_{-}^{n}+2(1-\theta)\left(\frac{Q_\lambda}{q}\right)^{n}+2\theta\left(\frac{Q_\lambda^{n}}{q^{n+1}}\right)=0. \tag{3.73}$$

Here, the subscripts $+$ and $-$ mean the upper and lower boundaries, respectively.

From the bottom boundary condition, $\tilde{w}(t,x,\lambda=0)\equiv 0$, which implies $\tilde{w}^{*}_{i,\frac{1}{2}}\equiv 0$, therefore, the predictor of the vertical velocity component $\tilde{w}^{*}$ can be obtained explicitly. Notice that, since the equation is defined at the middle of the cell (i,k), then the term Q_λ should be calculated at this location. Finally, the vertical velocity at the next time step is:

$$\frac{\tilde{w}_{+}^{n+1}-\tilde{w}_{+}^{*}}{\Delta t}+\frac{\tilde{w}_{-}^{n+1}-\tilde{w}_{-}^{*}}{\Delta t}+2\theta\left(\frac{\delta_\lambda}{q^{n+1}}\right)=0. \tag{3.74}$$

Again, with the bottom boundary condition, $\tilde{w}^{n+1}_{i,\frac{1}{2}}\equiv 0$, $\tilde{w}^{n+1}$ can also be calculated explicitly, after the unknown variable δ is obtained from Poisson's equation for pressure.

To have an overview of the momentum equation, we sum up the discretized momentum equations, respectively:

$$\frac{\tilde{u}^{n+1}-\tilde{u}^{n}}{\Delta t}+(\tilde{u}\tilde{u}_x)^{n}+\theta\left[Q_x^{n+1}-\left(\frac{\Phi_x}{q}\right)^{n+1}Q_\lambda^{n+1}\right]+(1-\theta)\left[Q_x^{n}-\left(\frac{\Phi_x}{q}\right)^{n}Q_\lambda^{n}\right]=-g\theta\eta_x^{n+1}-g(1-\theta)\eta_x^{n}, \tag{3.75}$$

$$\frac{\tilde{w}_{+}^{n+1}-\tilde{w}_{+}^{n}}{\Delta t}+\frac{\tilde{w}_{-}^{n+1}-\tilde{w}_{-}^{n}}{\Delta t}+(\tilde{u}\tilde{w}_x)_{+}^{n}+(\tilde{u}\tilde{w}_x)_{-}^{n}+2\theta\left(\frac{Q_\lambda}{q}\right)^{n+1}+2(1-\theta)\left(\frac{Q_\lambda}{q}\right)^{n}=0. \tag{3.76}$$

The Poisson equation for pressure can be obtained by taking directly the divergence operator on Eqn. (3.72) and Eqn. (3.74):

$$(q \cdot \text{Eqn. (3.72)})_x - (\Phi_x \cdot \text{Eqn. (3.72)})_\lambda + (\text{Eqn. (3.74)})_\lambda = 0,$$

with considering the divergence of the velocity field at the next time-step vanishes:

$$\text{div}_{\mathbf{\Lambda}}\, \tilde{\mathbf{u}}^{n+1} \equiv 0, \quad \tilde{\mathbf{u}}^{n+1} := (\tilde{u}^{n+1}, \tilde{w}^{n+1}).$$

Finally, it takes the form:

$$\Delta_{\mathbf{\Lambda}}\delta = \frac{\text{div}_{\mathbf{\Lambda}}\, \mathbf{u}^*}{\Delta t}, \quad \mathbf{u}^* := (u^*, w^*). \tag{3.77}$$

In summary, the main steps of the numerical code would be as follows:

1. Get the first predictor of horizontal velocity u^{**} from Eqn. (3.69).
2. Obtain q^{n+1} for the next time step from Eqn. (3.70).
3. Integrate q^{n+1} numerically in λ-direction to get Φ^{n+1}.
4. Calculate the second predictor of horizontal velocity u^* and the predictor of vertical velocity w^* from Eqn. (3.71) and Eqn. (3.73), respectively.
5. Solve the Poisson equation for dynamic pressure Eqn. (3.77) to get δ.
6. Update the corrector of both horizontal and vertical velocity u^{n+1} and w^{n+1} from Eqn. (3.72) and Eqn. (3.74), respectively.

3.6.3. Partial numerical results

A computational code was developed in Fortran and tested for the case of a stable periodic nonlinear wave in uniform wave depth. The initial solution is obtained from the so-called stream-function theory in a potential flow framework (Dean 1965), using the code steam_HT (Benoit, Luck, Chevalier, and Belorgey 2003). It also serves as a reference solution at any later time instants as the wave is propagating without deformation and a known phase celerity (denoted C, provided on output by the stream-function method).

We consider a periodic wave propagating in the positive x direction, in a mean water depth $H = 1.9$ m, with a wave amplitude (crest-to-trough height) $\eta = 0.2$ m and a wavelength $L = 37.5$ m.

The calculated wave period is $T \approx 8.727$ s, and the celerity is $C = \dfrac{L}{T} \approx 4.30\ \dfrac{m}{s}$.

The relative water depth $\dfrac{H}{L} \approx 0.05$ and the wave steepness is $\dfrac{\eta}{L} \approx 0.005$. The corresponding Ursell number is $U_r = \dfrac{\eta L^2}{H^3} \approx 41.0$. This wave condition is plotted on the Le Méhauté diagram (Le Méhauté 1976) in Fig. 3.5 (marked by "*"). The notation in this figure is different from that in this article, h in the figure is the mean

water depth H; H in the figure is the wave amplitude η; and τ is the wave period T. It can be verified that the chosen wave condition belongs to the shallow-water nonlinear regime.

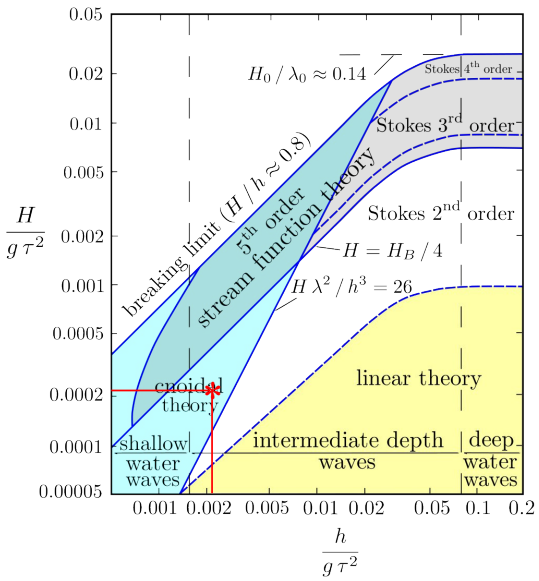

Figure 3.5. – The tested case marked on Le Méhauté diagram (the diagram was taken from Wikipedia)

The horizontal domain covers exactly one wavelength L and uses periodic lateral boundary conditions. The vertical range is discretized into 64 cells($\Delta x = \frac{37.5}{64}$m); the vertical domain is discretized into 40 cells ($\Delta\lambda = \frac{1}{40}$). The time step is discretized as: $\Delta t = \frac{T}{250} \approx 0.035$ s. The corresponding CFL number is around 0.21. The initial conditions of the simulations, namely Φ, $\tilde{u}$, $\tilde{w}$ and Q are imposed on the (x, λ) grid from the stream-function calculation.

Fig. 3.6 shows the corresponding numerical results of the physical unknowns, Φ, $\tilde{u}$, $\tilde{w}$, Q, and the value div $\tilde{\mathbf{u}}$.

In fact, the following numerical results are not obtained exactly from the scheme described above (but with an earlier version). Two parts are different between the earlier version scheme and the scheme described above:

1. The Keller-box scheme is not applied; this leads to a staggered grid being used, in other words, the dynamic pressure Q is stored at the center of the cell (i, k), instead of the middle of the upper boundary of this cell.
2. The idea of using the difference in dynamic pressure between two time steps, $\delta \coloneqq Q^{n+1} - Q^n$ is not yet implemented.

The numerical results are shown for three different levels, $\lambda = 0$ (seabed), $\lambda = 0.5$ and $\lambda = 1$ (free surface), which are represented by black, red, and blue lines, respectively. Remark that $\Phi(\lambda = 1)$ is the free surface evolution, which is shown by the blue line in the variable Φ. In Fig. 3.6a, the initial states are shown, and we can see that $\operatorname{div} \mathbf{u}$ is exactly zero initially. Fig. 3.6b, Fig. 3.6c and Fig. 3.6d show the numerical results when $t = 10\Delta t$, $t = 60\Delta t$ and $t = 100\Delta t$, respectively. One can observe that $\operatorname{div} \mathbf{u}$ increases in time, and the vertical velocity w increases afterwards (see the results when $t = 60\Delta t$, Fig. 3.6c).

In the present implementation, the numerical code blows up within a half-wave period (Fig. 3.6d). We anticipate that this problem might come from the inaccuracy in applying the vertical discretization, which plays an important role when calculating the vertical velocity and the pressure. Thus, using the Keller-box scheme and applying the concept of δ should allow us to have a more accurate pressure estimation. Tests in this direction are ongoing, in particular by implementing the two features mentioned above (Keller-box scheme + use of δ for the dynamic pressure).

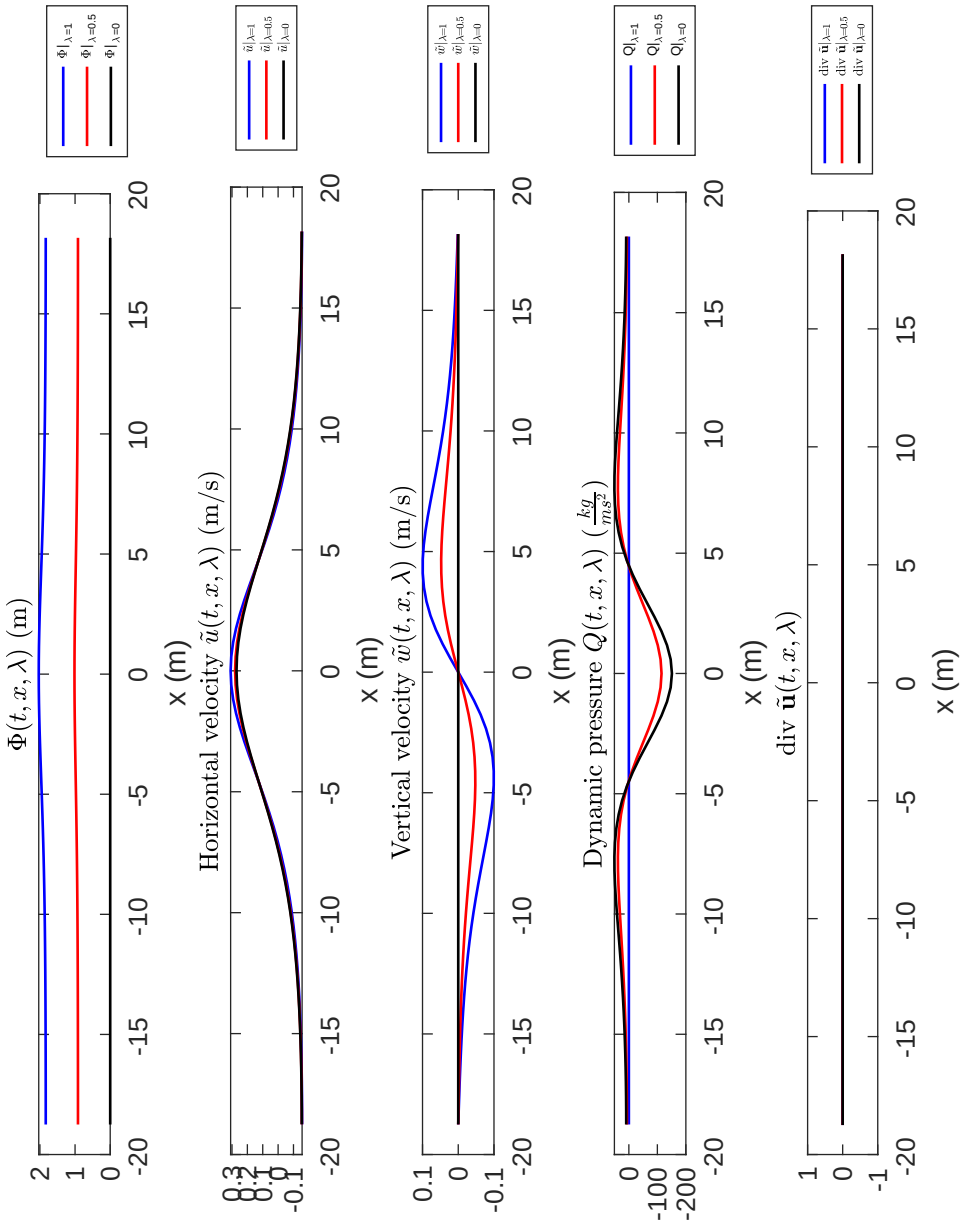

(a) Initial state, $t = 0$ s.

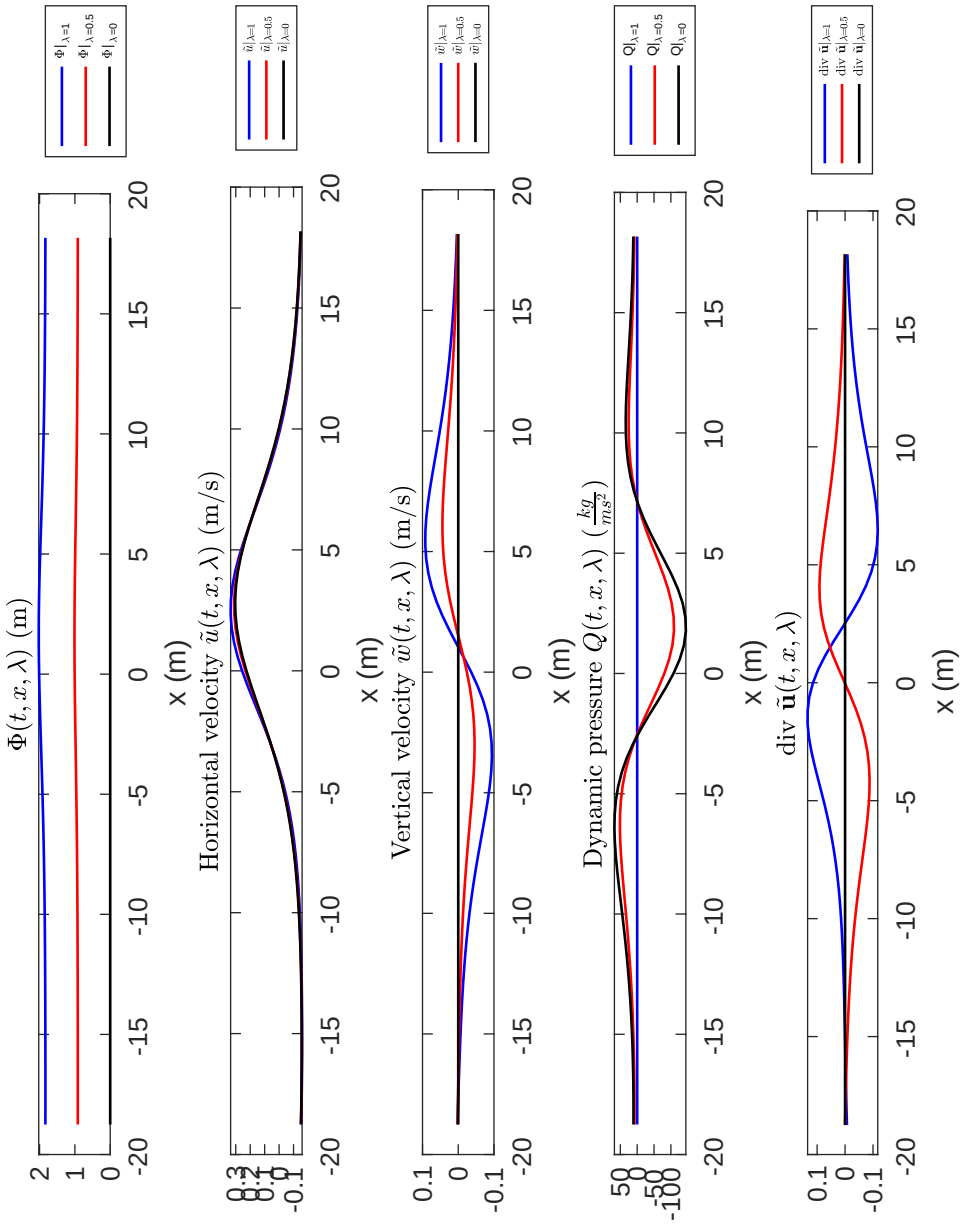

(b) $t = 10\Delta t = \dfrac{10}{250}T \approx 0.349$ s.

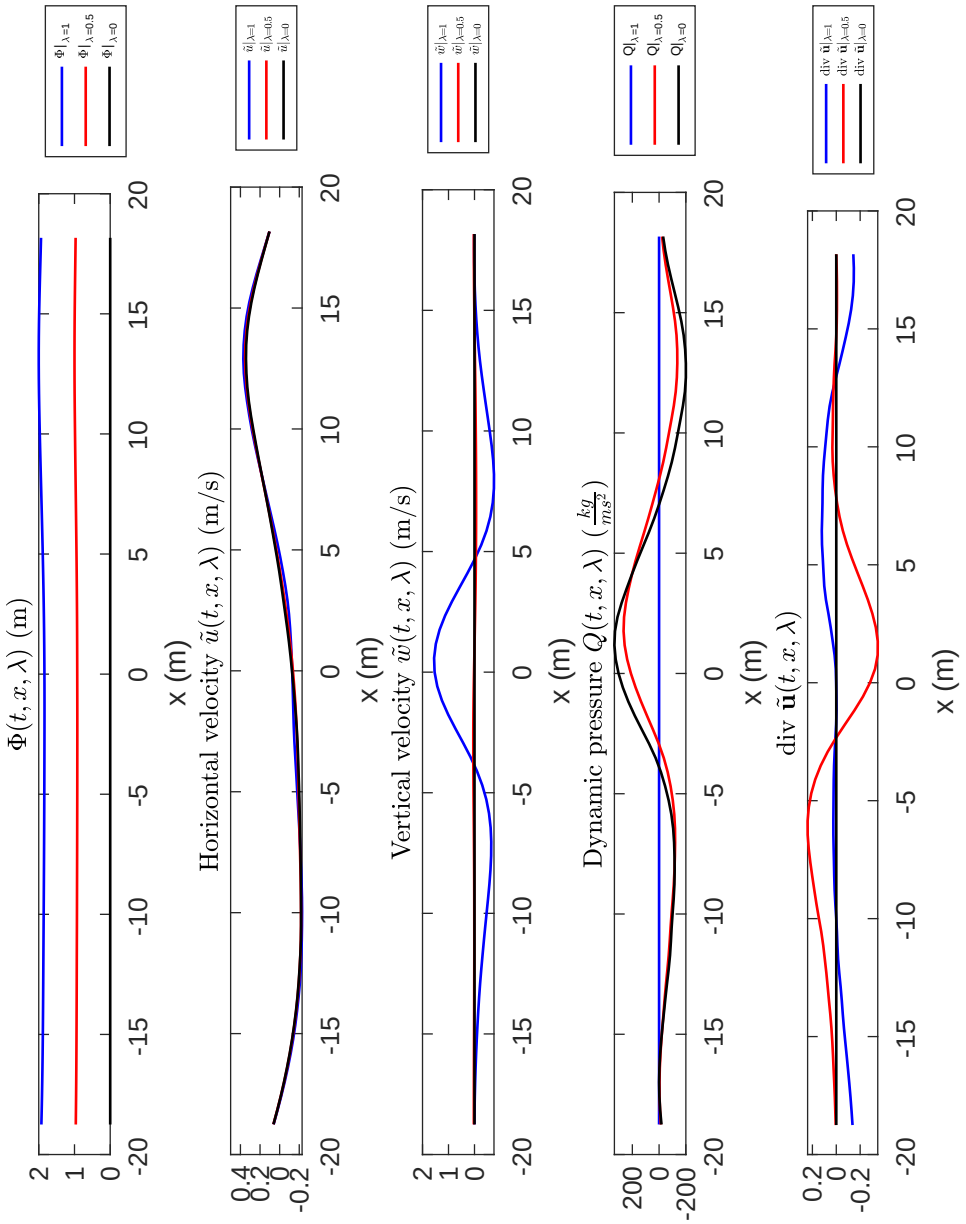

(c) $t = 60\Delta t = \dfrac{60}{250}T \approx 2.095$ s.

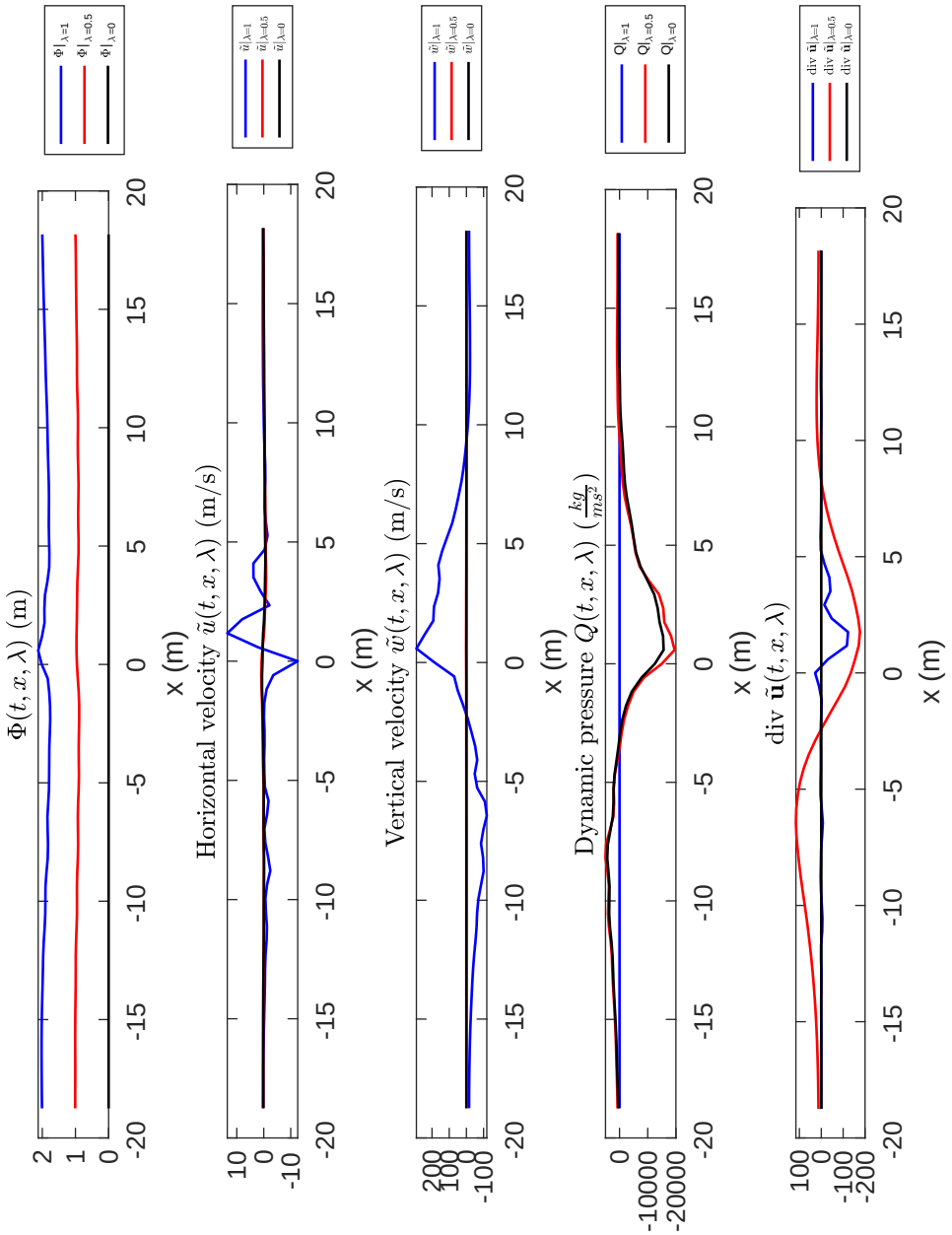

(d) $t = 100\Delta t = \dfrac{100}{250}T \approx 3.491$ s.

Figure 3.6. – Partial numerical results

3.7. Conclusion

In this work, the Euler equations and the equation of energy in semi-Lagrangian coordinates are derived. The bottom boundary condition of Poisson's equation of pressure is found, which depends on the curvature of the bottom topography $B_0(x)$ in the general case.

A numerical code was developed and tested on a flat-bottom case, $B_0(x) = -H$. However, several difficulties are faced while working on it. A significant problem is that the velocity field is not always divergence-free numerically, after updating the velocity field by the solution of Poisson's equation for pressure. This may be the reason the system becomes numerically unstable.

One of the possible methods to deal with this problem is using the concept of staggered grids, namely not storing all variables at the same location. On the other hand, solving a conservative system numerically might also reduce the value of $\operatorname{div} \mathbf{u}$. In other words, instead of calculating the unknown velocity $\tilde{u}$, and $\tilde{w}$ numerically from Eqn. (3.9), consider $\Phi_\lambda \tilde{u}$ and $\Phi_\lambda \tilde{w}$ as the unknown velocity field, and obtain the solution from Eqn. (3.18). Moreover, using the difference of the dynamic pressure between two time-steps ($\delta := Q^{n+1} - Q^n$) might also provide a more accurate solution while solving Poisson's equation for pressure, and also more accurate "correctors" of velocity fields. A couple of methods and strategies were already tried; however, the problem is not completely understood yet. Nevertheless, a possible numerical scheme is presented.

A complete numerical study for the flat-bottom case is needed as the basis of further numerical studies. A direct extension case of this work is to study the effect of the arbitrary smooth bottom topography acting on the pressure numerically.

Conclusion and perspective

The modulation equations for BBM equation is completely studied in Chapter 1. The boundary of modulational stability is found. The instability region can be approximated by $k > \sqrt{3}$, where k is the wave number.

A two-layer flow of ideal homogeneous fluid described by the Benney equations with continuous piecewise linear velocity profile is studied in Chapter 2. The total energy of this system is not convex. Hence the system can not be symmetrized by using the Godunov, Friedrichs, and Lax method. However, the system is hyperbolic, and the Riemann invariants for this system can be found explicitly. The study of the eigenfields has been done. Two eigenfields corresponding to the fast and slow surface waves are genuinely nonlinear in the sense of Lax. The third eigenfield corresponds to the vorticity transport is neither genuinely nonlinear nor linear degenerate. The region of parameters (ω_1, ω_2) where all three eigenfields are genuinely nonlinear is found. In this case, the "entropy" condition guarantees the shock stability for all fields. However, when the second characteristic field is neither genuinely nonlinear nor linear degenerate, a stable shock exists corresponding to the wrong "entropy" inequality. This unphysical result might be due to the assumption of the constant vorticities in both layers, $\omega_1 = \text{const.}$ and $\omega_2 = \text{const.}$ These vorticities are assumed not to change through the shock. Probably, a new two-layer flow model should be derived where the vorticity in both layers can change through the shock.

The Euler equations in semi-Lagrangian coordinates are formulated in Chapter 3. A curvature-depending bottom boundary condition for Poisson's equation for pressure is derived. Several difficulties are faced while doing numerical studies with a flat-bottom case. The most significant issue is that it is difficult to keep $\operatorname{div} \mathbf{u}$ vanishing numerically. Different numerical techniques should be tested to guarantee the condition $\operatorname{div} \mathbf{u} = 0$.

Bibliography

[APB24] Andreas Alexandris-Galanopoulos, George Papadakis, and Kostas Belibassakis. "A semi-Lagrangian Splitting framework for the simulation of non-hydrostatic free-surface flows". In: *Ocean Modelling* 187 (2024), p. 102290 (cit. on p. 16).

[BGT07] R Barros, SL Gavrilyuk, and VM Teshukov. "Dispersive nonlinear waves in two-layer flows with free surface. I. Model derivation and general properties". In: *Studies in Applied Mathematics* 119.3 (2007), pp. 191–211 (cit. on p. 19).

[BF67] T Brooke Benjamin and James E Feir. "The disintegration of wave trains on deep water Part 1. Theory". In: *Journal of Fluid Mechanics* 27.3 (1967), pp. 417–430 (cit. on p. 13).

[BBM72] Thomas Brooke Benjamin, Jerry Lloyd Bona, and John J Mahony. "Model equations for long waves in nonlinear dispersive systems". In: *Philosophical Transactions of the Royal Society of London. Series A, Mathematical and Physical Sciences* 272.1220 (1972), pp. 47–78 (cit. on pp. 12, 17).

[Ben73] DJ Benney. "Some properties of long nonlinear waves". In: *Studies in Applied Mathematics* 52.1 (1973), pp. 45–50 (cit. on pp. 13, 14).

[Ben+03] Michel Benoit, Marilyne Luck, Christophe Chevalier, and Michel Belorgey. "Near-bottom kinematics of shoaling and breaking waves: experimental investigation and numerical prediction". In: *Coastal Engineering 2002: Solving Coastal Conundrums*. World Scientific, 2003, pp. 306–318 (cit. on p. 112).

[BNR14] Sylvie Benzoni-Gavage, Pascal Noble, and Luis Miguel Rodrigues. "Slow modulations of periodic waves in Hamiltonian PDEs, with application to capillary fluids". In: *Journal of Nonlinear Science* 24 (2014), pp. 711–768 (cit. on p. 13).

[Che+17] Chesnokov, El, Gavrilyuk, and Pavlov. "Stability of shear shallow water flows with free surface". In: *SIAM Journal on Applied Mathematics* 77.3 (2017), pp. 1068–1087 (cit. on pp. 14, 54, 55).

[CSY05] C Mei Chiang, Michael Stiassnie, and Dick KP Yue. *Theory and Applications of Ocean Surface Waves: Part 1: Linear Aspects Part 2: Nonlinear Aspects*. World Scientific, 2005 (cit. on p. 17).

[Dav88] Stephen F Davis. “Simplified second-order Godunov-type methods”. In: *SIAM Journal on Scientific and Statistical Computing* 9.3 (1988), pp. 445–473 (cit. on p. 92).

[Dea65] Robert G Dean. “Stream function representation of nonlinear ocean waves”. In: *Journal of Geophysical Research* 70.18 (1965), pp. 4561–4572 (cit. on p. 112).

[Di +24] Bernard Di Martino, Chourouk El Hassanieh, Edwige Godlewski, et al. “Hyperbolicity of a semi-Lagrangian formulation of the hydrostatic free-surface Euler system”. In: *Nonlinearity* 38.1 (2024), p. 015018 (cit. on p. 16).

[FL71] Kurt O Friedrichs and Peter D Lax. “Systems of conservation equations with a convex extension”. In: *Proceedings of the National Academy of Sciences* 68.8 (1971), pp. 1686–1688 (cit. on p. 47).

[GLS23] Sergey Gavrilyuk, Yu-Hsi Lin, and Keh-Ming Shyue. “Hyperbolicity study of the modulation equations for the Benjamin–Bona–Mahony equation”. In: *Studies in Applied Mathematics* 151.2 (2023), pp. 536–554 (cit. on pp. 3, 25).

[GS21] Gavrilyuk and Shyue. “Singular solutions of the BBM equation: analytical and numerical study”. In: *Nonlinearity* 35.1 (2021), p. 388 (cit. on p. 13).

[GMS17] SL Gavrilyuk, NI Makarenko, and SV Sukhinin. *Waves in continuous media*. Vol. 11. Springer, 2017 (cit. on p. 17).

[God61] Godunov. “An interesting class of quasilinear systems”. In: *Dokl. Akad. Nauk SSSR*. Vol. 139. 1961, pp. 521–523 (cit. on p. 47).

[God59] SK0171 Godunov. “Finite difference methods for the computation of discontinuous solutions of the equations of fluid dynamics”. In: *Mat. Sb.* 47 (1959), pp. 271–306 (cit. on p. 91).

[HLL83] Amiram Harten, Peter D Lax, and Bram van Leer. “On upstream differencing and Godunov-type schemes for hyperbolic conservation laws”. In: *SIAM review* 25.1 (1983), pp. 35–61 (cit. on p. 92).

[HP16] Vera Mikyoung Hur and Ashish Kumar Pandey. “Modulational instability in nonlinear nonlocal equations of regularized long wave type”. In: *Physica D: Nonlinear Phenomena* 325 (2016), pp. 98–112 (cit. on p. 13).

[Lan13] David Lannes. *The water waves problem: mathematical analysis and asymptotics*. Vol. 188. American Mathematical Soc., 2013 (cit. on p. 17).

[Le 76] Bernard Le Méhauté. *An introduction to hydrodynamics and water waves*. Springer Science & Business Media, 1976 (cit. on p. 112).

[LeV92] Randall J LeVeque. *Numerical methods for conservation laws*. Vol. 132. Springer, 1992 (cit. on p. 90).

[Liu74] Tai Ping Liu. "The Riemann problem for general 2× 2 conservation laws". In: *Transactions of the American Mathematical Society* 199 (1974), pp. 89–112 (cit. on p. 47).

[Liu75] Tai-Ping Liu. "The Riemann problem for general systems of conservation laws". In: *Journal of Differential Equations* 18.1 (1975), pp. 218–234 (cit. on p. 47).

[Mit13] Dimitrios Mitsotakis. "A simple introduction to water waves". In: (2013) (cit. on p. 17).

[Miu80] RM Miura. "Explicit roots of the cubic polynomial and applications". In: *Appl. Math. Notes* 4 (1980), pp. 22–40 (cit. on p. 59).

[Nic06] RWD Nickalls. "Viete, Descartes and the cubic equation". In: *The Mathematical Gazette* 90.518 (2006), pp. 203–208 (cit. on p. 59).

[Phi57] Norman A Phillips. "A coordinate system having some special advantages for numerical forecasting". In: *Journal of the Atmospheric Sciences* 14.2 (1957), pp. 184–185 (cit. on p. 15).

[RG13] Richard and Gavrilyuk. "The classical hydraulic jump in a model of shear shallow-water flows". In: *Journal of Fluid Mechanics* 725 (2013), pp. 492–521 (cit. on p. 86).

[Ser99] Denis Serre. *Systems of Conservation Laws 1: Hyperbolicity, entropies, shock waves*. Cambridge University Press, 1999 (cit. on p. 47).

[SZ03] Guus Stelling and Marcel Zijlema. "An accurate and efficient finite-difference algorithm for non-hydrostatic free-surface flow with application to wave propagation". In: *International journal for numerical methods in fluids* 43.1 (2003), pp. 1–23 (cit. on p. 109).

[Sto19] James Johnston Stoker. *Water waves: The mathematical theory with applications*. Courier Dover Publications, 2019 (cit. on p. 14).

[Tes85] V. M. Teshukov. "On the hyperbolicity of long wave equations". In: *Doklady Akademii Nauk*. Vol. 284. 3. Russian Academy of Sciences. 1985, pp. 555–559 (cit. on p. 16).

[Tes92] V. M. Teshukov. "On Cauchy Problem for Long Wave Equations". In: *Free Boundary Problems in Continuum Mechanics: International Conference on Free Boundary Problems in Continuum Mechanics, Novosibirsk, July 15–19,1991*. Ed. by S. N. Antontsev, A. M. Khludnev, and K.-H. Hoffmann. Basel: Birkhäuser Basel, 1992, pp. 331–338. ISBN: 978-3-0348-8627-7. DOI: 10.1007/978-3-0348-8627-7_36. URL: https://doi.org/10.1007/978-3-0348-8627-7_36 (cit. on p. 16).

[Tor13] Eleuterio F Toro. *Riemann solvers and numerical methods for fluid dynamics: a practical introduction*. Springer Science & Business Media, 2013 (cit. on p. 90).

[Tso92] Taicheng Tso. *The zero dispersion limits of nonlinear wave equations*. The University of Arizona, 1992 (cit. on p. 13).

[Viè46] François Viète. *Francisci Vietae Fontenaeensis, De Aeqvationvm Recognitione Et Emendatione Tractatvs Dvo*. Laquehay, 1646 (cit. on p. 59).

[Wes09] Pieter Wesseling. *Principles of computational fluid dynamics*. Vol. 29. Springer Science & Business Media, 2009 (cit. on p. 109).

[Whi67] GB Whitham. "Non-linear dispersion of water waves". In: *Journal of Fluid Mechanics* 27.2 (1967), pp. 399–412 (cit. on p. 13).

[Whi11] Gerald Beresford Whitham. *Linear and nonlinear waves*. John Wiley & Sons, 2011 (cit. on p. 13).

[Zak80] Vladimir Evgen'evich Zakharov. "Benney equations and quasiclassical approximation in the method of the inverse problem". In: *Functional analysis and its applications* 14.2 (1980), pp. 89–98 (cit. on pp. 14, 15, 95).

[Zwi02] Daniel Zwillinger. *CRC standard mathematical tables and formulae*. chapman and hall/CRC, 2002 (cit. on p. 59).